The Gas Phase Ligand Exchange of Cadmium β-diketonate Complexes

by

Dominic Giovanni Silvestri

Submitted in Partial Fulfillment of the Requirements

for the Degree of

Master of Science

in the

Chemistry

Program

YOUNGSTOWN STATE UNIVERSITY

August, 2014

The Gas Phase Ligand Exchange of Cadmium β-diketonate Complexes

Dominic Giovanni Silvestri

I hereby release this thesis to the public. I understand that this thesis will be made available from the OhioLINK ETD Center and the Maag Library Circulation Desk for public access. I also authorize the University or other individuals to make copies of this thesis as needed for scholarly research.

Signature:

Dominic G. Silvestri, Student Date

Approvals:

Dr, Brian D. Leskiw, Thesis Advisor Date

Dr. Howard D. Mettee, Committee Member Date

Dr. Ganesaratnam K. Balendiran, Committee Member Date

Dr. Salvatore A. Sanders, Associate Dean of Graduate Studies Date

ABSTRACT

A series of gas-phase ligand exchange reactions involving Cadmium trifluorotrimethylacetylacetonate ($Cd(tftm)_2$) were examined using a triple quadrupole mass spectrometer. Multiple co-sublimation experiments were explored with various metal β-diketonates where several partial and complete ligand exchange processes were observed and are reported herein for the first time. In an attempt to elucidate possible mechanisms leading to the formation of the mixed ligand complex, select ion-neutral experiments were conducted within the collision cell of the triple quadrupole mass spectrometer.

Acknowledgements

First and foremost, I would like to thank my family and friends for their continued love and support. They have always encouraged me to pursue my goals and have always been there to lend a hand in times of need. It hasn't always been an easy road, and it's said that things worthwhile are never easy, but having them by my side has certainly made the journey much more gratifying.

I would like to thank Dr. Brian Leskiw for welcoming me into his research group and for his time and knowledge in helping me become not just a better student, but helping round me into a better individual. His constant availability and willingness to help not just me succeed, but my colleagues as well, will never go overlooked.

I would like to thank my committee members, Dr. Howard Mettee and Dr. Ganesaratnam Balendiran in assisting in the preparation of presenting my thesis. Also, Ray Hoff and Dr. Wang were helpful contributors and were there to assist in any problems faced with the instrumentation.

Finally the Youngstown State University chemistry department deserves a thank you, as well. Allowing me to continue my education in pursuit of a Master's Degree has opened up many opportunities that were not previously available to me. I hope to use the knowledge I gained here to make not just a career for myself, but to make a life for myself.

TABLE OF CONTENTS

List of Figures

List of Tables

List of Equations

Chapter 1
Literature Review

1.1 β-Diketonates

β-diketonates are used in a broad range of scientific fields and are often sought after due to their versatility. Metal β-diketonates are typically described as a coordination compound rather than an organometallic complex due to the type of bonding involved. The ligand metal bond of the coordination compound is covalent in nature, while an organometallic compound bond has a much stronger direct carbon-metal bond.[1] These complexes are used quite often because of their ability to be easily prepared, tenability through ligand selection, and volatile nature.[2-5] The applications of β-diketonate complexes are many and include fields of the deposition of metallic films[5], carbon-nantube structures[6] and in catalysis[7,8].

The usefulness of the β-diketonate complexes can also be attributed to the ease of altering the corresponding substituents. The complexes that will be investigated herein include metal acetylacetonates, $M(acac)_2$, metal trifluoromethylacetylacetonate, $M(tftm)_2$, metal hexafluoroacetylacetonates, M(hfac), and for the first time, metal diethylacetylacetonate, $M(eeac)_2$, and metal trifluoroacetylacetonate, M(tfac) complexes. The gas phase reactivity of the complexes will be investigated.

In an attempt to investigate the keto-enol tautomerization for this class of complexes Sloop et al.[9] studied multiple trifluorotrimethyl-β-diketonates using UV and IR spectroscopy and found that the enol form was in fact the preferred structure. This claim was supported by three examples presented in their paper. The first example incorporated an aromatic ring as one of the substituents, and the molecule demonstrated electron withdrawing properties that are favorable for enol positioning. The second

example added an *ortho* substituent to prevent the co-planarity of the ring that limited stability. Finally, when intramolecular hydrogen bonding opportunities of the carbonyl with adjacent heteroatoms become significant, the enol form was again observed to be favored. It should also be noted that chelation with a metal can be achieved by the loss of a proton and the bonding coordination of both oxygens.

1.2 Bonding in β-diketonates Complexes

When examining the properties that affect the bonding in β-diketonates, Ligand Field Theory[10] has been utilized to examine the metal-ligand interactions. This theory is of interest because certain properties, such as color and magnetism, can be described in coordination compounds. In addition to establishing some of these unique features, Ligand Field Theory is used to explain the fragmentation patterns of various metal β-diketonates in their respective mass spectra. Furthermore, since the geometries of these ligands are usually arranged as octahedral, tetrahedral or square planar, the theory assists in the explanation as how their geometries arise from the interaction between the ligand and the d-orbitals of the metal.[11] It is from these electrostatic interactions that the energies of the complexes can be established, although the equations are those that require extensive calculations. With regard to the energies produced from these orbitals, the oxidation states can also have an influence as well. Seeing as how the greater the difference in energy is proportional to the d-orbital splitting patterns, the oxidation state can also be determined from the energy difference.

1.3 β-diketonates & Mass Spectrometry

When examining the fragmentation patterns of β-diketonates complexes, there have been a plethora of techniques employed. These techniques include electron impact (EI)[12], chemical ionization (CI)[13], liquid secondary-ion mass spectrometry (LSIMS)[14], and matrix-assisted light desorption ionization (MALDI).[15] MacDonald and Shannon[16] were among the first to present information on the fragmentation of these species. Their worked consisted of acetylacetonate and benzolymethanes complexes that addressed general pathways. The biggest finding that occurred was the realization that the metal can retain its oxidation state due to the stability of the ligand.

Further research was pursued by Majer and Perry[17], who performed experiments examining the formation of mixed ligands in the gas phase. In their study, they obtained spectra that gave evidence for the formation of complexes consisting of two metal centers. They also proposed reaction pathways for this formation.

1.4 Mechanism of Ionization

The studies involved from this point forward are those of the positive ion mass spectrometry. Seeing as how the mass spectrometer will be the main instrument in examining the data, it is important to have an understanding of the process of ionization for the compounds at hand. In establishing mechanisms for ionization, it should be noted that 70eV electron impact is the most commonly used technique in mass spectrometry. It is from this technique that positive molecular ions are produced, as shown in Equation 1.1.

$$M(L)_n + e^- \rightarrow [M(L)_n]^+ + 2\ e^- \qquad (1.1)$$

Following the loss of an electron, the delocalization of the charge can occur over the complex or the charge can be centralized on the metal. However, it is the metal center that plays the largest role in the extent of the delocalization. The energy required to ionize a sample will depend on whether the d-orbitals are completely filled.

1.5 Application of β-diketonates

The application of β-diketonates is becoming increasingly examined due to the versatility of the compounds. Applications that β-diketonates are involved in, but not limited to, include the deposition of metallic films, removal of heavy metals from water, and carbon nanotube technology. Nieminen et. al.[18] examined the conditions at which lanthanum oxide could be deposited by using $La(thd)_3$. One of the major problems faced during deposition was the large carbon residue in the films. In using this specific β-diketonate, it was reported that the metallic deposition not only occurred, but at a lower temperature than previously reported, and with less carbon residue.

Kumar et.al.[19] found that β-diketonate functionalized styrene resins can be employed in the removal of heavy metals, such as nickel, chromium, and lead, from water. It was found that these compounds were useful in absorbing such heavy metals by calculating the kinetic absorption rates of these complexes. In the study, the functional molecule successfully removed the heavy metals from the water. Given the effectiveness of the functional molecule being able to remove heavy metals from water, the applications of β-diketonates have expanded to now also include environmental remediation.

Spijksma et. al.[20] examined the stability of the metal oxide nanostructures by modifying the substituents present on the molecule. Additional stability was found due to an increase in the metal-oxygen bond length and the increase in the number of substituents on the molecule forming di- and tri-substituted compounds instead of mono-substituted. As mentioned previously, the stable nature of β-diketonates is a sought after trait and the study presented can confirm that claim.

Chapter 2

Instrumentation

2.1 Mass Spectrometry

Mass spectrometry is an analytical tool used mainly to identify elemental composition. These instruments are used in a variety of applications in numerous scientific fields. Some examples where mass spectrometers are useful are environmental analysis, forensic analysis, clinical research, proteomics and genomics, and generation physio-chemical data.

Some of the more common types of mass spectrometers include quadrupole, time-of-flight, and double-focusing mass spectrometers. With advancements in technology, techniques have been developed to enhance the functionality of the mass spectrometers. Inductively coupled plasma mass spectrometry (ICPMS) is one type of technique that has been developed with such new technology.

Even with the new advancements and different types of mass spectrometers being produced, all of the instruments follow the same set of principles when samples are run and data is collected. The components of a mass spectrometer, as outlined in Figure 2.1, are an ion source, mass analyzer, ion detector, and data analyzer.

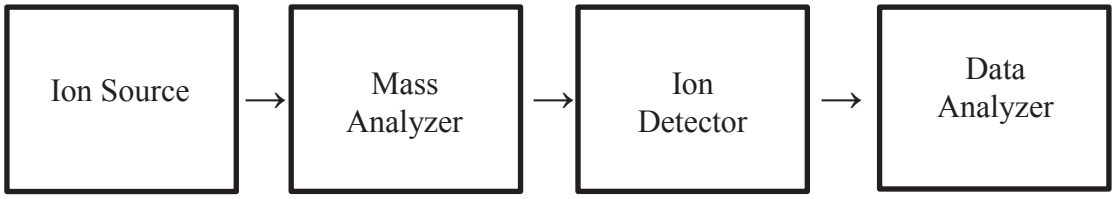

Figure 2.1: The four major parts of a generic mass spectrometer

2.2 Quadrupole Mass Analyzer

A quadrupole mass analyzer is most common mass spectrometer used. The ability of the instrument to perform scan rates over the entire spectrum in such a rapid amount of time is one of the advantages that is widely considered when using the quadrupole. The spectrometer, as depicted in Figure 2.2, is composed of four rods that run parallel to one another that act as the electrodes, and the ions are then accelerated in the space between the rods. Upon selecting a specific range for the masses to be analyzed, all molecules that do not fall within that range are turned off axis and do not reach the detector. The four rods are both positively and negatively charged, two positive and two negative, where the opposing potentials create an electric field that allows only ions with certain *m/z* to reach the detector.

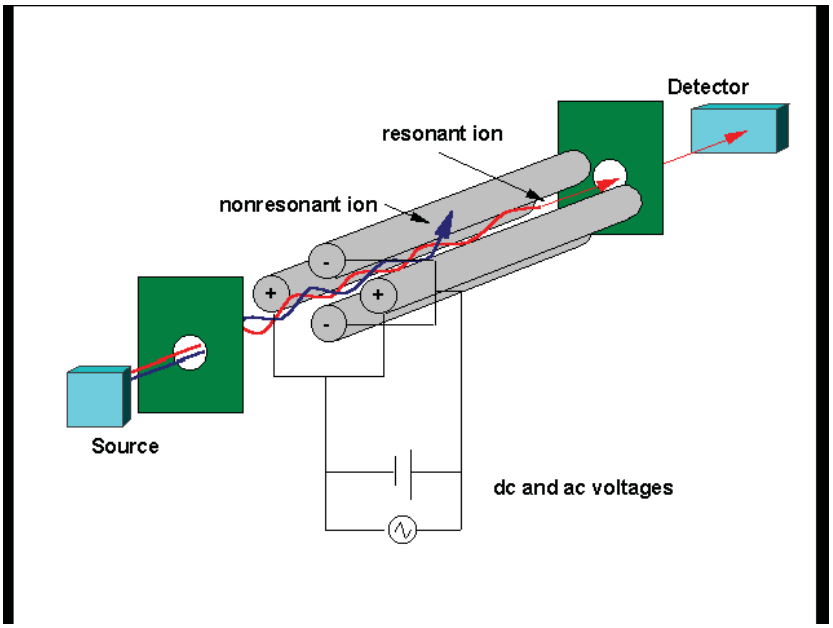

Figure 2.2: Schematic of a quadrupole mass spectrometer.

2.3 Triple Quadrupole

The triple quadrupole mass spectrometer has three quadrupoles arranged in succession, each one composed of, again, four cylindrical rods. The triple quad can be used to gather further information about the composition of the parent peak, or as in this case, used to determine mixed ligand combinations and possible mechanism formations. Quadrant 1, Q1, and Quadrant 3, Q3, of the spectrometer are used for similar purposes; their responsibility consists of filtering the ions according to the *m/z* ratio. The second quadrant is the region where a neutral species is introduced to react with the charged ions from quadrant 1. The collision cell, as this region is often referred to, can be used to create fragments of the original ions are that passed through Q1. However, when inducing collisions, it is important not to completely obliterate the species, but carefully monitor the ion signal for fragmentation.

2.4 Collision Cell

In the collision cell, as mentioned, fragmentation is often used for further analysis of parent ion composition; however, in the study being carried out here, it is an integral part in determining just the opposite – the formation of the metal ligand complexes. When attempting to determine such pathways there were many possible routes to be examined. During the ionization process, in which only the first quadrant was used, there were losses of specific masses that allowed for the identification of stable fragments. Fluorine migration, loss of *t*-butyl and ethyl groups, and only one equivalent of the ligand binding to the metal were all possible species that were of interest when introducing species into the collision cell. Once these specific masses were introduced, it was pretty clear whether the mixed ligand complex was formed.

Chapter 3
Experimental

3.1 Synthesis of Metal Hexafluoroacetylacetonate [$M(hfac)_2$]

All compounds were purchased from Sigma Aldrich and were investigated without any further purification. $M(hfac)_2$ was prepared at a concentration of 0.0250 M, as it was found to be suitable for mass spectrometric analysis.

3.2 Metal 2,4 Pentanedione [$M(acac)_2$]

The preparation of the samples were adapted from procedures by Lerach[14] and Watson & Lin[21]. The metal chloride was dissolved in 100 mL of room temperature de-ionized H_2O, in some cases toluene, and was stirred with a magnetic stir plate and a PTFE coated stir bar. Upon addition of the metal chloride to the H_2O, depending on the metal, two or three molar equivalents of the ligand, 2,4-pentanedione, *acac*, were added to the solution. Due to the immiscibility of the water and 2,4-pentanedione, a basic solution of 1:1 (v/v) NH_4OH: H_2O was added. Once the base was added, a precipitate would almost always immediately form. After completion, the precipitate was isolated via vacuum filtration. All samples were then verified by mass spectrometry if the precipitate was found.

3.2.1 $Ni(acac)_2$

The addition of 0.6988 g of the metal chloride ($NiCl_2$• 6 H_2O) and 0.60 mL of 2,4-pentanedione resulted in the solution changing to a light green color. The addition of 20 mL of 1:1 (v/v) NH_4OH: H_2O dropwise resulted in no immediate formation of precipitate. The mixture was stirred for 1 hour at room temperature, and the precipitate

was isolated via vacuum filtration resulting in a light blue homogeneous powder. The product was allowed to dry and was re-crystallized overnight by evaporation from methanol in a desiccator. Once dried, the newly formed compound was found to have a percent yield of 79.5%. A representative mass spectrum is presented in Figure 4.2.

3.2.2 $Pd(acac)_2$

The addition of 0.4337 g of the metal chloride ($PdCl_2$) and 0.4897 mL of 2,4-pentanedione resulted in the solution turning from a dark red to light yellow color. The addition of 20 mL of 1:1 (v/v) NH_4OH: H_2O resulted in no immediate formation of precipitate. The mixture was stirred for 1.5 hours at room temperature, however no precipitate formed.

Due to the lack of success in the first trial, a second trial was attempted with the addition of 0.1438 g of metal chloride and 0.1674 mL of 2,4-pentanedione to 100 mL of toluene. 20 mL of 1:1 (v/v) NH_4OH: H_2O was added dropwise and the solution was heated and stirred, but no precipitate formed.

3.2.3 $Ag(acac)_2$

The addition of 0.6126 g of the metal nitrate ($AgNO_3$) and 0.3703 mL of 2,4-pentanedione did not result in a color change of the solution. The addition of 20 mL of 1:1 (v/v) NH_4OH: H_2O resulted in the formation of oil droplets but upon stirring disappeared. The mixture was stirred for 1 hour at room temperature, but did not yield a precipitate.

3.2.4 $Fe(acac)_3$

The addition of 0.5690 g of the metal chloride ($FeCl_3$) and 0.6484 mL of 2,4-pentanedione did not result in a color change of the solution. The addition of 20 mL of 1:1 (v/v) NH_4OH: H_2O did not result in an immediate formation of a precipitate. The mixture was stirred for 2 hours at room temperature but the metal chloride did not dissolve fully into solution. This synthesis was unsuccessful.

3.2.5 $Cd(acac)_2$

The addition of 0.4429 g of the metal chloride ($CdCl_2$) and 0.4927 mL of 2,4-pentanedione to 100 mL of toluene did not result in a color change of the solution. Furthermore, the addition of 20 mL of 1:1 (v/v) NH_4OH: H_2O resulted in no immediate precipitate formation. An additional 40 mL 1:1 (v/v) NH_4OH: H_2O was added; the mixture was stirred for 1 hour on low heat, with no precipitate formation.

3.2.6 K(acac)

The addition of 0.4428 g of the metal chloride (KCl) and 0.5532 mL of 2,4-pentanedione did not result in a color change of the solution. The addition of 20 mL of 1:1 (v/v) NH_4OH: H_2O resulted in the formation of no precipitate. The mixture was stirred for 1 hour at room temperature and yielded no precipitate.

3.2.7 $Fe(acac)_2$

The addition of 0.5827 g of the metal chloride ($FeCl_2$) and 0.601 mL of 2,4-pentanedione resulted in the solution turning from clear to a deep red color. The addition

of 20 mL of 1:1 (v/v) NH_4OH: H_2O resulted in the formation of a red-orange precipitate. The mixture was stirred for 1 hour at room temperature, and the precipitate was isolated via vacuum filtration resulting in a homogeneous powder. The product was allowed to dry and re-crystallize overnight by evaporation from methanol in a desiccator.

3.2.8 $Ca(acac)_2$

The addition of 0.3070 g of the metal chloride ($CaCl_2$) and 0.641 mL of 2,4-pentanedione did not result in a change of the solution. The addition of 20 mL of 1:1 (v/v) NH_4OH: H_2O resulted in the formation of no precipitate. The mixture was stirred for 1 hour at low heat and was considered unsuccessful as no precipitate was formed.

3.2.9 $Cu(acac)_2$

The addition of 0.3836 g of the metal chloride ($CuCl_2$) and 0.584 mL of 2,4-pentanedione did not result in a color change of the solution. The addition of 20 mL of 1:1 (v/v) NH_4OH: H_2O resulted in the formation of a white precipitate. The mixture was stirred for 1 hour at room temperature, and the precipitate was isolated via vacuum filtration resulting in a homogeneous powder. The product was allowed to dry and was re-crystallized overnight by evaporation from methanol in a desiccator.

3.3 Metal 1,1,1-trifluoro-5,5-dimethyl-2,4-hexanedione [$M(tftm)_2$]

The preparation of the samples were adapted from procedures by Hunter[1], Lerach[14] and Watson & Lin[21]. The metal chloride was dissolved in 100 mL of room temperature de-ionized H_2O, or in some cases, in toluene, and was stirred with a

magnetic stir plate and a PTFE coated stir bar. Upon addition of the metal chloride to the H_2O, depending on the metal, one, two, or three molar equivalents of 1,1,1-trifluoro-5,5-dimethyl-2,4-hexanedione were added to the solution. Due to the immiscibility of the mixture, a basic solution of 1:1 (v/v) NH_4OH: H_2O was added. Once the base was added, a precipitate would almost always immediately form. After completion, the precipitate was isolated via vacuum filtration. All samples were then verified by mass spectrometry if the precipitate was found.

3.3.1 $Fe(tftm)_3$

The addition of 0.3161 g of the metal chloride ($FeCl_3$) and 0.6067 mL of 1,1,1-trifluoro-5,5-dimethyl-2,4-hexanedione were added to 100 mL of toluene, which did not result in a color change of the solution. The addition of 40 mL of 1:1 (v/v) NH_4OH: H_2O did not result in the immediate formation of a precipitate. The mixture was stirred for 1 hour at room temperature, and a red precipitate formed in the aqueous layer. The organic layer was decanted off and the aqueous layer was evaporated to dryness. The product was re-crystallized overnight by evaporation from methanol in a desiccator.

3.3.2 $Ni(tftm)_2$

The addition of 0.3957 g of the metal chloride ($NiCl_2$• 6 H_2O) and 0.560 mL of 1,1,1-trifluoro-5,5-dimethyl-2,4-hexanedione to 100 mL of distilled H_2O resulted in the solution turning light blue in color. The addition of 20 mL of 1:1 (v/v) NH_4OH: H_2O resulted in the formation of a light blue precipitate. The mixture was stirred for 1 hour at room temperature, and the precipitate was isolated via vacuum filtration resulting in a

homogeneous powder. The product was allowed to dry and was re-crystallized overnight by evaporation from methanol in a desiccator.

3.3.3 Li(tftm)

The addition of 0.2824 g of the metal chloride (LiCl) and 0.6416 mL of 1,1,1-trifluoro-5,5-dimethyl-2,4-hexanedione did not result in a color change of the solution. The addition of 20 mL of 1:1 (v/v) NH_4OH: H_2O did not result in the immediate formation of a precipitate. The mixture was stirred for 1 hour at room temperature but no precipitate formed.

3.3.4 $Co(tftm)_2$

The addition of 0.3950 g of the metal chloride ($CoCl_2$• 6 H_2O) and 0.5776 mL of 1,1,1-trifluoro-5,5-dimethyl-2,4-hexanedione resulted in the solution turning brown in color. The addition of 20 mL of 1:1 (v/v) NH_4OH: H_2O resulted in the formation of an orange precipitate. The mixture was stirred for 1 hour at room temperature, and the precipitate was isolated via vacuum filtration resulting in a homogeneous powder. The product was allowed to dry and was re-crystallized overnight by evaporation from methanol in a desiccator. Once dried, the newly formed compound was found to have a percent yield of 67.3%. A representative mass spectrum is presented in Figure 6.2.

3.3.5 $Ca(tftm)_2$

The addition of 0.1920 g of the metal chloride ($CaCl_2$) and 0.6027 mL of 1,1,1-trifluoro-5,5-dimethyl-2,4-hexanedione did not result in a color change of the solution. The addition of 20 mL of 1:1 (v/v) NH_4OH: H_2O resulted in the formation of a white

precipitate. The mixture was stirred for 1 hour at room temperature, and the precipitate was isolated via vacuum filtration resulting in a homogeneous powder. The product was allowed to dry and was re-crystallized overnight by evaporation from methanol in a desiccator.

3.3.6 K(tftm)

The addition of 0.2399 g of the metal chloride (KCl) and 0.554 mL of 1,1,1-trifluoro-5,5-dimethyl-2,4-hexanedione did not result in a color change of the solution. The addition of 20 mL of 1:1 (v/v) NH_4OH: H_2O did not result in the immediate formation of a precipitate. The mixture was stirred for 1 hour at low heat, but no precipitate formed.

3.3.7 $Mn(tftm)_2$

The addition of 0.2106 g of the metal chloride ($MnCl_2$) and 0.583 mL of 1,1,1-trifluoro-5,5-dimethyl-2,4-hexanedione resulted in the solution turning yellow in color. The addition of 20 mL of 1:1 (v/v) NH_4OH: H_2O resulted in the formation of an orange precipitate. The mixture was stirred for 1 hour at room temperature, and the precipitate was isolated via vacuum filtration resulting in a homogeneous powder. The product was allowed to dry and was re-crystallized overnight by evaporation from methanol in a desiccator.

3.3.8 $Cu(tftm)_2$

The addition of 0.2416 g of the metal chloride ($CuCl_2$) and 0.5717 mL of 1,1,1-trifluoro-5,5-dimethyl-2,4-hexanedione resulted in the solution turning blue in color. The addition of 20 mL of 1:1 (v/v) NH_4OH: H_2O resulted in the formation of a royal blue precipitate. The mixture was stirred for 1 hour at room temperature, and the precipitate was isolated via vacuum filtration resulting in a homogeneous powder. The product was allowed to dry and was re-crystallized overnight by evaporation from methanol in a desiccator.

3.3.9 $Fe(tftm)_2$

The addition of 0.3484 g of the metal chloride ($FeCl_2$) and 0.582 mL of 1,1,1-trifluoro-5,5-dimethyl-2,4-hexanedione resulted in the solution turning orange in color. The addition of 20 mL of 1:1 (v/v) NH_4OH: H_2O resulted in the formation of a dark, rust colored precipitate. The mixture was stirred for 1 hour at low heat, and the precipitate was isolated via vacuum filtration resulting in a homogeneous powder. The product was allowed to dry and was re-crystallized overnight by evaporation from methanol in a desiccator.

3.3.10 $Zn(tftm)_2$

The addition of 0.2238 g of the metal chloride ($ZnCl_2$) and 0.569 mL of 1,1,1-trifluoro-5,5-dimethyl-2,4-hexanedione did not result in a color change of the solution. The addition of 20 mL of 1:1 (v/v) NH_4OH: H_2O resulted in the formation of a white precipitate. Although initially appeared upon the addition of the base, after the mixture

was stirred for 1 hour on low heat, the precipitate was no longer visible. Due to a lack of a precipitate, the reaction was unsuccessful.

3.3.11 $Pd(tftm)_2$

The addition of 0.2690 g of the metal chloride ($PdCl_2$) and 0.523 mL of 1,1,1-trifluoro-5,5-dimethyl-2,4-hexanedione did not result in a color change of the solution. The addition of 20 mL of 1:1 (v/v) NH_4OH: H_2O did not result in the immediate formation of a precipitate. The mixture was stirred for 2.5 hours at room temperature, in which after the first hour a white precipitate began to form. The precipitate was isolated via vacuum filtration resulting in a homogeneous powder, and the product was allowed to dry and was re-crystallized overnight by evaporation from methanol in a desiccator. Once dried, the newly formed compound was found to have a percent yield of 43.7%. A representative mass spectrum is presented in Figure 6.5.

3.3.12 $Cd(tftm)_2$

The addition of 0.2812 g of the metal chloride ($CdCl_2$) and 0.658 mL of 1,1,1-trifluoro-5,5-dimethyl-2,4-hexanedione did not result in a color change of the solution. The addition of 20 mL of 1:1 (v/v) NH_4OH: H_2O resulted in the formation of a white precipitate. The mixture was stirred for 1 hour at room temperature, and the precipitate was isolated via vacuum filtration resulting in a homogeneous powder. The product was allowed to dry and was re-crystallized overnight by evaporation from methanol in a desiccator. Once dried, the newly formed compound was found to have a percent yield of 60.0%. A representative mass spectrum is presented in Figure 4.1.

3.3.13 $Al(tftm)_3$

The addition of 0.2956 g of the metal chloride ($AlCl_3$• 6 H_2O) and 0.5912 mL of 1,1,1-trifluoro-5,5-dimethyl-2,4-hexanedione were added to 100 mL of toluene and resulted in the solution becoming cloudy. The addition of 40 mL of 1:1 (v/v) NH_4OH: H_2O resulted in the formation of a white precipitate. The mixture was stirred for 1 hour at room temperature, and the precipitate formed in the organic layer. The aqueous layer was filtered off and the toluene layer was evaporated. The product was allowed to dry and was re-crystallized overnight by evaporation from methanol in a desiccator.

3.3.14 $Mg(tftm)_2$

The addition of 0.3660 g of the metal chloride ($MgCl_2$• 6 H_2O) and 0.626 mL of 1,1,1-trifluoro-5,5-dimethyl-2,4-hexanedione resulted in the solution turning white in color. The addition of 20 mL of 1:1 (v/v) NH_4OH: H_2O resulted in the formation of a white precipitate. The mixture was stirred for 1 hour on low heat, and the precipitate was isolated via vacuum filtration resulting in a homogeneous powder. The product was allowed to dry and was re-crystallized overnight by evaporation from methanol in a desiccator. Once dried, the newly formed compound was found to have a percent yield of 92.4%. A representative mass spectrum is presented in Figure 6.4.

3.3.15 Ag(tftm)

The addition of 0.3590 g of the metal chloride (AgCl) and 0.429 mL of 1,1,1-trifluoro-5,5-dimethyl-2,4-hexanedione did not result in a color change of the solution. The addition of 20 mL of 1:1 (v/v) NH_4OH: H_2O did not result in the immediate

formation of a precipitate. The mixture was stirred for 1 hour on low heat, and the precipitate formed later during the stirring and then isolated via vacuum filtration resulting in a homogeneous powder. The product was allowed to dry and was re-crystallized overnight by evaporation from methanol in a desiccator.

3.4 Metal 3,5-Heptanedione [$M(eeac)_2$]

The preparation of the samples were adapted from procedures by by Hunter[1], Lerach[14] and Watson & Lin[21]. The metal chloride was dissolved in 100 mL of room temperature de-ionized H_2O, or in some cases toluene, and was stirred with a magnetic stir plate and a PTFE coated stir bar. Upon addition of the metal chloride to the H_2O, depending on the metal, one, two, or three molar equivalents of 3,5-heptanedione were added to the solution. Due to the immiscibility of the mixture, a basic solution of 1:1 (v/v) NH_4OH: H_2O was added. Once the base was added, a precipitate would almost always immediately form. After completion, the precipitate was isolated via vacuum filtration. All samples were then verified by mass spectrometry if the precipitate was found.

3.4.1 $Ni(eeac)_2$

The addition of 0.5660 g of the metal chloride ($NiCl_2$• 6 H_2O) and 0.645 mL of 3,5-heptanedione resulted in the solution turning light green in color. The addition of 20 mL of 1:1 (v/v) NH_4OH: H_2O dropwise resulted in a light blue formation of precipitate. The mixture was stirred for 1 hour on low heat, and the precipitate was isolated via vacuum filtration resulting in a light blue homogeneous powder. The product was allowed to dry

and was re-crystallized overnight by evaporation from methanol in a desiccator. Once dried, the newly formed compound was found to have a percent yield of 41.1%. A representative mass spectrum is presented in Figure 4.2.

3.4.2 Li(eeac)

The addition of 0.2364 g of the metal chloride (LiCl) and 0.7521 mL of 3,5-heptanedione did not result in a color change of the solution. The addition of 20 mL of 1:1 (v/v) NH_4OH: H_2O did not result in the immediate formation of a precipitate. The mixture was stirred for 1 hour on low heat and no precipitate formed.

3.4.3 $Ca(eeac)_2$

The addition of 0.2808 g of the metal chloride ($CaCl_2$) and 0.686 mL of 3,5-heptanedione did not result in a color change of the solution. The addition of 20 mL of 1:1 (v/v) NH_4OH: H_2O did not result in the immediate formation of a precipitate. The mixture was stirred for 1 hour on low heat and no precipitate formed.

3.4.4 K(eeac)

The addition of 0.3513 g of the metal chloride (KCl) and 0.608 g of 3,5-heptanedione did not result in a color change of the solution. The addition of 20 mL of 1:1 (v/v) NH_4OH: H_2O did result in the formation of oil droplets but not a solid precipitate. The mixture was stirred for 1 hour on low heat. After the solution was stirred, the oil droplets dissipated and no precipitate was evident.

3.4.5 $Mn(eeac)_2$

The addition of 0.3134 g of the metal chloride ($MnCl_2$) and 0.653 mL of 3,5-heptanedione resulted in the solution turning orange in color. The addition of 20 mL of 1:1 (v/v) NH_4OH: H_2O resulted in the formation of a black precipitate. The mixture was stirred for 1 hour on low heat, and the precipitate was isolated via vacuum filtration resulting in a homogeneous powder. The product was allowed to dry and was re-crystallized overnight by evaporation from methanol in a desiccator.

3.4.6 $Cu(eeac)_2$

The addition of 0.3126 g of the metal chloride ($CuCl_2$) and 0.635 mL of 3,5-heptanedione resulted in the solution turning light blue in color. The addition of 20 mL of 1:1 (v/v) NH_4OH: H_2O resulted in the formation of a purple precipitate. The mixture was stirred for 1 hour on low heat, and the precipitate was isolated via vacuum filtration resulting in a homogeneous powder. The product was allowed to dry and was re-crystallized overnight by evaporation from methanol in a desiccator.

3.4.7 $Fe(eeac)_2$

The addition of 0.3039 g of the metal chloride ($FeCl_2$) and 0.651 mL of the ligand resulted in the solution turning orange-brown in color. The addition of 20 mL of 1:1 (v/v) NH_4OH: H_2O resulted in the formation of a brown precipitate. The mixture was stirred for 1 hour on low heat, and the precipitate was isolated via vacuum filtration resulting in a homogeneous powder. The product was allowed to dry and was re-crystallized overnight by evaporation from methanol in a desiccator.

3.4.8 $Co(eeac)_2$

The addition of 0.4408 g of the metal chloride ($CoCl_2$•6 H_2O) and 0.645 mL of 3,5-heptanedione resulted in the solution turning blue in color. The addition of 20 mL of 1:1 (v/v) NH_4OH: H_2O resulted in the formation of a peach colored solution. The mixture was stirred for 2 hour at room temperature and allowed to stand overnight. The precipitate was isolated via vacuum filtration resulting in a homogeneous, red powder. The product was allowed to dry and was re-crystallized overnight by evaporation from methanol in a desiccator. Once dried, the newly formed compound was found to have a percent yield of 28.0%. A representative mass spectrum is presented in Figure 6.1.

3.4.9 $Zn(eeac)_2$

The addition of 0.3188 g of the metal chloride ($ZnCl_2$) and 0.632 mL of 3,5-heptanedione did not result in a color change of the solution. The addition of 20 mL of 1:1 (v/v) NH_4OH: H_2O did not result in the immediate formation of a precipitate. The mixture was stirred for 1 hour on low heat and no precipitate formed.

3.4.10 $Pd(eeac)_2$

The addition of 0.3637 g of the metal chloride ($PdCl_2$) and 0.560 mL of 3,5-heptanedione did not result in a color change of the solution. The addition of 20 mL of 1:1 (v/v) NH_4OH: H_2O resulted in the formation of no immediate precipitate. The mixture was stirred for 1 hour on low heat and no precipitate formed.

3.4.11 $Cd(eeac)_2$

The addition of 0.3747 g of the metal chloride ($CdCl_2$) and 0.551 mL of 3,5-heptanedione did not result in a color change of the solution. The addition of 20 mL of 1:1 (v/v) NH_4OH: H_2O did not result in the immediate formation of a precipitate. The mixture was stirred for 1 hour on low heat and no precipitate formed.

3.4.12 Ag(eeac)

The addition of 0.4655 g of the metal chloride (AgCl) and 0.431 mL of 3,5-heptanedione did not result in a color change of the solution. The addition of 20 mL of 1:1 (v/v) NH_4OH: H_2O did not result in the immediate formation of a precipitate. The mixture was stirred for 1 hour on low heat and no precipitate formed.

3.4.13 $Mg(eeac)_2$

The addition of 0.5457 g of the metal chloride ($MgCl_2$•6 H_2O) and 0.724 mL of 3,5-heptanedione did not result in a color change of the solution, but did appear to become more viscous. The addition of 20 mL of 1:1 (v/v) NH_4OH: H_2O resulted in the formation of a white precipitate. The mixture was stirred for 1 hour on low heat, and the precipitate was isolated via vacuum filtration resulting in a homogeneous powder. The product was allowed to dry and was re-crystallized overnight by evaporation from methanol in a desiccator. Once dried, the newly formed compound was found to have a percent yield of 32.1%. A representative mass spectrum is presented in Figure 6.3.

3.5 Metal 1,3-Diphenyl-1,3-propanedione [$M(dbm)_2$]

The preparation of the samples were adapted from procedures by by Hunter[1], Lerach[14] and Watson & Lin[21]. The metal chloride was dissolved in 100 mL of room temperature de-ionized H_2O, or in some cases toluene, and was stirred with a magnetic stir plate and a PTFE coated stir bar. Upon addition of the metal chloride to the H_2O, depending on the metal, one, two, or three molar equivalents of 1,3-diphenyl-1,3-propanedione were added to the solution. Due to the immiscibility of the water and ligand, a basic solution of 1:1 (v/v) NH_4OH: H_2O was added and a precipitate would almost always immediately form. After completion, the precipitate was isolated via vacuum filtration. All samples were then verified by mass spectrometry if the precipitate was found.

3.5.1 $Ni(dbm)_2$

The addition of 0.3516 g of the metal chloride ($NiCl_2$• 6 H_2O) and 0.6632 g of 1,3-diphenyl-1,3-propanedione resulted in the solution turning green in color. The addition of 20 mL of 1:1 (v/v) NH_4OH: H_2O resulted in the formation of a light blue precipitate. The mixture was stirred for 1 hour on low heat, and the precipitate was isolated via vacuum filtration resulting in a homogeneous powder. The product was allowed to dry and was re-crystallized overnight by evaporation from methanol in a desiccator.

3.5.2 $Cu(dbm)_2$

The addition of 0.2195 g of the metal chloride ($CuCl_2$) and 0.6620 g of 1,3-diphenyl-1,3-propanedione resulted in the solution turning dark blue in color. The addition of 20 mL of 1:1 (v/v) NH_4OH: H_2O resulted in the formation of a light yellow precipitate. The mixture was stirred for 1 hour on low heat, and the precipitate was isolated via vacuum filtration resulting in a homogeneous powder. The product was allowed to dry and was re-crystallized overnight by evaporation from methanol in a desiccator.

3.5.3 $Zn(dbm)_2$

The addition of 0.2116 g of the metal chloride ($ZnCl_2$) and 0.6901 g of 1,3-diphenyl-1,3-propanedione did not result in a color change of the solution. The addition of 20 mL of 1:1 (v/v) NH_4OH: H_2O did not result in the immediate formation of a precipitate. After the mixture was stirred for 1 hour on low heat, a pale yellow precipitate was present and was isolated via vacuum filtration resulting in a homogeneous powder. The product was allowed to dry and was re-crystallized overnight by evaporation from methanol in a desiccator.

3.5.4 $Co(dbm)_2$

The addition of 0.3515 g of the metal chloride ($CoCl_2$• 6 H_2O) and 0.6629 g of 1,3-diphenyl-1,3-propanedione resulted in the solution turning blue-green in color. The addition of 20 mL of 1:1 (v/v) NH_4OH: H_2O did not result in the immediate formation of a precipitate. The mixture was stirred for several hours on low heat and the precipitate

formed that was mustard in color. The precipitate was then isolated via vacuum filtration resulting in a homogeneous powder. The product was allowed to dry and was re-crystallized overnight by evaporation from methanol in a desiccator.

3.5.5 $Mg(dbm)_2$

The addition of 0.3225 g of the metal chloride ($MgCl_2$• 6 H_2O) and 0.9486 g of 1,3-diphenyl-1,3-propanedione resulted in the solution turning yellow in color. The addition of 20 mL of 1:1 (v/v) NH_4OH: H_2O resulted in the formation of a yellow precipitate. The mixture was stirred for 1 hour on low heat, and the precipitate was isolated via vacuum filtration resulting in a homogeneous powder. The product was allowed to dry and was re-crystallized overnight by evaporation from methanol in a desiccator.

3.5.6 $Cd(dbm)_2$

The addition of 0.2451 g of the metal chloride ($CdCl_2$) and 0.5997 g of 1,3-diphenyl-1,3-propanedione resulted in the solution turning yellow in color, similar to that of the magnesium solution. The addition of 20 mL of 1:1 (v/v) NH_4OH: H_2O resulted in the formation of a yellow precipitate. The mixture was stirred for 1 hour on low heat, and the precipitate was isolated via vacuum filtration resulting in a homogeneous powder. The product was allowed to dry and was re-crystallized overnight by evaporation from methanol in a desiccator.

3.5.7 $Pd(dbm)_2$

The addition of 0.2396 g of the metal chloride ($PdCl_2$) and 0.6062 g of 1,3-diphenyl-1,3-propanedione did not result in a color change of the solution. The addition of 20 mL of 1:1 (v/v) NH_4OH: H_2O did not result in the immediate formation of a precipitate. The mixture was stirred for 1 hour on low heat, and an orange colored precipitate did form. The substance was isolated via vacuum filtration resulting in a homogeneous powder. The product was allowed to dry and was re-crystallized overnight by evaporation from methanol in a desiccator.

3.5.8 Li(dbm)

The addition of 0.1375 g of the metal chloride (LiCl) and 0.7275 g of 1,3-diphenyl-1,3-propanedione resulted in the solution turning yellow in color. The addition of 20 mL of 1:1 (v/v) NH_4OH: H_2O resulted in the formation of a light yellow precipitate. The mixture was stirred for 1 hour on low heat, and the precipitate was isolated via vacuum filtration resulting in a homogeneous powder. The product was allowed to dry and was re-crystallized overnight by evaporation from methanol in a desiccator.

3.5.9 $Ca(dbm)_2$

The addition of 0.1704 g of the metal chloride ($CaCl_2$) and 0.6885 g of 1,3-diphenyl-1,3-propanedione resulted in the solution turning yellow in color. The addition of 20 mL of 1:1 (v/v) NH_4OH: H_2O resulted in the formation of a yellow precipitate. The mixture was stirred for 1 hour on low heat, and the precipitate was isolated via vacuum

filtration resulting in a homogeneous powder. The product was allowed to dry and was re-crystallized overnight by evaporation from methanol in a desiccator.

3.5.10 K(dbm)

The addition of 0.2123 g of the metal chloride (KCl) and 0.6443 g of 1,3-diphenyl-1,3-propanedione did not result in a color change of the solution. The addition of 20 mL of 1:1 (v/v) NH_4OH: H_2O resulted in the formation of a yellow precipitate. The mixture was stirred for 1 hour on low heat, and the precipitate was isolated via vacuum filtration resulting in a homogeneous powder. The product was allowed to dry and was re-crystallized overnight by evaporation from methanol in a desiccator.

3.5.11 $Mn(dbm)_2$

The addition of 0.1875 g of the metal chloride ($MnCl_2$) and 0.6705 g of 1,3-diphenyl-1,3-propanedione resulted in the solution turning orange in color. The addition of 20 mL of 1:1 (v/v) NH_4OH: H_2O resulted in the formation of a yellow precipitate. The mixture was stirred for 1 hour on low heat, and the precipitate was isolated via vacuum filtration resulting in a homogeneous powder. The product was allowed to dry and was re-crystallized overnight by evaporation from methanol in a desiccator.

3.5.12 $Fe(dbm)_2$

The addition of 0.2946 g of the metal chloride ($FeCl_2$• 4 H_2O) and 0.6678 g of 1,3-diphenyl-1,3-propanedione resulted in the solution turning a light brown in color. The addition of 20 mL of 1:1 (v/v) NH_4OH: H_2O resulted in the formation of a dark brown

precipitate. The mixture was stirred for 1 hour on low heat, and the precipitate was isolated via vacuum filtration resulting in a homogeneous powder. The product was allowed to dry and was re-crystallized overnight by evaporation from methanol in a desiccator.

3.5.13 $Al(dbm)_3$

The addition of 0.2602 g of the metal chloride ($AlCl_3$• 6 H_2O) and 0.7211 g of 1,3-diphenyl-1,3-propanedione to 100 mL of toluene did not result in a color change of the solution. The addition of 20 mL of 1:1 (v/v) NH_4OH: H_2O did not result in the immediate formation of a precipitate. The mixture was stirred for 2 hour on low heat and allowed to sit overnight. After sitting, a white precipitate had formed in the organic layer, which was separated and evaporated. The product was recovered and was re-crystallized overnight by evaporation in a desiccator.

3.5.14 $Ag(dbm)_2$

The addition of 0.3378 g of the metal chloride (AgCl) and 0.5092 g of 1,3-diphenyl-1,3-propanedione did not result in the color change of the solution. The addition of 20 mL of 1:1 (v/v) NH_4OH: H_2O failed to result in the formation of a precipitate. The mixture was stirred for several hours on low heat, the reaction was deemed unsuccessful.

3.6 Metal 1,1,1-Trifluoro-2,4-pentanedione [$M(tfac)_2$]

The preparation of the samples were adapted from procedures by Hunter[1], Lerach[14] and Watson & Lin[21]. The metal chloride was dissolved in 100 mL of room

temperature de-ionized H_2O, or in some cases toluene, and was stirred with a magnetic stir plate and a PTFE coated stir bar. Upon addition of the metal chloride to the H_2O, depending on the metal, one, two, or three molar equivalents of the corresponding ligand were added to the solution. Due to the immiscibility of the water and 1,1,1-trifluoro-2,4-pentanedione, a basic solution of 1:1 (v/v) NH_4OH: H_2O was added. Once the base was added, a precipitate would almost always immediately form. After completion, the precipitate was isolated via vacuum filtration. All samples were then verified by mass spectrometry if the precipitate formed.

3.6.1 $Al(tfac)_3$

The addition of 0.3734 g of the metal chloride ($AlCl_3$• 6 H_2O) and 0.558 mL of 1,1,1-trifluoro-2,4-pentanedione did not result in a color change of the solution. The addition of 20 mL of 1:1 (v/v) NH_4OH: H_2O did not result in the immediate formation of a precipitate. The mixture was stirred for 1 hour on low heat, but was unsuccessful due to lack of precipitate formation.

3.6.2 Ag(tfac)

The addition of 0.4104 g of the metal chloride (AgCl) and 0.347 mL of 1,1,1-trifluoro-2,4-pentanedione did not result in a color change of the solution. The addition of 20 mL of 1:1 (v/v) NH_4OH: H_2O did not result in the immediate formation a precipitate. The mixture was stirred for 1 hour on low heat, but was unsuccessful due to lack of precipitate formation.

3.6.3 $Ca(tfac)_2$

The addition of 0.2744 g of the metal chloride ($CaCl_2$) and 0.6097 mL of 1,1,1-trifluoro-2,4-pentanedione did not result in a color change. Initially, the addition of 20 mL of 1:1 (v/v) NH_4OH: H_2O resulted in the formation of a white precipitate, but after stirring the substance was no longer visible. The solution stirred for 1 hour on low heat, but was unsuccessful due to lack of precipitate formation.

3.6.4 $Co(tfac)_2$

The addition of 0.4879 g of the metal chloride ($CoCl_2$• 6 H_2O) and 0.4957 mL of 1,1,1-trifluoro-2,4-pentanedione resulted in the solution turning teal in color. The addition of 20 mL of 1:1 (v/v) NH_4OH: H_2O resulted in the formation of a tan precipitate. The mixture was stirred for 1 hour on low heat, and the precipitate was isolated via vacuum filtration resulting in a homogeneous powder. The product was allowed to dry and was re-crystallized overnight by evaporation from methanol in a desiccator.

3.6.5 $Cd(tfac)_2$

The addition of 0.3283 g of the metal chloride ($CdCl_2$) and 0.4330 mL of 1,1,1-trifluoro-2,4-pentanedione did not result in a color change of the solution. The addition of 20 mL of 1:1 (v/v) NH_4OH: H_2O resulted in the formation of a white precipitate. The mixture was stirred for 1 hour on low heat, and the precipitate was isolated via vacuum filtration resulting in a homogeneous powder. The product was allowed to dry and was re-crystallized overnight by evaporation from methanol in a desiccator.

3.6.6 $Ni(tfac)_2$

The addition of 0.2650 g of the metal chloride ($NiCl_2$• 6 H_2O) and 0.496 mL of 1,1,1-trifluoro-2,4-pentanedione did not result in a color change of the solution. The addition of 20 mL of 1:1 (v/v) NH_4OH: H_2O resulted in the formation of a white precipitate. A precipitate did form after the mixture was stirred for 1 hour on low heat. The precipitate was isolated via vacuum filtration resulting in a homogeneous powder. The product was allowed to dry and was re-crystallized overnight by evaporation from methanol in a desiccator. Once dried, the newly formed compound was found to have a percent yield of 41.1%. A representative mass spectrum is presented in Figure 4.4.

3.6.7 $Cu(tfac)_2$

The addition of 0.2751 g of the metal chloride ($CuCl_2$) and 0.489 mL of 1,1,1-trifluoro-2,4-pentanedione resulted in the solution turning dark blue in color. The addition of 20 mL of 1:1 (v/v) NH_4OH: H_2O resulted in the formation of a black precipitate. The mixture was stirred for 1 hour on low heat, and the precipitate was isolated via vacuum filtration resulting in a homogeneous powder. The product was allowed to dry and was re-crystallized overnight by evaporation from methanol in a desiccator.

3.6.8 $Zn(tfac)_2$

The addition of 0.2739 g of the metal chloride ($ZnCl_2$) and 0.487 mL of 1,1,1-trifluoro-2,4-pentanedione resulted in the solution turning orange in color. The addition of 20 mL of 1:1 (v/v) NH_4OH: H_2O resulted in the formation of an orange precipitate.

The mixture was stirred for 1 hour on low heat, and the precipitate was isolated via vacuum filtration resulting in a homogeneous powder. The product was allowed to dry and was re-crystallized overnight by evaporation from methanol in a desiccator.

3.7 Metal 3-Methyl-2,4-pentanedione [$M(3Mac)_2$]

The preparation of the samples were adapted from procedures by Hunter[1], Lerach[14] and Watson & Lin[21]. The metal chloride was dissolved in 100 mL of room temperature de-ionized H_2O, or in some cases toluene, and was stirred with a magnetic stir plate and a PTFE coated stir bar. Upon addition of the metal chloride to the H_2O, depending on the metal, one, two, or three molar equivalents of the corresponding ligand were added to the solution. Due to the immiscibility of the water and 3-methyl-2,4-pentanedione, a basic solution of 1:1 (v/v) NH_4OH: H_2O was added. Once the base was added, a precipitate would almost always immediately form. After completion, the precipitate was isolated via vacuum filtration. All samples were then verified by mass spectrometry if the precipitate was found.

3.7.1 $Co(3Mac)_2$

The addition of 0.6212 g of the metal chloride ($CoCl_2$• 6 H_2O) and 0.608 mL of 3-methyl-2,4-pentanedione resulted in the solution turning pink in color. The addition of 20 mL of 1:1 (v/v) NH_4OH: H_2O resulted in the formation of a grey precipitate. The mixture was stirred for 1 hour on low heat, and the precipitate was isolated via vacuum filtration

resulting in a homogeneous powder. The product was allowed to dry and was re-crystallized overnight by evaporation from methanol in a desiccator.

3.7.2 Li(3Mac)

The addition of 0.2647 g of the metal chloride (LiCl) and 0.721 mL of 3-methyl-2,4-pentanedione resulted in the solution turning green in color. The addition of 20 mL of 1:1 (v/v) NH_4OH: H_2O did not result in the immediate formation of a precipitate. The mixture was stirred for 1 hour on low heat, but was unsuccessful due to lack of precipitate formation.

3.7.3 $Mg(3Mac)_2$

The addition of 0.3382 g of the metal chloride ($MgCl_2$• 6 H_2O) and 0.6910 mL of 3-methyl-2,4-pentanedione did not result in a color change of the solution. The addition of 20 mL of 1:1 (v/v) NH_4OH: H_2O did not result in the immediate formation of a precipitate. The mixture was stirred for 1 hour on low heat and allowed to sit overnight, but was unsuccessful due to lack of precipitate formation.

3.7.4 $Ca(3Mac)_2$

The addition of 0.3102 g of the metal chloride ($CaCl_2$) and 0.6504 mL of 3-methyl-2,4-pentanedione did not result in a color change of the solution. The addition of 20 mL of 1:1 (v/v) NH_4OH: H_2O did not result in the immediate formation of a precipitate. The mixture was stirred for 1 hour on low heat, but was unsuccessful due to lack of precipitate formation.

3.7.5 $Mn(3Mac)_2$

The addition of 0.3724 g of the metal chloride ($MnCl_2 \cdot H_2O$) and 0.6163 mL of 3-methyl-2,4-pentanedione resulted in the solution turning orange-brown in color. The addition of 20 mL of 1:1 (v/v) NH_4OH: H_2O resulted in the formation of a dark brown precipitate. The mixture was stirred for 1 hour on low heat, and the precipitate was isolated via vacuum filtration resulting in a homogeneous powder. The product was allowed to dry and was re-crystallized overnight by evaporation from methanol in a desiccator.

3.7.6 $Fe(3Mac)_3$

The addition of 0.7150 g of the metal chloride ($FeCl_3 \cdot 6\ H_2O$) and 0.6143 mL of 3-methyl-2,4-pentanedione resulted in the solution turning red in color. The addition of 20 mL of 1:1 (v/v) NH_4OH: H_2O resulted in the formation of a rust colored precipitate. The mixture was stirred for 1 hour on low heat, and the precipitate was isolated via vacuum filtration resulting in a homogeneous powder. The product was allowed to dry and was re-crystallized overnight by evaporation from methanol in a desiccator.

3.7.7 $Cu(3Mac)_2$

The addition of 0.3455 g of the metal chloride ($CuCl_2$) and 0.5981 mL of 3-methyl-2,4-pentanedione resulted in the solution turning light green in color. The addition of 20 mL of 1:1 (v/v) NH_4OH: H_2O did not result in the immediate formation of a precipitate. The mixture was stirred for 1 hour on low heat, but was unsuccessful due to lack of precipitate formation.

3.7.8 $Zn(3Mac)_2$

The addition of 0.3510 g of the metal chloride ($ZnCl_2$) and 0.5943 mL of 3-methyl-2,4-pentanedione did not result in the color change of the solution. The addition of 20 mL of 1:1 (v/v) NH_4OH: H_2O did not result in the immediate formation of a precipitate. The mixture was stirred for 1 hour on low heat, but was unsuccessful due to lack of precipitate formation.

3.7.9 $Pd(3Mac)_2$

The addition of 0.3973 g of the metal chloride ($PdCl_2$) and 0.521 mL of 3-methyl-2,4-pentanedione did not result in a color change of the solution. The addition of 20 mL of 1:1 (v/v) NH_4OH: H_2O did not result in the immediate formation of a precipitate, as the metal chloride did not immediately go into solution. The mixture was stirred for 1 hour on low heat, but was unsuccessful due to lack of precipitate formation.

3.7.10 $Cd(3Mac)_2$

The addition of 0.4035 g of the metal chloride ($CdCl_2$) and 0.651 mL of 3-methyl-2,4-pentanedione did not result in a color change of the solution. The addition of 20 mL of 1:1 (v/v) NH_4OH: H_2O resulted in the formation of a brown precipitate. The mixture was stirred for 1 hour on low heat, but was unsuccessful due to lack of precipitate formation.

3.7.11 $Al(3Mac)_3$

The addition of 0.4898 g of the metal chloride ($AlCl_3$• 6 H_2O) and 0.709 mL of 3-methyl-2,4-pentanedione to 100 mL of toluene did not result in the color change of the solution. The addition of 20 mL of 1:1 (v/v) NH_4OH: H_2O resulted in the formation of a brown precipitate. The mixture was stirred for 2 hours and a white precipitate had formed in the organic layer, which was separated and rotovapped. The product was then scraped and dissolved in methanol allowed to dry and was re-crystallized overnight by evaporation in a desiccator.

3.7.12 $Fe(3Mac)_2$

The addition of 0.5267 g of the metal chloride ($FeCl_2$) and 0.614 mL of 3-methyl-2,4-pentanedione resulted in the solution turning brown-orange in color. The addition of 20 mL of 1:1 (v/v) NH_4OH: H_2O resulted in the formation of a brown precipitate. The mixture was stirred for 1 hour on low heat, and the precipitate was isolated via vacuum filtration resulting in a homogeneous powder. The product was allowed to dry and was re-crystallized overnight by evaporation from methanol in a desiccator.

3.7.13 Ag(3Mac)

The addition of 0.4896 g of the metal chloride (AgCl) and 0.393 mL of 3-methyl-2,4-pentanedione did not result in the color change of the solution. The addition of 20 mL of 1:1 (v/v) NH_4OH: H_2O resulted in the formation of a white precipitate. The mixture was stirred for 1 hour on low heat, and the precipitate was isolated via vacuum filtration

resulting in a homogeneous powder. The product was allowed to dry and was re-crystallized overnight by evaporation from methanol in a desiccator.

3.7.14 $Ni(3Mac)_2$

The addition of 0.6227 g of the metal chloride ($FeCl_2$• 6 H_2O) and 0.608 mL of 3-methyl-2,4-pentanedione resulted in the solution turning blue in color. The addition of 20 mL of 1:1 (v/v) NH_4OH: H_2O did not result in the immediate formation of a precipitate. A precipitate did form after the mixture was stirred for 1 hour on low heat. The precipitate was isolated via vacuum filtration resulting in a homogeneous powder. The product was allowed to dry and was re-crystallized overnight by evaporation from methanol in a desiccator.

3.8 Metal 2,2,6,6-Tetramethyl-3,5-heptanedione [$M(tmeac)_2$]

The preparation of the samples were adapted from procedures by Hunter[1], Lerach[14] and Watson & Lin[21]. The metal chloride was dissolved in 100 mL of room temperature de-ionized H_2O, or in some cases toluene, and was stirred with a magnetic stir plate and a PTFE coated stir bar. Upon addition of the metal chloride to the H_2O, depending on the metal, one, two, or three molar equivalents of the corresponding ligand were added to the solution. Due to the immiscibility of the water and 2,2,6,6-tetramethyl-3,5-heptanedione, a basic solution of 1:1 (v/v) NH_4OH: H_2O was added. Once the base was added, a precipitate would almost always immediately form. After completion, the precipitate was isolated via vacuum filtration. All samples were then verified by mass spectrometry if the precipitate was found.

3.8.1 $Al(tmeac)_3$

The addition of 0.3145 g of the metal chloride ($AlCl_3$• 6 H_2O) and 0.8098 mL of 2,2,6,6-tetramethyl-3,5-heptanedione did not result in the color change of the solution. The addition of 20 mL of 1:1 (v/v) NH_4OH: H_2O did not result in the immediate formation of a precipitate. The mixture was stirred for 1 hour on low heat, but was unsuccessful due to lack of precipitate formation.

3.8.2 Ag(tmeac)

The addition of 0.3744 g of the metal chloride (AgCl) and 0.5357 mL of 2,2,6,6-tetramethyl-3,5-heptanedione did not result in the color change of the solution. The addition of 20 mL of 1:1 (v/v) NH_4OH: H_2O did not result in the immedaite formation of a precipitate. The mixture was stirred for 1 hour on low heat, but was unsuccessful due to lack of precipitate formation.

3.8.3 $Cd(tmeac)_2$

The addition of 0.2836 g of the metal chloride ($CdCl_2$) and 0.6509 mL of 2,2,6,6-tetramethyl-3,5-heptanedione did not result in the color change of the solution. The addition of 20 mL of 1:1 (v/v) NH_4OH: H_2O did not result in the immediate formation of a precipitate. A precipitate did form after the mixture was stirred for 1 hour on low heat. The precipitate was isolated via vacuum filtration resulting in a homogeneous powder. The product was allowed to dry and was re-crystallized overnight by evaporation from methanol in a desiccator.

3.9 Instrumentation and Mass Spectrometric Parameter

The mass spectrometer technique that was implemented when gathering the spectra for each of the different complexes was positive ion electron ionization. These spectra were obtained using a Finnigan MAT TSQ/SSQ 7000 triple quadrupole mass spectrometer. Under this technique, the samples were introduced by a direct insertion probe containing a Re filament. The spectrum generated had a mass range from *m/z* 50 to *m/z* 650, but no significant data was collected beyond *m/z* 530. Source pressures were maintained at 10^{-6} torr with the source temperature held at 160 ˚ C and a manifold temperature maintained at 80˚ C. Normal trials were run for 10 minutes with a heating ramp starting 150 mA and ending around 950 mA. Depending on the ligand used, sublimation and co-sublimation would occur at different points in each trial, so a 10 minute trial was found to be sufficient. All samples were synthesized as described in sections 3.1.2-3.1.8 and the M(hfac) samples were obtained from Sigma-Aldrich without any further examination.

A 1.0 μL sample of 0.0250 M solution of the complex was initially added to a custom made, two filament loop and was set to dry before being inserted into the ionization chamber. During co-sublimation, the two filament loop was also implemented with one sample being placed on one loop and the second sample being placed on the opposite loop, 2 mm away. The reason for the double loop was so that no reaction would take place between the two samples before entering the ionization chamber. However, the separation of the two samples was unnecessary and would essentially match the results when using a single loop filament. The gas phase ligand exchange results dominate the

mass spectra in each experiment and any non-gas phase process was minimal, if at all, present.

Furthermore, the co-sublimation reactions were also explored in the collision cell by first selecting a particular ion and reacting it with a neutral target. These reactions were examined to help determine the role of which compound forms the mixed ligand and which is the neutral compound, i.e. determining the mechanism of formation. Again, a 1.0 μL sample was placed on the insertion probe and then into the ionization chamber and a neutral gas was released into the collision cell to react with the ionized substance. A specific mass was selected in the first quadrupole to pass through into the collision cell and react. Masses were selected based on the loss of different groups throughout the ionization process, i.e. fluorine migration, loss of a *tBu* group, etc. During this process, the mixed ligands were in fact observed in the collision cell.

Chapter 4

Investigations of Mass Selected Reactions Involving Cadmium Trifluorotrimethylacetylacetonate and Nickel β-Diketonate Complexes

4.1 Introduction

Transition metal β-diketonate complexes have recently acquired some added interest, especially experiments conducted in the gas phase. A reason for this spike in attention is due to the variety of available metal and ligand combinations and their overall stability. In addition to metal β-diketonate complexes being very stable, it should be noted that their seemingly inherent catalytic properties, relating to both carbon nanotubes and metallic films, make these complexes sought after. Furthermore, due to the ease in which these complexes can be prepared, many different substituents can be incorporated leading to the formation of several novel metal β-diketonate complexes.

This Chapter presents for the first time the 70 EI mass spectra of $Cd(tftm)_2$ as well as the mixed ligand species following the co-sublimation of cadmium trifluorotrimethylacetylacetonate ($Cd(tftm)_2$) with three nickel β-diketonate complexes. This Chapter also examines the stability of species consisting of 1,1,1-trifluoro-5,5-dimethyl-2,4 hexanedione, 3,5-heptanedione, and 1,1,1-trifluoro-2,4-pentanedione bound with cadmium and nickel.

When examining the resulting mass spectra, the natural abundances of the metal center plays a helpful role in identifying which particular peak contains the metal.

Cadmium metal has eight isotopic masses, with the highest abundance, 28.7%, being the mass at 114 amu. The seven remaining isotopes are listed in order of increasing mass: 106, 108, 110, 111, 112, 113, and 116 amu. These masses are found in an abundance of 1.25%, 0.89%, 12.49%, 12.80%, 24.13%, 12.22%, and 7.49%, respectively. From these natural abundances, an isotopic pattern in Figure 4.1 is readily observed within the spectra.

The results presented in this Chapter help further the understanding of the gas phase ligand exchange between complexes consisting of different metals and ligands. Ligand exchange products formed via select ion-neutral ligand reactions within the collision cell of a triple quadrupole mass spectrometer are also reported for the first time for this class of complexes.

4.2 $Cd(tftm)_2$

Several mass spectra have been collected in the positive EI mode and will be presented in this Chapter along with an accompanying Table describing the relative ion intensities for all complexes observed. The fragmentation patterns that some of these complexes undergo are consistent with literature[22,23,24]. Figure 4.1 is the positive EI mass spectrum of $Cd(tftm)_2$ with the resulting ion intensities listed in Table 4.1. Experiments presented in this Chapter, and again in Chapter 5, will consist of co-sublimation reactions involving $Cd(tftm)_2$ with other β-diketonate complexes. Attempts will also be made to determine the reaction pathway in the formation of the mixed ligand complex.

The molecular ion $[Cd(tftm)_2]^+$ appearing at m/z = 504 is present in Figure 4.1. With this particular sample, however, there are traces of sodium within the sample, which results in the addition of +23 to the ion, totaling the m/z to 527. This trace of sodium has

also been documented using the scanning electron microscope (SEM) with additional SEM data presented in the Appendix. The sodium contamination is not existent in any of the other ions present, including the fragmented species of interest, and is likely an artifact of synthesis. A loss of a tertiary butyl group, *t*Bu at *m/z* = 57 amu, is the first fragmentation of the complex at *m/z* = 447. This fragment is often the most intense in the spectrum, resulting in it being the base peak as well. At the peak of *m/z* = 309, the complete loss of what amounts to one intact tftm ligand is observed, followed by a loss of a second *t*Bu group at *m/z* = 252. There is no loss of a CF_3 group nor any evidence of fluorine migration, which is the loss of CF_2, when the metal center is bound by one ligand, as was the case in Hunter's findings[23] using a different metal center.

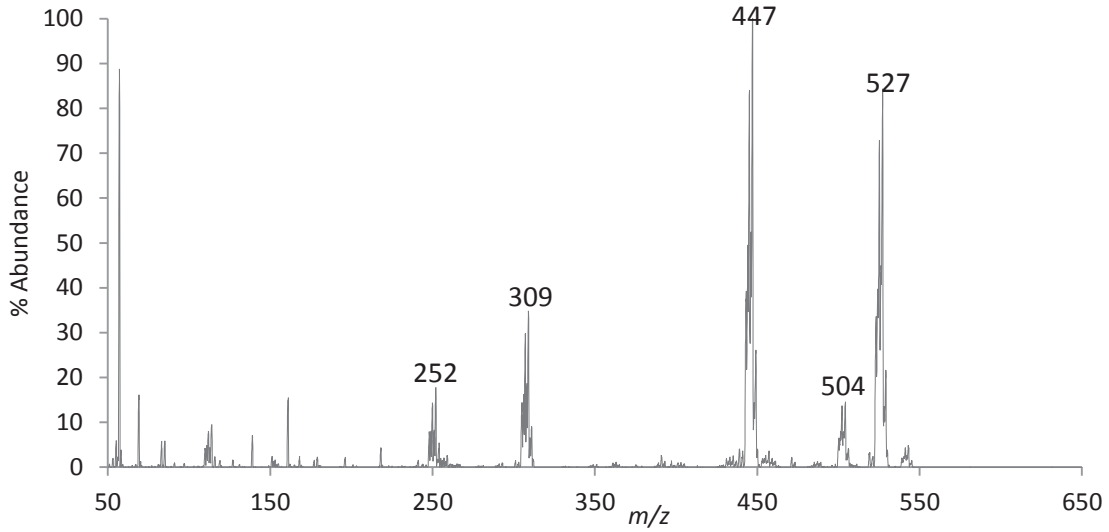

Figure 4.1: The 70 eV positive EI mass spectra for $Cd(tftm)_2$. Masses labeled represent the molecular ion and typical fragments of their respective parent compounds.

m/z	Species	Rel. Ab.
504	$[Cd(tftm)_2]^+$	15
447	$[Cd(tftm\text{-}t\text{Bu})(tftm)]^+$	100*
390	$[Cd(tftm\text{-}t\text{Bu})(tftm\text{-}t\text{Bu})]^+$	1*
309	$[Cd(tftm)]^+$	35*
252	$[Cd(tftm\text{-}t\text{Bu})]^+$	18*

Table 4.1: Relative positive ion intensities of single metal species to their respective base peaks as presented in Figure 4.1. Isobaric ion intensities indicated by *.

As seen in Table 4.1, the loss of a tertiary butyl group, *t*Bu, is common in the trifluorotrimethylacetylacetonate ligand, and can be observed at *m/z* = 447. It is here that the loss of the *t*Bu is represented as the base peak in the spectrum. The loss of a second *t*Bu group can be observed at *m/z* = 390, as well as the loss of an intact (tftm) ligand at *m/z* = 309. The same type of fragmentation occurs within the molecule even with one ligand present; where the loss of the remaining *t*Bu group followed by the second can be seen at *m/z* = 252.

The possible chemical pathways that lead to the formation of the observed ions that can occur during co-sublimation involving $[Cd(tftm)_2]^+$ ions are presented in Equations 4.1 - 4.5.

$$[Cd(tftm)_2]^+ + M(acac)(acac) \rightarrow [Cd(acac)(acac)]^+ + M(tftm)(tftm)_2 \quad (4.1)$$

$$[Cd(tftm)_2]^+ + M(acac)(acac) \rightarrow [Cd(tftm)(acac)]^+ + M(tftm)(acac) \quad (4.2)$$

$$[Cd(tftm)(tftm\text{-}t\text{Bu})]^+ + M(acac)(acac) \rightarrow [Cd(tftm\text{-}t\text{Bu})(acac)]^+ + M(tftm)(acac) \quad (4.3)$$

$$[Cd(tftm)]^+ + M(acac)(acac) \rightarrow [Cd(acac)]^+ + M(tftm)(acac) \quad (4.4)$$

$$[Cd(tftm\text{-}t\text{Bu})]^+ + M(acac)(acac) \rightarrow [Cd(acac)]^+ + M(tftm\text{-}t\text{Bu})(acac) \quad (4.5)$$

While a complete exchange occurring during co-sublimation reactions is a desirable outcome, the observation of a mixed ligand or even a partial exchange is encouraging when looking to establish legitimacy of the reaction. The co-sublimation experiments that will appear later in this Chapter show evidence of ligand exchange as well as fragmentation thereof.

4.3 $Ni(acac)_2$

Figure 4.2 is the positive EI mass spectrum of $Ni(acac)_2$. This complex has been presented elsewhere[23], but as an overview, the fragmentation pattern will be discussed with the relative ion intensities presented in Table 4.2. The $[Ni(acac)_2]^+$ molecular ion peak can be observed at *m/z* = 256. The loss of a methyl group is recorded at *m/z* = 241, and is a very common fragmentation route for this complex. In the loss of an intact *acac* ligand a peak is observed at *m/z* = 157 and again, the loss of a methyl group can be seen in the spectrum at *m/z* = 142.

4.4 $Ni(eeac)_2$

Figure 4.3 is the positive EI mass spectrum of $Ni(eeac)_2$ and is presented for the first time with the relative ion intensities listed in Table 4.3. The $[Ni(eeac)_2]^+$ molecular ion is present given the ion signal at *m/z* = 312. Similar to the loss of the *t*Bu groups in the trifluorotrimethylacetylacetonate complexes, the loss of an ethyl group at *m/z* = 283, is a very common fragmentation route for this ligand. In the loss of an intact *eeac* ligand, the resulting ion peak is observed at *m/z* = 185, followed by the loss of an ethyl group can at *m/z* = 156.

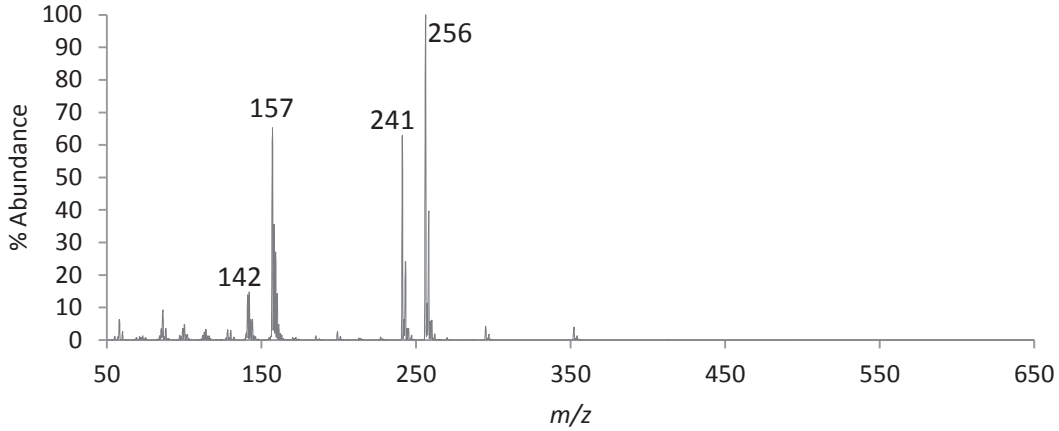

Figure 4.2: The 70 eV positive EI mass spectra for $Ni(acac)_2$. Masses labeled represent the molecular ion and typical fragments of their respective parent compounds.

m/z	Species	Rel. Ab.
256	$[Ni(acac)_2]^+$	100
241	$[Ni(acac)_2\text{-}CH_3]^+$	63
226	$[Ni(acac\text{-}CH_3)(acac\text{-}CH_3)]^+$	<1
157	$[Ni(acac)]^+$	65
142	$[Ni(acac\text{-}CH_3)]^+$	15

Table 4.2: Relative positive ion intensities of single metal species to their respective base peaks as presented in Figure 4.2. Isobaric ion intensities indicated by *.

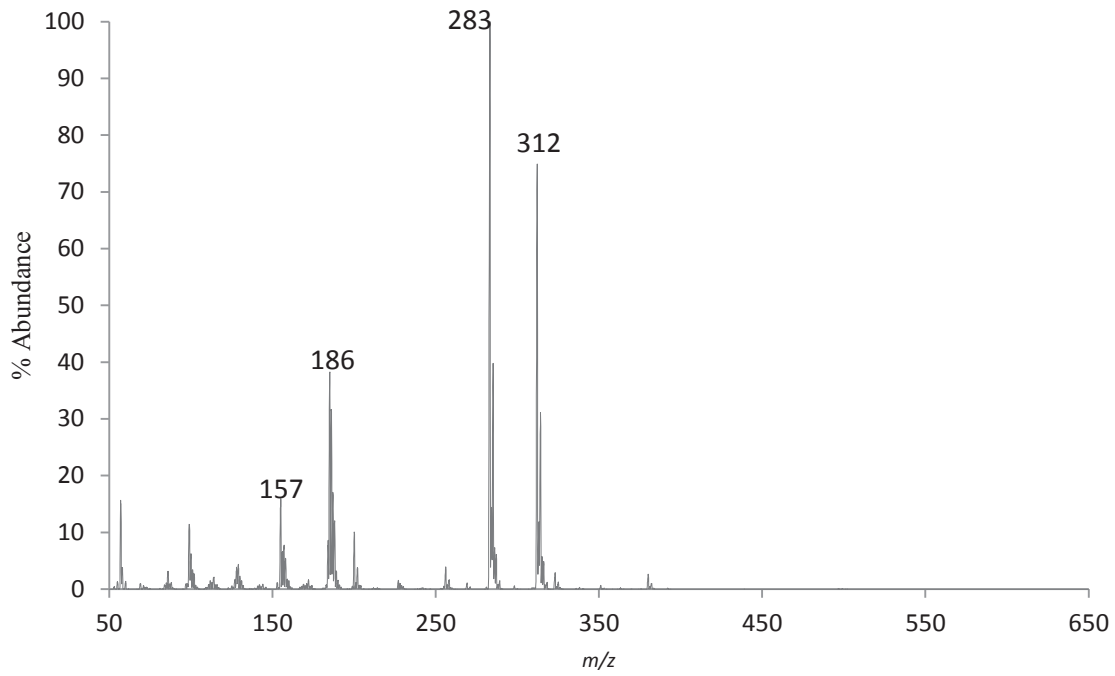

Figure 4.3: The 70 eV positive EI mass spectra for $Ni(eeac)_2$. Masses labeled represent the molecular ion and typical fragments of their respective parent compounds.

m/z	Species	Rel. Ab.
312	$[Ni(eeac)_2]^+$	75
283	$[Ni(eeac\text{-}Et)(eeac)]^+$	100
254	$[Ni(eeac\text{-}Et)(eeac)]^+$	<1*
186	$[Ni(eeac)]^+$	38
157	$[Ni(eeac\text{-}Et)]^+$	7
127	$[Ni(eeac\text{-}2Et)]^+$	2

Table 4.3: Relative positive ion intensities of single metal species to their respective base peaks as presented in Figure 4.3. Isobaric ion intensities indicated by *.

4.5 $Ni(tfac)_2$

Figure 4.4 is the positive EI mass spectrum of $Ni(tfac)_2$ and is presented for the first time. Relative ion intensities are listed in Table 4.4 where the molecular ion peak can be observed at *m/z* = 364. As is common with the ligands having a terminal alkyl chain, the methyl group is lost as a fragment and the resulting ion is observed at *m/z* = 349. Similar to that of the hexafluoroacetylacetonate ligand, where both (CF_3) groups are lost

creating a stable fragment, the same loss channel occurs with the *tfac* ligand, with the loss of the lone (CF_3) group at *m/z* = 295. The loss of the ligand was observed at *m/z* = 211, while the fluorine migration peak was present at *m/z* = 161.

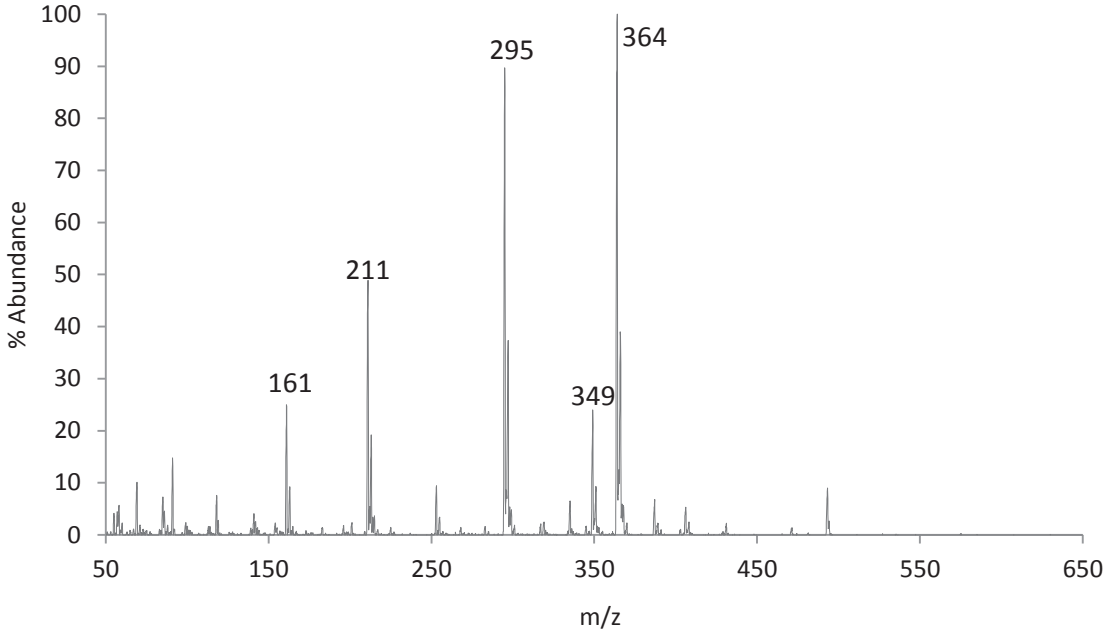

Figure 4.4: The 70 eV positive EI mass spectra for $Ni(tfac)_2$. Masses labeled represent the molecular ion and typical fragments of their respective parent compounds.

m/z	Species	Rel. Ab.
364	$[Ni(tfac)_2]^+$	100
349	$[Ni(tfac\text{-}CH_3)]^+$	21
295	$[Ni(tfac\text{-}CF_3)]^+$	90
211	$[Ni(tfac)]^+$	49
196	$[Ni(tfac\text{-}CH_3)]^+$	2
151	$[Ni(tfac\text{-}CF_2)]^+$	<1

Table 4.4: Relative positive ion intensities of single metal species to their respective base peaks as presented in Figure 4.4. Isobaric ion intensities indicated by *.

4.6 Co-Sublimation of $Cd(tftm)_2$ and $Ni(acac)_2$

In addition to reproducing both Figures 4.1 and 4.2 in Figures 4.5a and 4.5b, respectively, which conveniently serve as reference spectra for the comparison of the hetero-metal gas-phase reactions, Figures 4.5c includes the co-sublimation of $Ni(acac)_2$ and $Cd(tftm)_2$. The relative abundances in Figure 4.5a and 4.5b were presented in Tables 4.1 - 4.2. Similarly, Table 4.5 contains the relative ion abundances for Figure 4.5c. In using the data presented in each of the Tables, one can conclude that an actual ligand exchange did occur given the appreciable ion signal occurring at the appropriate mass corresponding to the expected ligand exchange product.

In addition to the ligand exchange species now being present, several fragmented species are present as well in Figure 4.5c. Any partial or complete exchanges that may have taken place are highlighted in bold within the co-sublimation mass spectra. Upon further inspection of Figure 4.5c, not only did the mixed ligand complex in fact form at m/z = 352, but this species was also in the highest abundance. The loss of a *t*Bu group from the mixed ligand, *m/z* = 295, was also in high abundance. In discussing these partial exchanges, we will see that the loss of the tertiary butyl group is a common component among possible mechanism pathways.

It should be noted that when the samples were placed on the inlet probe in a methanol solution, the two samples were placed on the probe at the same time, using a single loop and a double loop. Upon further review, it was determined that there was little difference in the outcome of the reaction if a double loop was used, where each sample was placed on its respective loop, and when samples were placed together on the same loop.

When determining which species are more likely to be ions during the co-sublimation experiments, it is important to consider which species sublimes first. Given the increased volatility of the more fluorinated derivative, that species will appear first in the spectrum and when the second species sublimes, it is only then possible for the mixed complex to form. When looking at the equations that describe the mixed ligand formation, the mass-selected experiments can be used to support particular mechanistic pathways.

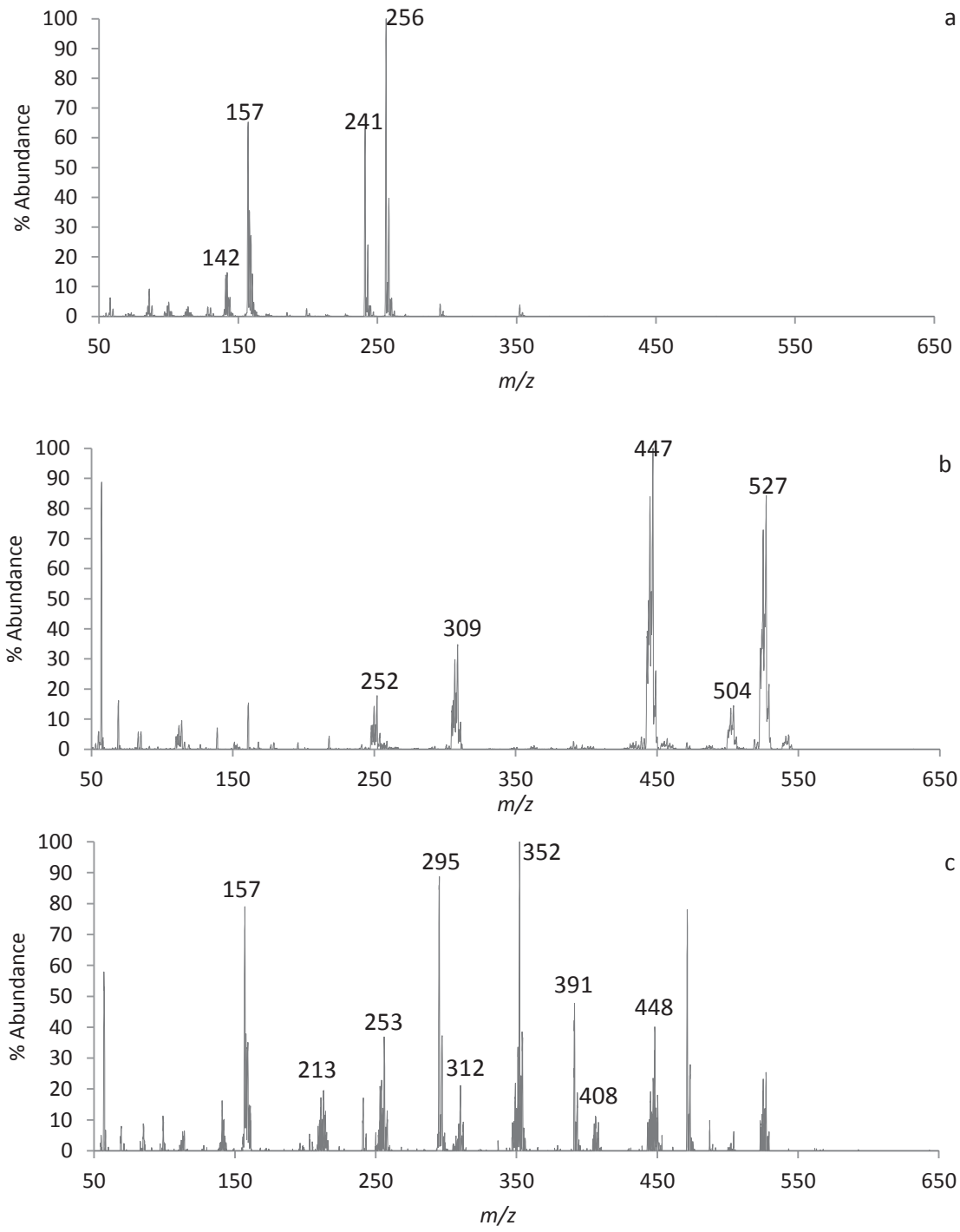

Figure 4.5: The 70eV positive EI mass spectra of (a) $Ni(acac)_2$, (b) $Cd(tftm)_2$, and (c) the co-sublimation of $Ni(acac)_2$ and $Cd(tftm)_2$. Masses labeled in (a) and (b) represent the molecular ion and typical fragments of their respective parent compounds. Masses labeled in (c) correspond to the intact ligand gas phase product and fragments thereof.

m/z	Species	Rel. Ab.	m/z	Species	Rel. Ab.
504	$[Cd(tftm)_2]^+$	15	256	$[Ni(acac)_2]^+$	100
447*	$[Cd(tftm\text{-}t\text{Bu})(tftm)]^+$	100	241	$[Ni(acac\text{-}CH_3)(acac)]^+$	63
390*	$[Cd(tftm\text{-}t\text{Bu})(tftm\text{-}t\text{Bu})]^+$	1	226	$[Ni(acac\text{-}CH_3)(acac\text{-}CH_3)]^+$	<1
309*	$[Cd(tftm)]^+$	35	157	$[Ni(acac)]^+$	65
252*	$[Cd(tftm\text{-}t\text{Bu})]^+$	18	142	$[Ni(acac\text{-}CH_3)]^+$	15
312	$[Cd(acac)_2]^+$	8	448*	$[Ni(tftm)_2]^+$	40
408	$[Cd(tftm)(acac)]^+$	9	352*	$[Ni(tftm)(acac)]^+$	100
351*	$[Cd(tftm\text{-}t\text{Bu})(acac)]^+$	34	295*	$[Ni(tftm\text{-}t\text{Bu})(acac)]^+$	89
213	$[Cd(acac)]^+$	20	391*	$[Ni(tftm\text{-}t\text{Bu})(tftm)]^+$	48
			253*	$[Ni(tftm)]^+$	21

Table 4.5: Relative ion intensities of hetero-metal species to their respective base peaks as presented in Figure 4.5. Isobaric ion intensities indicated by *.

4.7 Selected Reaction of $[Cd(tftm)_2]^+$, $[Cd(tftm)(tftm\text{-}t\text{Bu})]^+$, and $[Cd(tftm)]^+$ with $Ni(acac)_2$

Presented in Figure 4.6 is the mass-selected spectra of $[Cd(tftm)(tftm)]^+$ and fragments following a reaction with neutral $Ni(acac)_2$ within the collision cell of the triple quadrupole mass spectrometer. The parent peak was selected by only allowing one mass to pass through Quadrant 1, while all remaining ion masses were filtered out. From here, the selected mass would then interact with the neutral species that was introduced into the collision cell. This is a useful process because it assists in determining which particular ion is a major contributor in the formation of the mixed ligand during the co-sublimation experiments. All spectra were collected in cation mode with an *m/z* = 504, 447, and 309 corresponding to the mass selected species of interest. After each particular ion was introduced to the collision cell containing $Ni(acac)_2$ species, product masses were then scanned in Quadrant 3, producing a full spectrum. It is with these respective spectra that the mechanism of the metal-ligand exchange can be investigated.

In comparing the relative ion intensities with those of the single metal and hetero-metal experiments presented in Figure 4.5, the data is clear in identifying which ions correspond to the newly formed compounds. Under normal collision cell conditions, it is more conducive for the samples to be broken apart, or fragmented, to determine structural composition of the intended molecule. However, in this case the collision cell is used for preferentially selecting masses that would give better insight into determining just how the mixed ligand species would form and whether the selected ion is potentially an active participant in the source during co-sublimation. The relative intensities of the co-sublimation samples, as well as the presence of the mixed ligand species upon the mass selection of particular ions are essential in identifying possible reaction pathways.

The spectra presented in Figure 4.6 corresponds to mass-selected $[Cd(tftm)(tftm)]^+$ reacting with $Ni(acac)_2$ within the collision cell at different times on the chromatogram throughout the same sample trial. The times selected were arbitrary in nature, and were merely selected on whether or not they were germane to the reaction. While the majority of the resulting ions in Figure 4.6 are fragments of the selected ion, one peak in particular is quite interesting in that it corresponds to a complete exchange in the formation of $[Cd(acac)_2]^+$ at m/z = 312. Equation 4.6 is a possible reaction pathway supporting the formation of this ion. This does not preclude other possible reactions; no reactions were prevalent when the intact molecular ion was mass-selected during the selective reaction experiments.

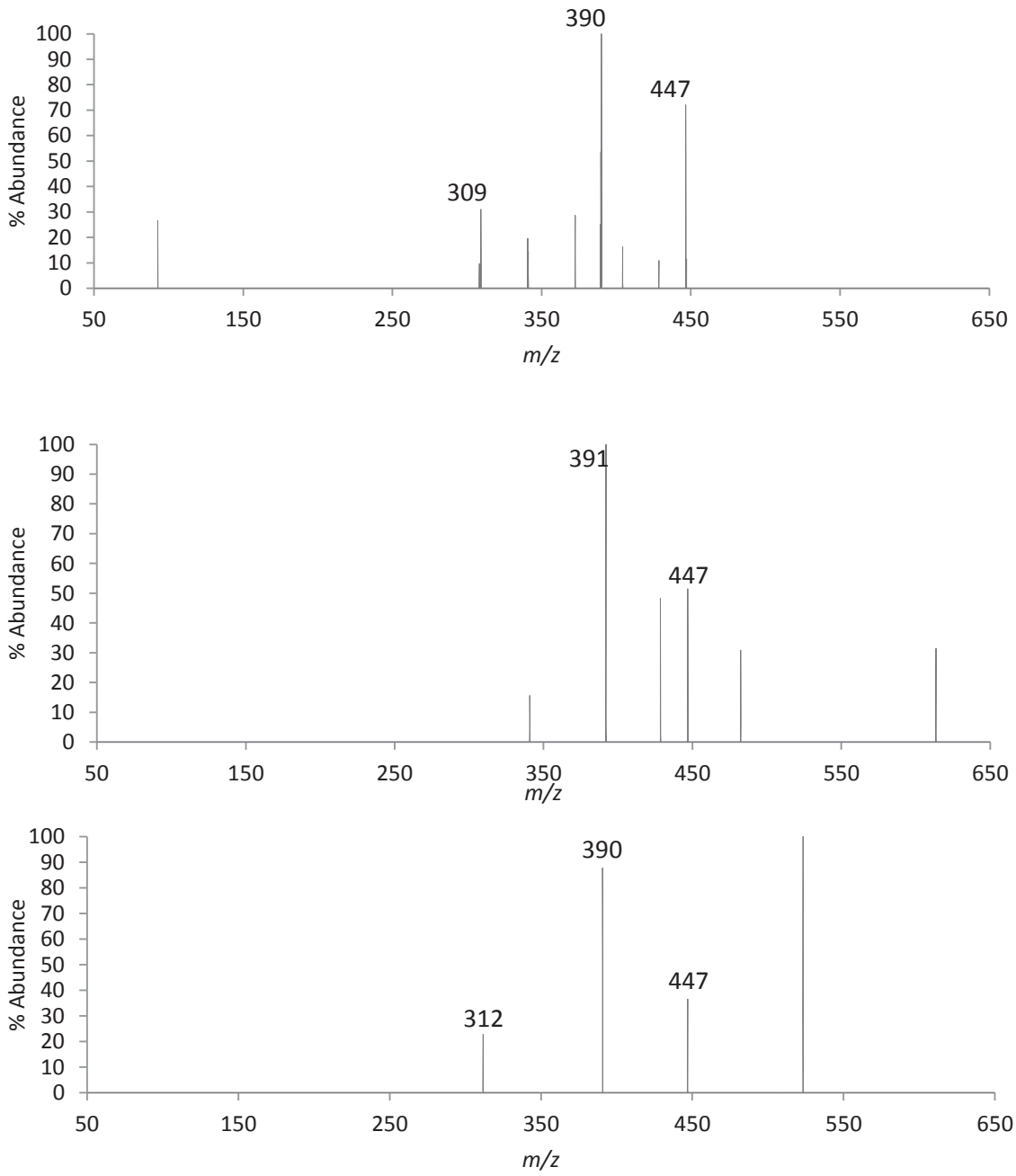

Figure 4.6: The positive EI mass selected spectrum of $[Cd(tftm)(tftm)]^+$ and neutral $Ni(acac)_2$ at the mass of 504 in the collision cell at different times in the chromatogram.

$$[Cd(tftm)(tftm)]^+ + Ni(acac)_2 \rightarrow [Cd(acac)(acac)]^+ + Ni(tftm)(tftm) \quad (4.6)$$

The data presented in Figure 4.7 is the resulting mass spectra following the mass selection of $[Cd(tftm)(tftm\text{-}t\text{Bu})]^+$ at *m/z* = 447, and the specific reaction with a neutral $Ni(acac)_2$ target within the collision cell. Interestingly, the peak at *m/z* = 353 in the top spectra of Figure 4.7 is similar to the expected mass of the nickel mixed ligand, i.e. $[Ni(tftm)(acac)]^+$. This value is one more mass unit than is expected, but without isotopic patterns for additional evidence, an absolute confirmation is not available. Nonetheless, an ion at m/z = 351 would also be of interest given that it would correspond to a known stable fragment of the cadmium mixed ligand. The middle spectrum also contains an ion with a *m/z* = 407 which falls within the isotope range of $[Cd(tftm)(acac)]^+$. Equations 4.7 - 4.9 illustrate possible mechanisms leading to the formation of the aforementioned ions of interest.

$$[Cd(tftm)(tftm\text{-}t\text{Bu})]^+ + Ni(acac)_2 \rightarrow [Ni(tftm)(acac)]^+ + Cd(tftm\text{-}t\text{Bu})(acac) \quad (4.7)$$

$$[Cd(tftm)(tftm\text{-}t\text{Bu})]^+ + Ni(acac)_2 \rightarrow [Cd(tftm\text{-}t\text{Bu})(acac)]^+ + Ni(tftm\text{-}t\text{Bu})(acac) \quad (4.8)$$

$$[Cd(tftm)(tftm\text{-}t\text{Bu})]^+ + Ni(acac)_2 \rightarrow [Cd(tftm)(acac)]^+ + Ni(tftm)(acac) \quad (4.9)$$

The bottom spectrum presented in Figure 4.7 has an interesting peak at *m/z* = 449 which may describe the complete exchange and the formation of $[Ni(tftm)_2]^+$. With a quick comparison with Figure 4.5c, and noting the presence of several peaks around m/z = 449, the reaction presented in Equation 4.10 may in fact be an active pathway.

$$[Cd(tftm)(tftm\text{-}t\text{Bu})]^+ + Ni(acac)_2 + t\text{Bu} \rightarrow [Ni(tftm)(tftm)]^+ + Cd(acac)(acac) \quad (4.10)$$

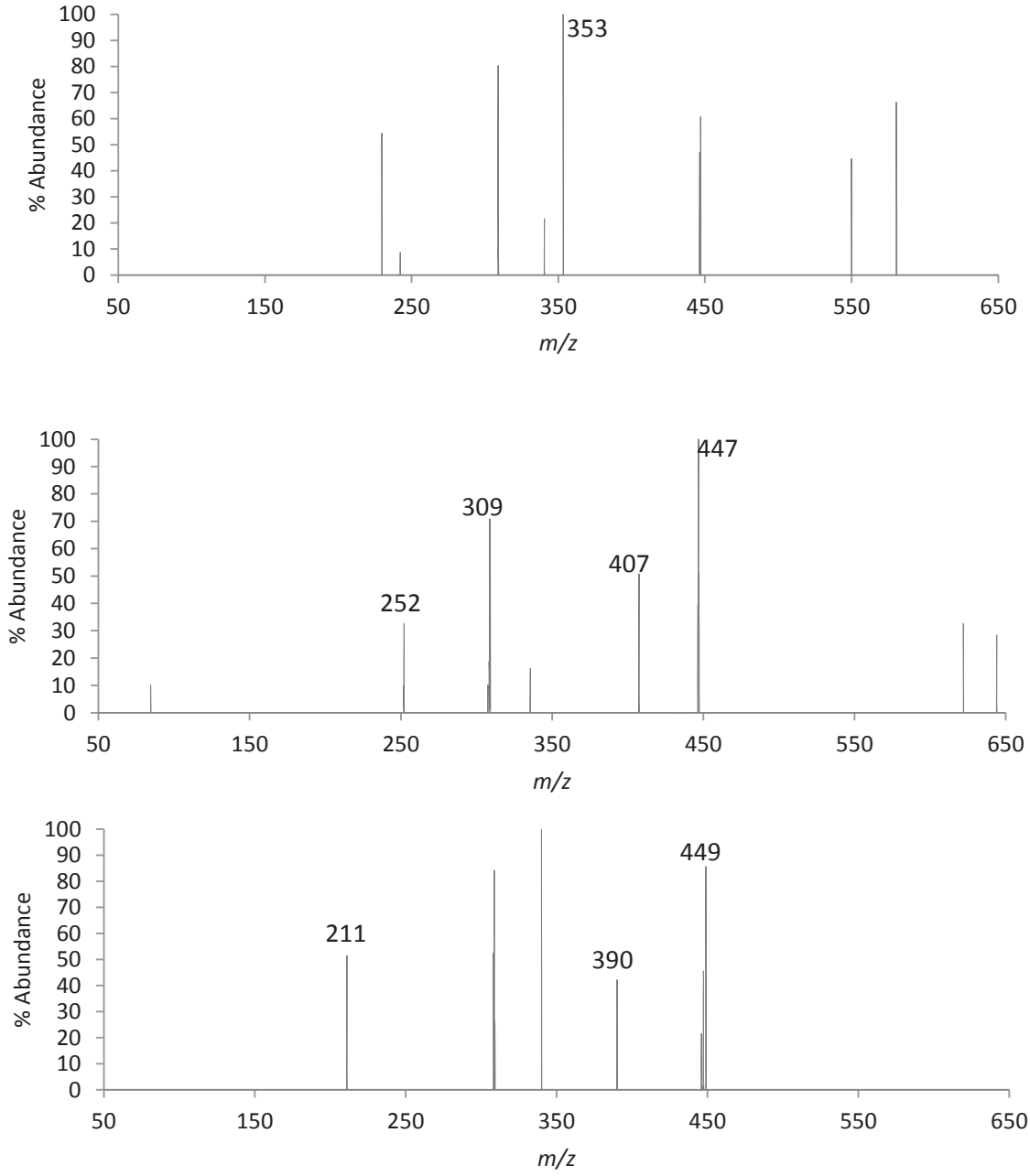

Figure 4.7: The positive EI mass selected spectrum of $[Cd(tftm)(tftm\text{-}t\text{Bu})]^+$ and neutral $Ni(acac)_2$ at the mass of 447 in the collision cell.

Another cadmium-containing fragment that was mass-selected and reacted with neutral $Ni(acac)_2$ was $[Cd(tftm)]^+$ at m/z = 309. As presented in Figure 4.8, there were a few peaks of particular interest and include the mixed ligand species $[Cd(tftm)(acac)]^+$ at m/z = 408 and the partial exchange species $[Ni(tftm)]^+$ at m/z = 253.

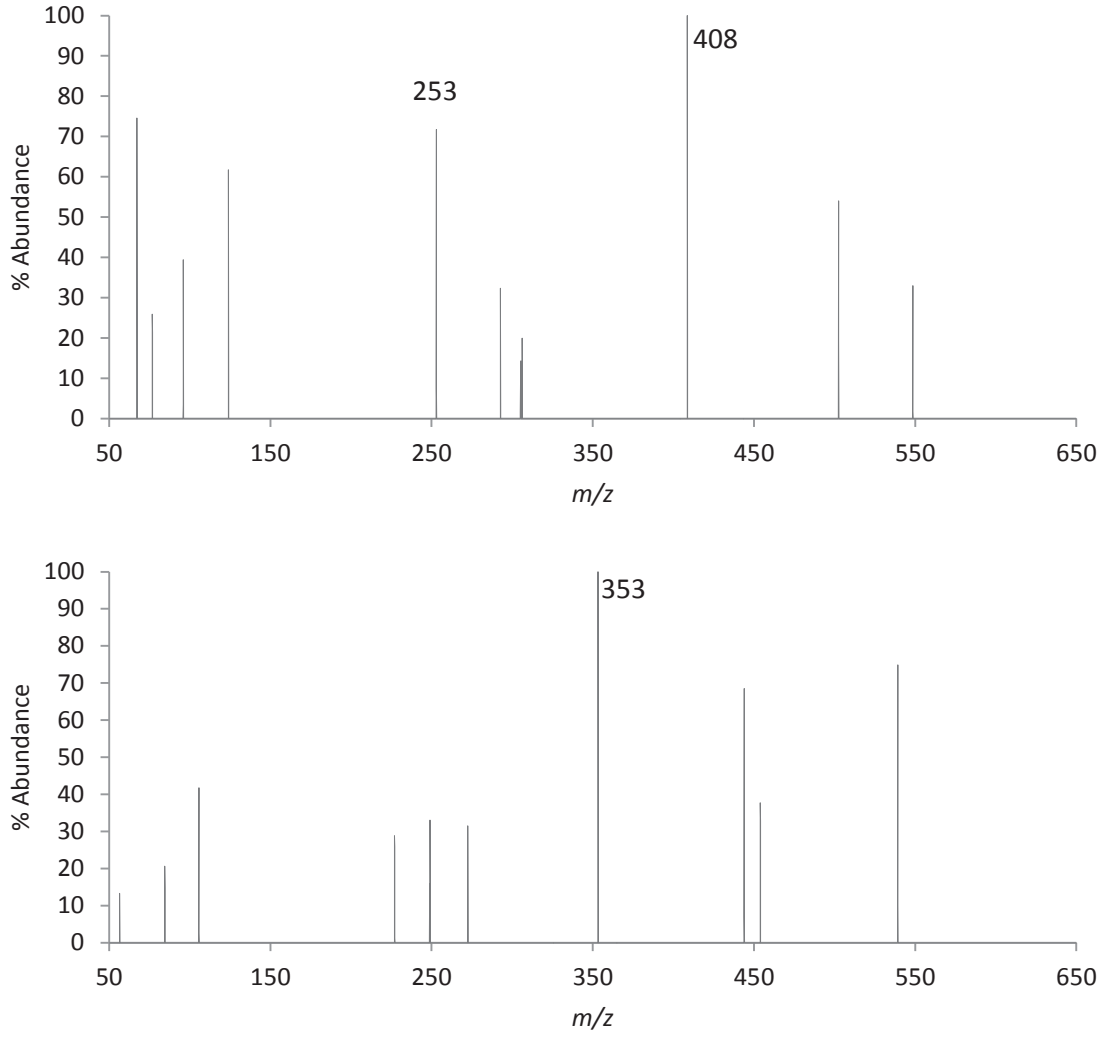

Figure 4.8: The positive EI mass selected spectrum of $[Cd(tftm)]^+$ and neutral $Ni(acac)_2$ at the mass of 309 in the collision cell.

Detecting the $[Cd(tftm)(acac)]^+$ complex after the selective reaction is a good indication that the selected mass is one that should be considered further during the formation of the mixed ligand. Having both the mixed ligand of one complex, and the partial exchange of another in the same spectrum as well as evidence for $[Ni(tftm)(acac)]^+$ at *m/z* = 352, which is isobaric with $[Cd(acac)(tftm\text{-}t\text{Bu})]^+$ at *m/z* = 351, is very encouraging when determining which selected masses are useful. Presented in Equations 4.11 - 4.13 are possible reaction pathways describing the results presented in Figure 4.8.

$$[Cd(tftm)]^+ + Ni(acac)_2 \rightarrow [Cd(tftm)(acac)]^+ + Ni(acac) \quad (4.11)$$

$$[Cd(tftm)]^+ + Ni(acac)_2 \rightarrow [Ni(tftm)]^+ + Cd(tftm)(acac) \quad (4.12)$$

$$[Cd(tftm)]^+ + Ni(acac)_2 \rightarrow [Ni(acac)(tftm)]^+ + Cd(acac) \quad (4.13)$$

.

4.8 Co-sublimation of $Cd(tftm)_2$ and $Ni(eeac)_2$

In attempt to establish how reactive $Cd(tftm)_2$ is in the gas phase, co-sublimation reactions with $Ni(eeac)_2$ were performed. Similar to the setup of the previous section, the individual spectra are first reproduced from earlier Figures with the co-sublimation results stacked vertically for comparison purposes. Presented in Figure 4.9a is the mass spectrum of $Ni(eeac)_2$ and is reproduced from Figure 4.3 and clearly shows the $[Ni(eeac)_2]^+$ molecular ion is present given the ion signal at *m/z* = 312. A very common fragmentation route for this ligand is the loss of an ethyl group at *m/z* = 283. In the loss of an intact (eeac) ligand, the resulting ion peak is observed at *m/z* = 186, followed by the loss of an ethyl group at *m/z* = 157. The mass peaks present in Figure 4.9b, which corresponds to the $Cd(tftm)_2$ sublimation, are reproduced from Figure 4.1 and also correspond to the four peaks that are mass-selected for the collision cell reactions. The parent peak at *m/z* = 504 followed by the loss of a *t*Bu group, resulting in the peak at *m/z* = 447, are both present in the spectrum. The ion $[Cd(tftm)]^+$ is observed at *m/z* = 309, while the subsequent loss of a *t*Bu from the single intact ligand is present at *m/z* = 252. Figure 4.9c includes the co-sublimation of $Cd(tftm)_2$ and $Ni(eeac)_2$ and is vertically stacked for ease of comparison with the corresponding relative intensities presented in Table 4.6.

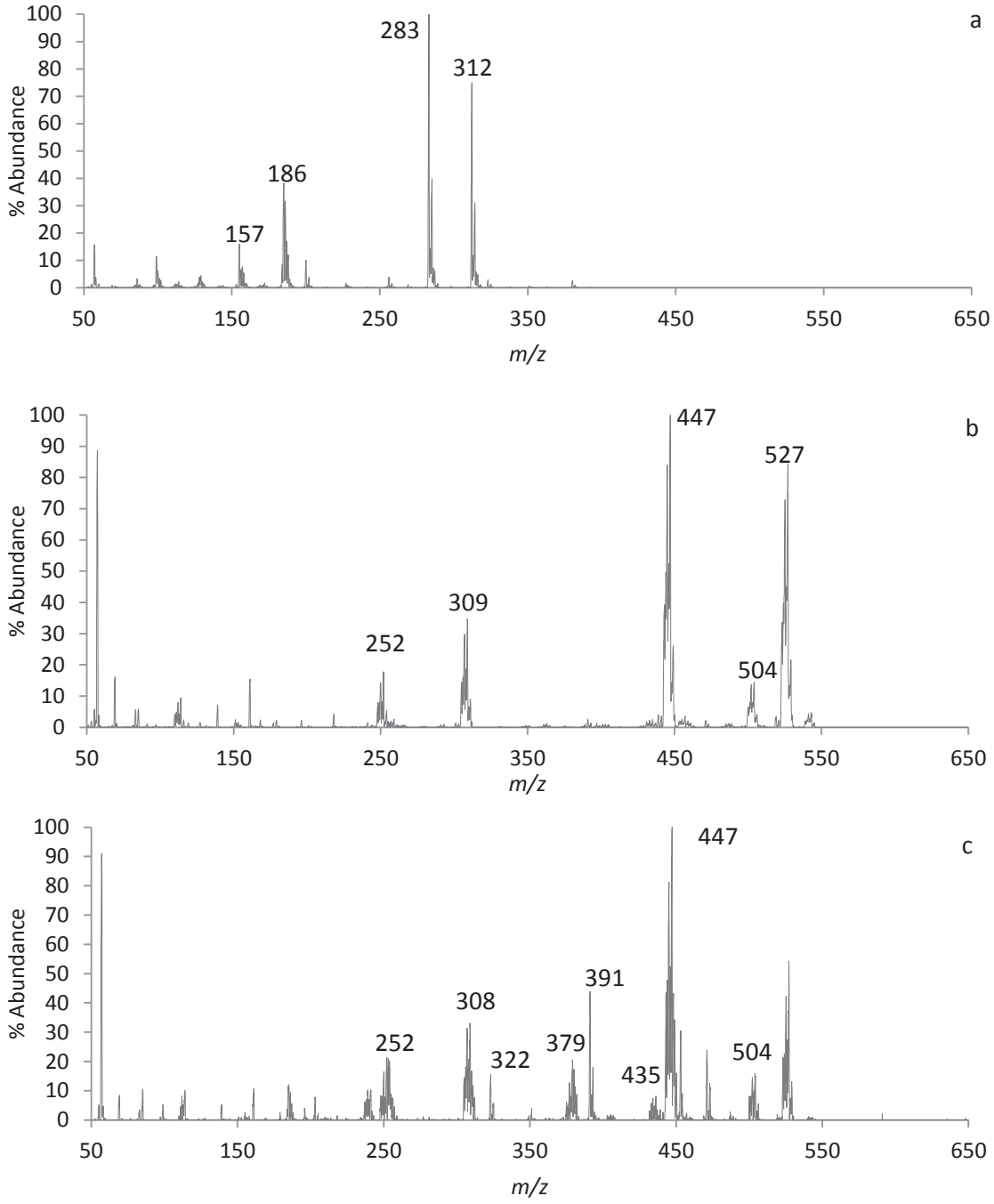

Figure 4.9: The positive EI mass spectra of (a) $Ni(eeac)_2$, (b) $Cd(tftm)_2$, and (c) the co-sublimation of $Ni(eeac)_2$ and $Cd(tftm)_2$. Masses labeled in (a) and (b) represent the molecular ion and typical fragments of their respective parent compounds. Masses labeled in (c) correspond to the intact ligand gas phase product and fragments thereof.

In examining Figure 4.9c, the ligand exchange involving the formation of $[Ni(tftm)(eeac)]^+$ at *m/z* = 379 was observed as was the formation of $[Cd(eeac\text{-}Et)(eeac\text{-}Et)]^+$ at *m/z* = 308. Interestingly, *m/z* = 391 corresponds to the loss of a *t*Bu group from the nearly complete exchange product involving nickel, i.e. $[Ni(tftm)(tftm\text{-}tBu)]^+$. The intensities are obtained from the single-metal sublimations, as well as the co-sublimations of the two samples placed into the reaction chamber on the same probe. What adds to the difficulty of describing such a process is the multitude of isobaric masses, in which one or more ions share the same *m/z*, during the co-sublimation reaction.

m/z	Species	Rel. Ab	m/z	Species	Rel. Ab
504	$[Cd(tftm)_2]^+$	16	312	$[Ni(eeac)_2]^+$	8
447*	$[Cd(tftm\text{-}tBu)(tftm)]^+$	100	283	$[Ni(eeac\text{-}Et)(eeac)]^+$	<1
390*	$[Cd(tftm\text{-}tBu)(tftm\text{-}tBu)]^+$	4	186	$[Ni(eeac)]^+$	12
309*	$[Cd(tftm)]^+$	33	157	$[Ni(eeac\text{-}Et)]^+$	1
252*	$[Cd(tftm\text{-}tBu)]^+$	21	448*	$[Ni(tftm)_2]^+$	43
435	$[Cd(tftm)(eeac)]^+$	5	379*	$[Ni(tftm)(eeac)]^+$	21
406	$[Cd(tftm)(eeac\text{-}Et)]^+$	1	391*	$[Ni(tftm\text{-}tBu)(tftm)]^+$	44
378*	$[Cd(tftm\text{-}tBu)(eeac)]^+$	8	322	$[Ni(tftm\text{-}tBu)(eeac)]^+$	1
366	$[Cd(eeac)_2]^+$	1	253*	$[Ni(tftm)]^+$	21
308	$[Cd(eeac\text{-}Et)(eeac\text{-}Et)]^+$	21			
211	$[Cd(eeac\text{-}Et)]^+$	1			

Table 4.6: Relative ion intensities of hetero-metal species to their respective base peaks as presented in Figure 4.9. Isobaric ion intensities lndicated by *.

4.9 Selected Reaction of $[Cd(tftm)_2]^+$, $[Cd(tftm)(tftm\text{-}tBu)]^+$, $[Cd(tftm)]^+$, and $[Cd(tftm\text{-}tBu)]^+$ with $Ni(eeac)_2$

In an attempt to understand the gas phase reactions occurring during the co-sublimation experiments, selective reactions utilizing various $Cd(tftm)_2$ cations and $Ni(eeac)_2$ were investigated. Similarly, as presented in the previous section using $Ni(acac)_2$ as the neutral target, the detection of particular ions, namely the mixed ligand

complexes, can be used to support one pathway over another. It is through the spectra presented in Figure 4.10 in which particular masses are selected using the first quadrant and introduced into the collision cell that provide the most insight into the mechanism pathway. The two spectra presented in Figure 4.10 reflect different times on the chromatogram throughout the same sample trial. The mass spectra presented in this section correspond to the mass-selected collision cell reactions of $[Cd(tftm)(tftm)]^+$, $[Cd(tftm)(tftm\text{-}t\text{Bu})]^+$, $[Cd(tftm)]^+$, and $[Cd(tftm\text{-}t\text{Bu}]^+$ with a neutral $Ni(eeac)_2$ target. The molecular ions for following equations listed below are the reaction schemes that help support the observed results that can account for the formation of the gas-phase ligand exchange complex. The fragmentation patterns for *eeac* vary from those of *acac* in that an ethyl group is the substituent lost as opposed to a methyl group. However, in looking at the volatility of the two species when co-sublimation occurs, again, the cadmium complex is the first to sublime.

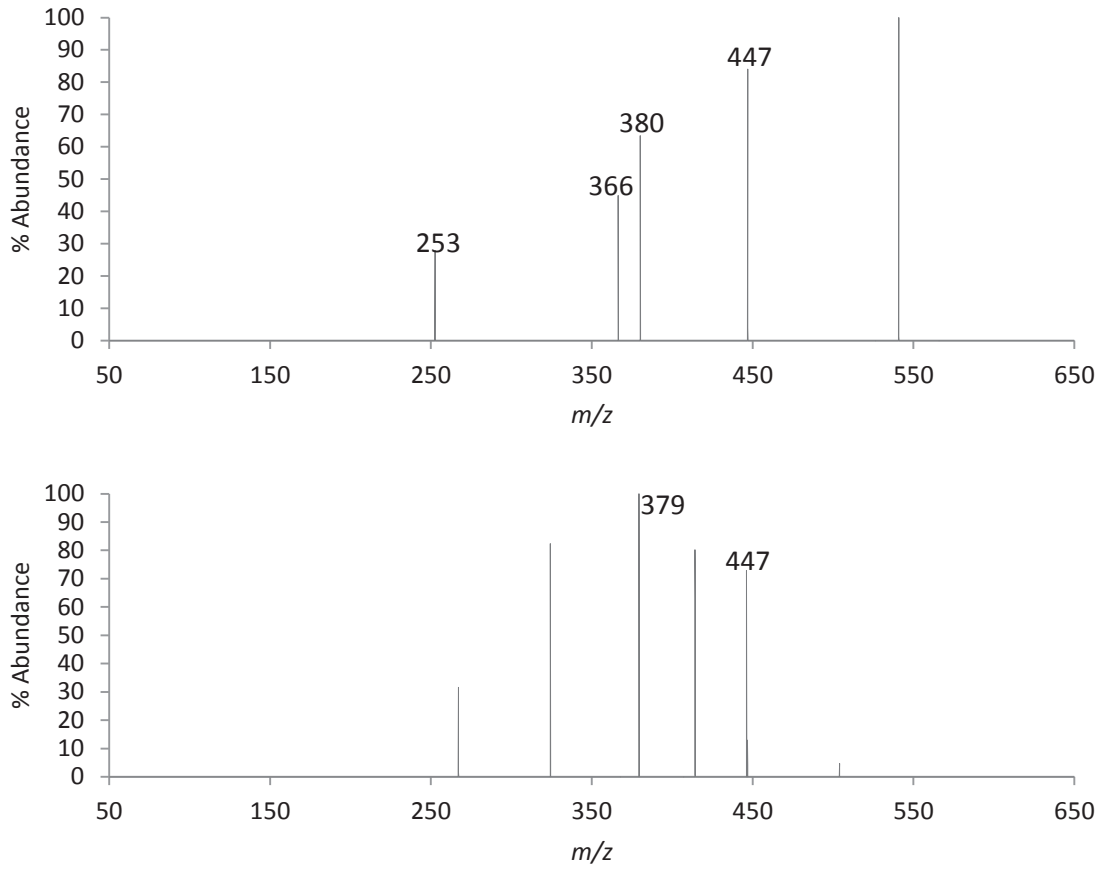

Figure 4.10: The positive EI mass selected spectrum of $[Cd(tftm)(tftm)]^+$ and neutral $Ni(eeac)_2$ at the mass of 504 in the collision cell.

In selecting the molecular ion peak, $[Cd(tftm)(tftm)]^+$, at *m/z* = 504 in Figure 4.10 we begin to gather evidence that not only does a mixed ligand form but there is also evidence that supports a complete exchange as well. In comparing Equation 4.14 and the first spectrum of Figure 4.10, an isobaric peak at *m/z* = 380 for the possible formation of either Ni(eeac)(tftm) at *m/z* = 379 and Cd(tftm-*t*Bu)(eeac) at *m/z* = 378 is present.

$$[Cd(tftm)(tftm)]^+ + Ni(eeac)_2 \rightarrow [Cd(tftm\text{-}tBu)(eeac)]^+ + Ni(tftm)(eeac) + tBu \qquad (4.14)$$

Upon further analysis of the first mass spectrum in Figure 4.10, we see what amounts to the complete exchange of $[Cd(eeac)_2]^+$ at *m/z* = 366. What is exciting about this result is

that while the complete exchange is not observed under co-sublimation conditions, there is experimental evidence that such an exchange is still possible. Furthermore, the peak at *m/z* = 253 is indicative of a single *tftm* attached to the nickel center, which corresponds to a fragmented exchange as well as $[Cd(tftm\text{-}t\text{Bu})]^+$ at *m/z* = 252. Seeing as how *m/z* = 447 also can be described as an isobaric peak, it is possible that a complete exchange yielding $Ni(tftm)_2$ at *m/z* = 448 cannot be ruled out.

The second spectrum in Figure 4.10 has the mixed ligand peak present at *m/z* = 379. What is significant about having the peak in both spectra is that the formation occurred at different times throughout the experiment. As previously mentioned, it is possible for the peak to represent either of the mixed ligand formations, the loss of a *t*Bu group in the cadmium complex and the complete mixed nickel complex, so the identity of the peak is not absolutely certain.

In evaluating the data from the second mass selected ion, $[Cd(tftm)(tftm\text{-}t\text{Bu})]^+$, there are many useful peaks present that give validity to the equations presented in this Section. The ion resulting from the loss of a tertiary butyl group seems to be a major contributor in the formation of not just the mixed ligand but in the complete exchange as well. It is in Equation 4.15 and 4.16 that we can use the observed peaks from Figure 4.11 to determine if the selected mass is reactive in the presence of neutral $Ni(eeac)_2$.

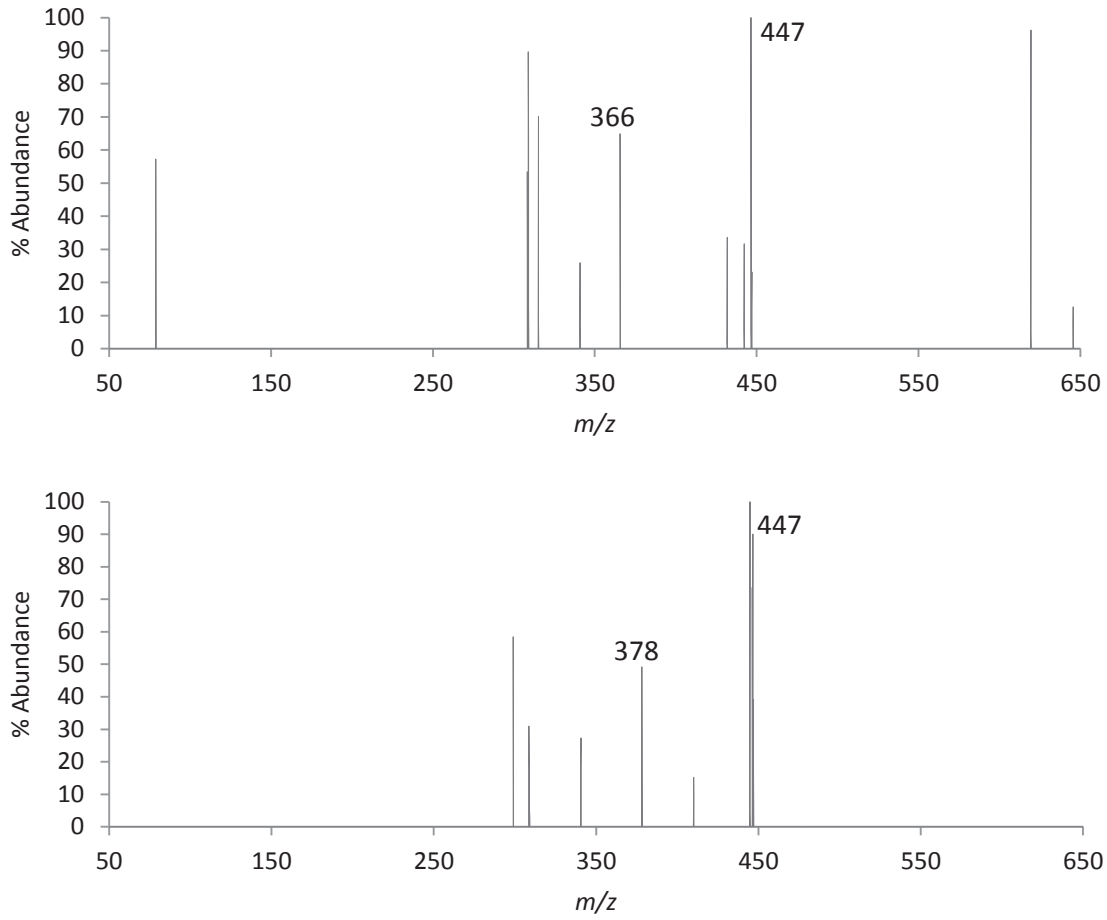

Figure 4.11: The positive EI mass selected spectrum of $[Cd(tftm)(tftm\text{-}t\text{Bu})]^+$ and neutral $Ni(eeac)_2$ at the mass of 447 in the collision cell.

$$[Cd(tftm)(tftm\text{-}t\text{Bu})]^+ + Ni(eeac)_2 \rightarrow [Cd(eeac)(eeac)]^+ + Ni(tftm\text{-}t\text{Bu})(tftm) \qquad (4.15)$$

$$[Cd(tftm)(tftm\text{-}t\text{Bu})]^+ + Ni(eeac)_2 \rightarrow [Cd(tftm\text{-}t\text{Bu})(eeac)]^+ + Ni(tftm)(eeac) \qquad (4.16)$$

When considering the sublimation experiments presented in Figure 4.9c, evidence for the formation of both mixed ligand products at *m/z* = 435 and *m/z* = 379 is clear. Once more, the isobaric peaks existing make it more difficult in establishing which peaks belong to which complex. In the first spectrum it is possible to see a possible complete

exchange with both species, given the presence of $[Cd(eeac)_2]^+$, at *m/z* = 366, and $[Ni(tftm)_2]^+$, at *m/z* = 448, due to possible overlap of the peak at *m/z* = 447. The cluster of isobaric peaks in Figure 4.9c indicate the possibility of multiple ion masses being present. $[Ni(tftm)_2]^+$ can be observed at *m/z* = 448, but additionally can be seen with the loss of a *t*Bu group at *m/z* 391.The mixed ligand complex at *m/*z = 379 and the loss of a *t*Bu at *m/z* = 322 is also present, which can support the validity of Equation 4.16. As was the case with $[Ni(tftm\text{-}tBu)(eeac)]^+$, the mixed ligand for the cadmium complex with a loss of a *t*Bu, $[Cd(tftm\text{-}tBu)(eeac)]^+$, is also visible in the Figure 4.10c at *m/z* = 378. Again, the loss of the *t*Bu in the cadmium mixed ligand complex is consistent with Equation 4.16.

With Equation 4.15 and 4.16 garnering much support from the existing peaks in Figure 4.9c, it is very possible that the mechanism of not just the mixed ligand formation, but in the complete exchanges as well, hinges on the $[Cd(tftm)(tftm\text{-}tBu)]^+$ ion. Moreover, the information presented in the mass selected data can only strengthen the previous claim.

The selected ion mass at *m/z* = 309 corresponding to $[Cd(tftm)]^+$, shows a few interesting peaks in the spectra presented in Figure 4.12. In using these mass spectra, we may be able to get a better understanding as to whether or not this specific ion is involved in the mixed ligand formation between the cadmium and nickel species.

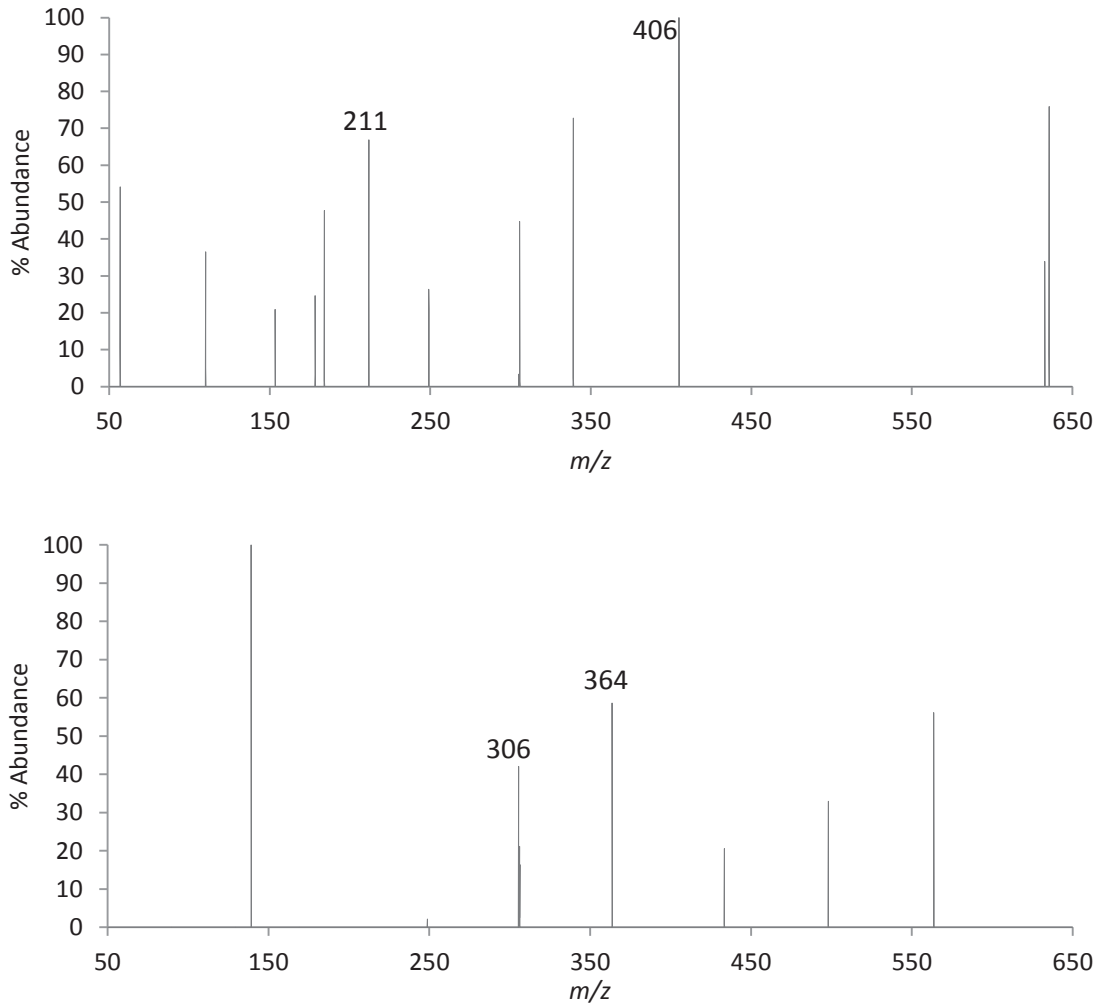

Figure 4.12: The positive EI Mass selected spectrum of $[Cd(tftm)]^+$ and neutral $Ni(eeac)_2$ at the mass of 309 in the collision cell.

Equations 4.17 and 4.18 prove to be very insightful when examining the data from both the co-sublimation and mass-selected spectra. $[Cd(tftm)]^+$ does not appear to be directly responsible in the formation of the intact mixed ligand $[Cd(tftm)(eeac)]^+$, but instead, the formation of the exchanged products with the loss of an ethyl group.

$$[Cd(tftm)]^+ + Ni(eeac)_2 \rightarrow [Cd(tftm)(eeac\text{-}Et)]^+ + Ni(eeac) + Et \quad (4.17)$$

$$[Cd(tftm)]^+ + Ni(eeac)_2 \rightarrow [Cd(eeac\text{-}Et)]^+ + Ni(tftm)(eeac) + Et \quad (4.18)$$

In the first spectrum of Figure 4.12 there are two peaks of interest that share similar fragmentation patterns. First, the peak at *m/z* = 406 corresponds to the cadmium

mixed ligand complex with what amounts to the loss of an ethyl group, $[Cd(tftm)(eeac\text{-}Et)]^+$ and second peak of interest is observed at *m/z* = 211, corresponding to $[Cd(eeac\text{-}Et)]^+$. In the second spectrum, the two emphasized peaks have masses two units less than their nominal masses. If the species in the spectrum are in fact two less than their actual masses, it can be assumed that the peak at *m/z* = 364 would correspond to the complete cadmium exchange resulting in $[Cd(eeac)_2]^+$, and the second peak at *m/z* = 306 would correspond to the loss of two ethyl groups from the exchanged complex, resulting in $[Cd(eeac\text{-}Et)(eeac\text{-}Et)]^+$.

The last of the selected masses for the collision cell reactions is *m/z* = 252, which corresponds to $[Cd(tftm\text{-}t\text{Bu})]^+$ and is presented in Figure 4.13. With $[Cd(tftm\text{-}t\text{Bu})]^+$ as the selected ion reacting with neutral $Ni(eeac)_2$, both the complete exchange at *m/z* = 366 corresponding to $[Cd(eeac)_2]^+$ and the mixed ligand product, $[Cd(tftm)(eeac)]^+$, at *m/z* = 435 are observed. Equations 4.19 and 4.20 describe these reactions accordingly.

$$[Cd(tftm\text{-}t\text{Bu})]^+ + Ni(eeac)_2 + t\text{Bu} \rightarrow [Cd(tftm)(eeac)]^+ + Ni(eeac) \quad (4.19)$$

$$[Cd(tftm\text{-}t\text{Bu})]^+ + Ni(eeac)_2 \rightarrow [Cd(eeac)_2]^+ + Ni(tftm\text{-}t\text{Bu}) \quad (4.20)$$

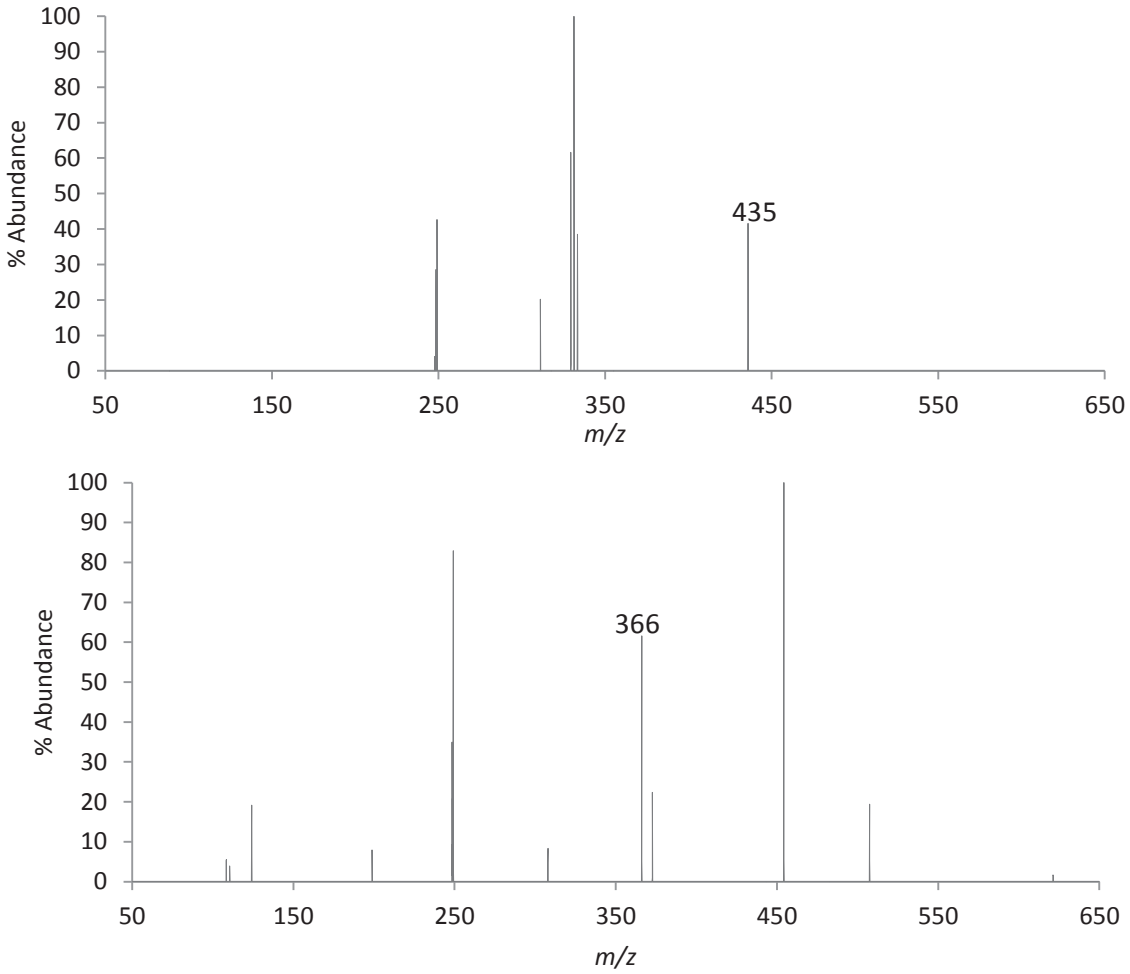

Figure 4.13: The positive EI mass selected spectrum of $[Cd(tftm\text{-}tBu)]^+$ and neutral $Ni(eeac)_2$ at the mass of 252 in the collision cell.

4.10 Co-sublimation of $Cd(tftm)_2$ and $Ni(tfac)_2$

In an attempt to further document and understand gas phase ligand exchange, $Cd(tftm)_2$ was also co-sublimed with $Ni(tfac)_2$. The peaks observed in the co-sublimation of $Cd(tftm)_2$ and $Ni(tfac)_2$ are presented in Figure 4.14 with the corresponding relative abundances listed in Table 4.7. Figure 4.14a is reproduced from Figure 4.4 and corresponds to the mass spectrum of $Ni(tfac)_2$. Figure 4.14b is the mass spectrum for $Cd(tftm)_2$ and Figure 4.14c is the corresponding co-sublimation. The peak at m/z = 462 and 406 correspond to the formation of the mixed ligand complexes $[Cd(tftm)(tfac)]^+$ and $[Ni(tftm)(tfac)]^+$, respectively. Additional fragments of the mixed ligand species are also clearly presented.

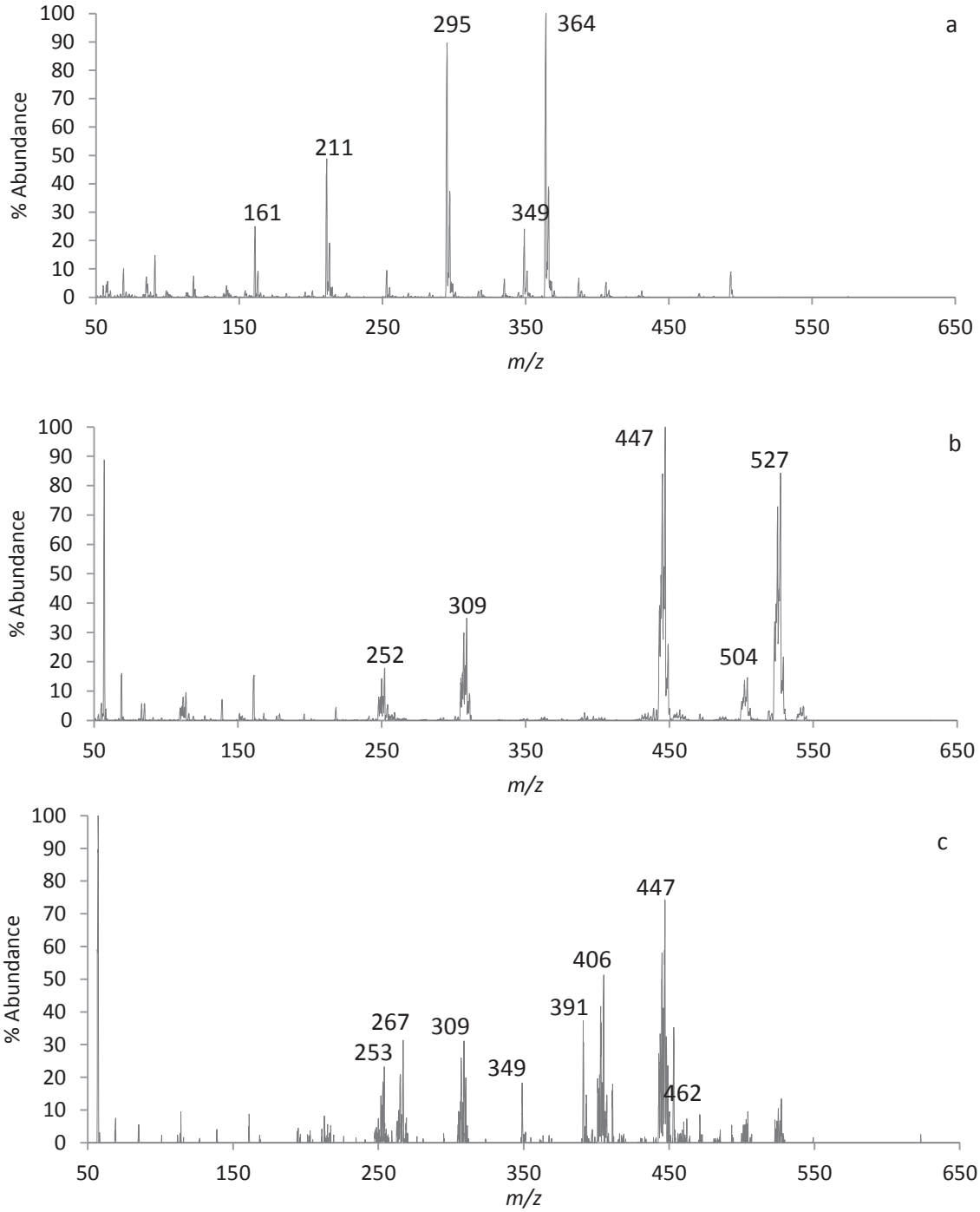

Figure 4.14: The Positive EI mass spectra of (a) $Ni(tfac)_2$, (b) $Cd(tftm)_2$, and (c) the co-sublimation of $Ni(tfac)_2$ and $Cd(tftm)_2$. Masses labeled in (a) and (b) represent the molecular ion and typical fragments of their respective parent compounds. Masses labeled in (c) correspond to the intact ligand gas phase product and fragments thereof.

m/z	Species	Rel. Ab	m/z	Species	Rel. Ab
504	$[Cd(tftm)_2]^+$	16	364	$[Ni(tfac)_2]^+$	8
447*	$[Cd(tftm\text{-}tBu)(tftm)]^+$	100	349	$[Ni(tfac\text{-}CH_3)(tfac)]^+$	<1
390*	$[Cd(tftm\text{-}tBu)(tftm\text{-}tBu)]^+$	4	295	$[Ni(tfac)(tfac\text{-}CF_3)]^+$	12
309*	$[Cd(tftm)]^+$	33	211	$[Ni(tfac)]^+$	1
252*	$[Cd(tftm\text{-}tBu)]^+$	21	161	$[Ni(tfac\text{-}CF_2)]^+$	<1
420	$[Cd(tfac)_2]^+$	1	448*	$[Ni(tftm)_2]^+$	32
462	$[Cd(tftm)(tfac)]^+$	7	406*	$[Ni(tftm)(tfac)]^+$	10
405*	$[Cd(tftm\text{-}tBu)(tfac)]^+$	51	349	$[Ni(tftm\text{-}tBu)(tfac)]^+$	18
393*	$[Cd(tftm)(tfac\text{-}CF_3)]^+$	15	391*	$[Ni(tftm\text{-}tBu)(tftm)]^+$	37
267	$[Cd(tfac)]^+$	31	253*	$[Ni(tftm)]^+$	19
252*	$[Cd(tfac\text{-}CH_3)]^+$	14			

Table 4.7: Relative ion intensities of hetero-metal species to their respective base peaks as presented in Figure 4.14. Isobaric ion intensities indicated by *.

4.11 Selected Reaction of $[Cd(tftm)_2]^+$ and $[Cd(tftm)(tftm\text{-}tBu)]^+(tftm)]^+$ with $Ni(tfac)_2$

The formation of peaks present in Figure 4.14c were examined through a series of selective reactions. The mechanistic role of $[Cd(tftm)(tftm)]^+$ in the presence of $Ni(tfac)_2$ can be examined by interpreting the results presented in Figure 4.15.

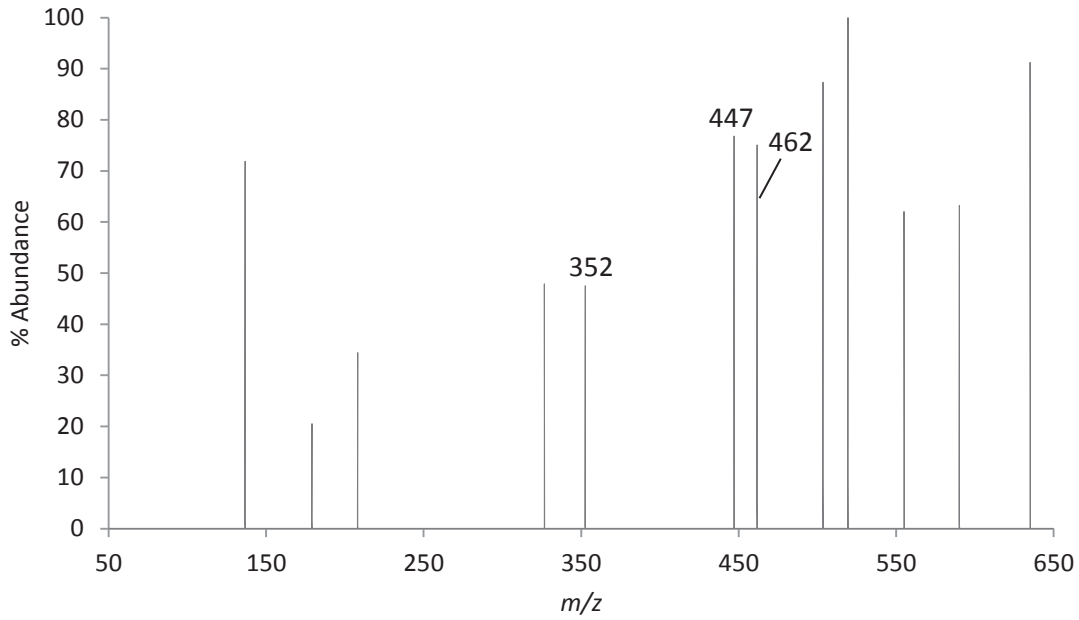

Figure 4.15: The positive EI mass selected spectrum of $[Cd(tftm)(tftm)]^+$ and neutral $Ni(tfac)_2$ at the mass of 504 in the collision cell.

Given the presence of a peak at *m/z* = 462, which corresponds to the mixed ligand complex of the cadmium species, it appears $[Cd(tftm)(tftm)]^+$ may be mechanistically active according to Equation 4.21.

$$[Cd(tftm)(tftm)]^+ + Ni(tfac)_2 \rightarrow [Cd(tftm)(tfac)]^+ + Ni(tftm)(tfac) \qquad (4.21)$$

The mechanism presented in Equation 4.22 describes the formation of $[Cd(tftm)(tfac\text{-}CF_3)]^+$ at *m/z* = 393. This mass is isobaric with the complete exchange $[Ni(tftm)(tftm\text{-}t\text{Bu})]^+$ at *m/z* = 391.

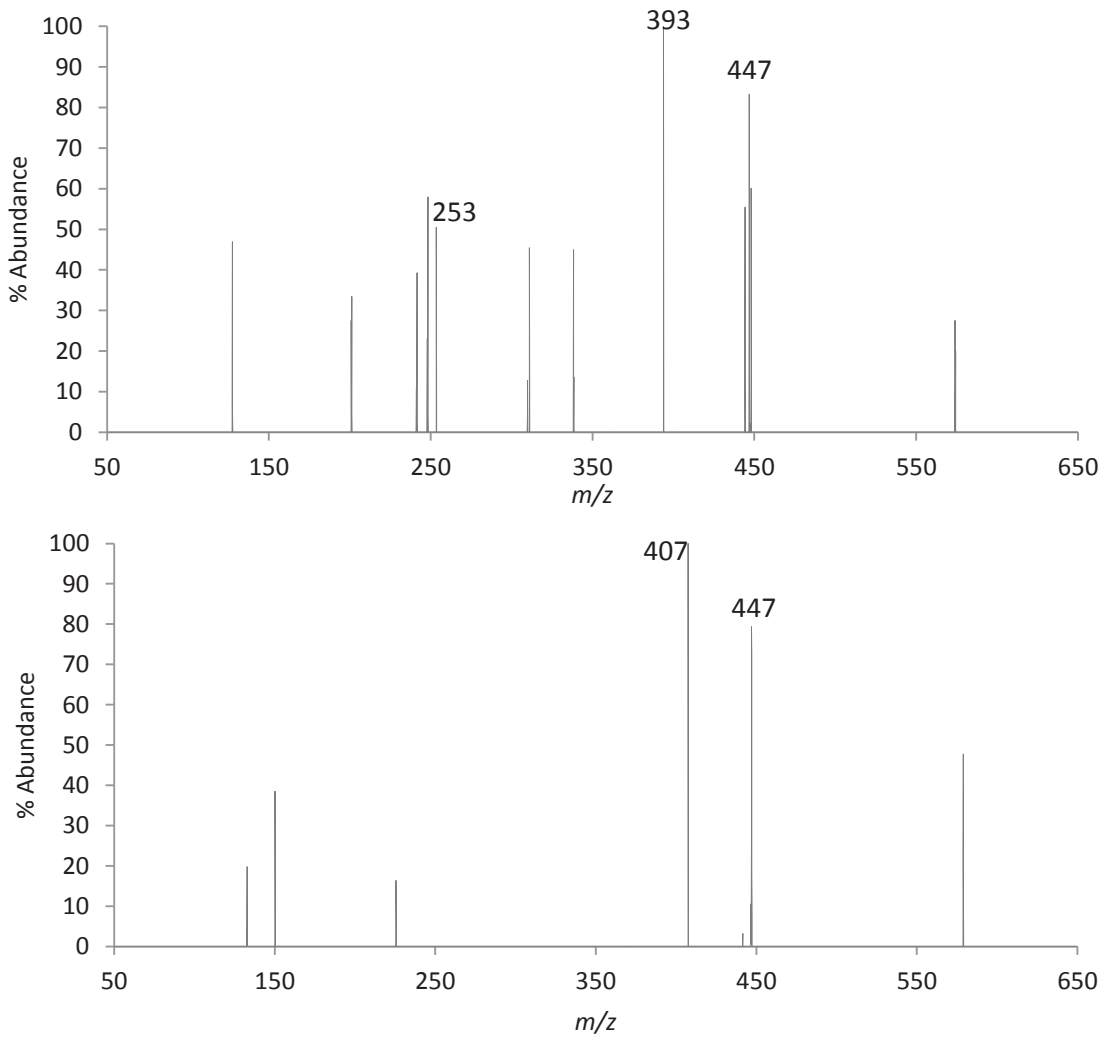

Figure 4.16: The positive EI Mass selected spectrum of $[Cd(tftm)(tftm\text{-}t\text{Bu})]^+$ and neutral $Ni(tfac)_2$ at the mass of 447 in the collision cell.

$$[Cd(tftm)(tftm\text{-}t\text{Bu})]^+ + Ni(tfac)_2 \rightarrow [Cd(tftm)(tfac\text{-}CF_3)]^+ + Ni(tftm\text{-}t\text{Bu})(tfac) + CF_3 \quad (4.22)$$

Moreover, the peak at *m/z* = 253 is consistent with the loss of an intact ligand from the complete exchange product, $[Ni(tftm)]^+$ at *m/z* = 253. $[Ni(tftm)(tfac)]^+$ at *m/z* = 406 may also be present in Figure 4.16. Additional selective reactions using $[Cd(tftm)]^+$ as well as $[Cd(tftm\text{-}t\text{Bu})]^+$ as the selected ion were also attempted, but provided inconclusive results.

Chapter 5

Investigations of Co-sublimation Reactions Involving Cadmium Trifluorotrimethylacetylacetonate and Transition Metal β-Diketonate Complexes

5.1 Introduction

In this Chapter, a variety of gas-phase reactions are examined where $Cd(tftm)_2$ is co-sublimed with several different transition metal β-diketonate complexes, including copper, zinc, nickel, and palladium as the metal centers. The data presented in Chapter 4 describing the behavior of the nickel β-diketonate complexes will not be reproduced here, nor will any mass selected experiments using the collision cell. Proposed mechanisms describing the gas phase reactions in this Chapter are similar to what was presented in Chapter 4. The data presented here is consistent with other experiments and serves as a stepping stone toward additional research and understanding.

The material presented in this Chapter is of great interest due to the proclivity of the reactions being quite successful. The exchanges that occurred throughout each trial, whether it is complete or partial ligand exchange, are all vital in giving the proposed thesis validity. Furthermore, previous claims made by Hunter and Lerach[1,14] state that the starting material, that is co-sublimed, is not reaction specific, and any combination will likely yield a mixed ligand complex. In this Chapter, $Cd(tftm)_2$ is co-sublimed with several different β-diketonate complexes and ligand exchange is, in fact, observed to occur.

5.2 Co-sublimation of $Cd(tftm)_2$ and $Cu(acac)_2$

The mass spectrometric data describing the sublimation of $Cu(acac)_2$, $Cd(tftm)_2$, as well as the co-sublimation of $Cd(tftm)_2$ and $Cu(acac)_2$ is presented in Figure 5.1, and is vertically stacked for ease of comparison. Figure 5.1a illustrates the single $Cu(acac)_2$ spectrum and the corresponding fragmentation pattern that is typically associated with this species. Notable peaks that can be observed in the three spectrum are listed in Table 5.1, and include the parent peak at m/z = 261, the loss of a methyl group at m/z = 246, the loss of second methyl group at m/z = 231, the loss of an entire acac ligand at m/z = 162, and the loss of a methyl group from only one intact acac ligand at m/z = 147. The mass spectrum of $Cd(tftm)_2$ is reproduced in Figure 5.1b, which is the same spectrum that is represented from Figure 4.1, just over a different range. The co-sublimation $Cd(tftm)_2$ and $Cu(acac)_2$ is presented in Figure 5.1c, where both species can react in the gas phase and undergo ligand exchange, whether it be a partial, mixed, or complete exchange. The ion peaks observed in Figure 5.1c are exclusive to the results following the co-sublimation ligand exchange and are not present in the individual spectrum. Table 5.1 reports the m/z ratios, the exchanged single species, mixed ligand and fragmented species, as well as corresponding the relative abundances. In assessing the ligand exchange in Figure 5.1c it would appear that the copper complex was more likely to form than the cadmium complexes, which is comparable to the data presented in Section 4.2.

m/z	Species	Rel. Ab.	m/z	Species	Rel. Ab.
408	$[Cd(tftm)(acac)]^+$	8	453	$[Cu(tftm)_2]^+$	23
312	$[Cd(acac)_2]^+$	4	396	$[Cu(tftm)(tftm\text{-}t\text{Bu})]^+$	35
213	$[Cd(acac)]^+$	14	339	$[Cu(tftm\text{-}t\text{Bu})(tftm\text{-}t\text{Bu})]^+$	54
504	$[Cd(tftm)_2]^+$	15	357	$[Cu(tftm)(acac)]^+$	59
447	$[Cd(tftm)(tftm\text{-}t\text{Bu})]^+$	100	300	$[Cu(tftm\text{-}tBu)(acac)]^+$	100
309	$[Cd(tftm)]^+$	35	261	$[Cu(acac)_2]^+$	100
252	$[Cd(tftm\text{-}t\text{Bu})]^+$	18	246	$[Cu(acac)(acac\text{-}CH_3)]^+$	51
			231	$[Cu(acac\text{-}CH_3)(acac\text{-}CH_3)]^+$	39
			162	$[Cu(acac)]^+$	43
			147	$[Cu(acac\text{-}CH_3)]^+$	45

Table 5.1: Relative ion abundances of the $Cd(tftm)_2$ and $Cu(acac)_2$ species, as well as the co-sublimation of $Cd(tftm)_2$ and $Cu(acac)_2$ as presented in Figure 5.1c.

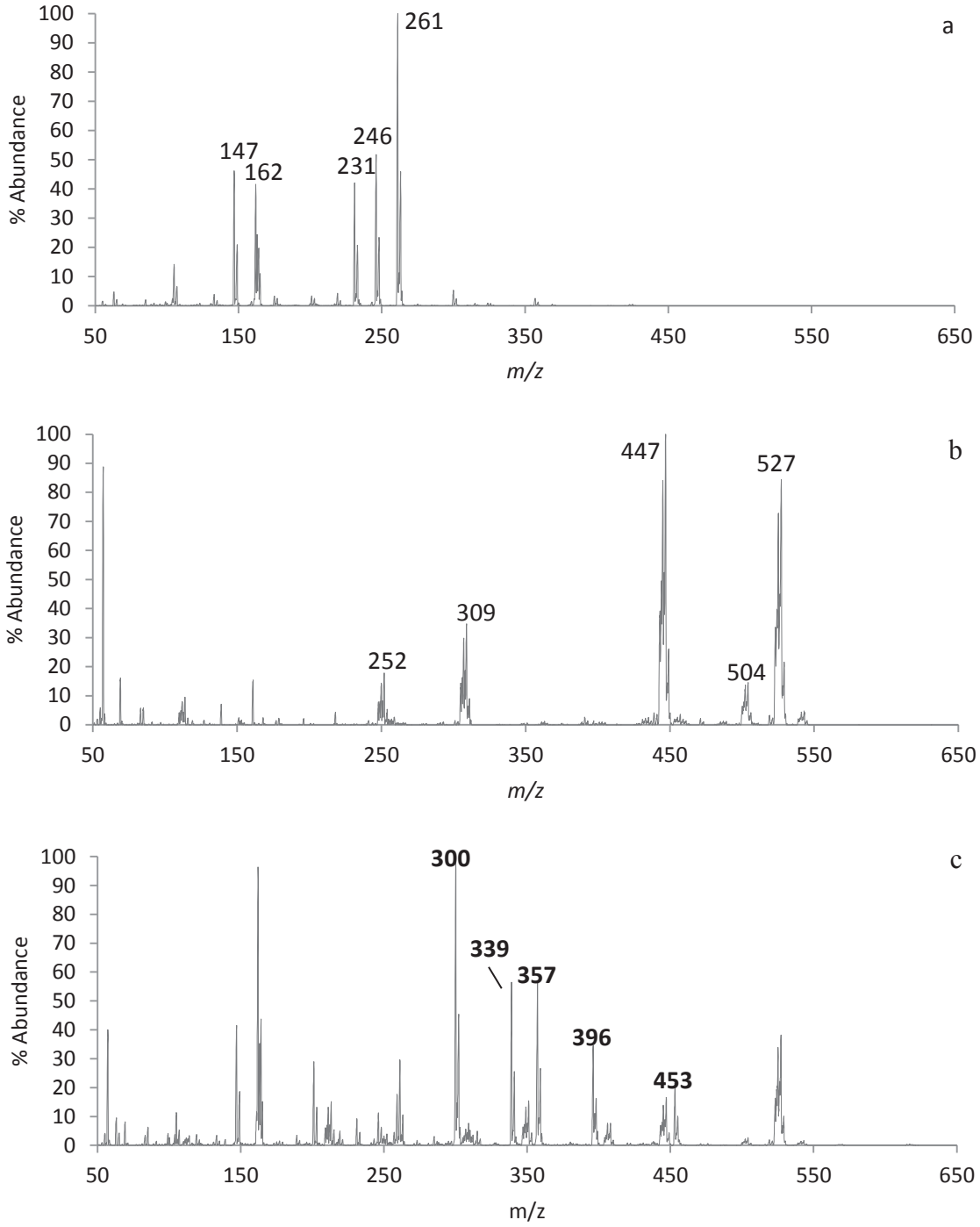

Figure 5.1: The positive EI mass spectra of (a) $Cu(acac)_2$, (b) $Cd(tftm)_2$, and (c) the co-sublimation of $Cu(acac)_2$ and $Cd(tftm)_2$. Masses labeled in (a) and (b) represent the molecular ion and typical fragments of their respective parent compounds. Masses labeled in (c) correspond to the intact ligand gas phase product and fragments thereof.

5.3: Co-sublimation of $Cd(tftm)_2$ and $Cu(eeac)_2$

The mass spectrometric data describing the sublimation of $Cu(eeac)_2$, $Cd(tftm)_2$, as well as the co-sublimation $Cd(tftm)_2$ and $Cu(eeac)_2$ is presented for the first time in Figure 5.2, and is vertically stacked for ease of comparison. Figure 5.2a illustrates the single $Cu(eeac)_2$ spectrum and the corresponding fragmentation pattern that is typically associated with this species. Notable peaks that can be observed in the three spectra are listed in Table 5.2, and include the parent peak $[Cu(eeac)_2]^+$ at *m/z* = 315, the loss of an ethyl group at *m/z* = 286, and the loss of second ethyl group at *m/z* = 257. The loss of an entire *eeac* ligand to produce $[Cd(eeac)]^+$ at *m/z* = 189 and the loss of a ethyl group from only one intact *eeac* ligand at *m/z* = 160 were also observed.

The mass spectrum of $Cd(tftm)_2$ is reproduced in Figure 5.2b, which is the same spectrum that is represented from Figure 4.1, just over a different mass range. The co-sublimation $Cd(tftm)_2$ and $Cu(eeac)_2$ is presented in Figure 5.2c, where both species can react in the gas phase and undergo ligand exchange, whether it be a partial or complete exchange. The ion peaks observed in Figure 5.2c are exclusive to the results following the co-sublimation ligand exchange and are not present in the individual spectrum. Table 5.2 reports the m/z ratios, the exchanged single species, mixed ligand and fragmented species, as well as the corresponding relative abundances. In assessing the ligand exchange in Figure 5.2c, it would appear that the copper complex was more likely to form than the cadmium complexes, which is comparable to the data presented in Section 4.2.

The masses present at both *m/z* = 435 and 384, respectively, confirm the formation of a mixed ligand for both complexes. There is also a complete exchange

observed at *m/z* = 453, which represents $[Cu(tftm)_2]^+$. Isobaric peaks are another aspect to consider when examining the peaks present in the spectra. This occurs when two different species overlap at the same nominal mass to form a cluster of peaks. For instance, $[Cu(tftm\text{-}t\text{Bu})(tftm\text{-}t\text{Bu})]^+$ appears at *m/z* 339, while the most abundant isotope for $[Cd(eeac)(eeac\text{-}Et)]^+$ appears at *m/z* 337, creating a much broader ion signal. It is from the single-metal spectra, using the isotopic pattern, which we can establish if the isobaric peaks are present in the hetero-metal spectrum.

m/z	**Species**	**Rel. Ab.**	**m/z**	**Species**	**Rel. Ab.**
435	$[Cd(tftm)(eeac)]^+$	3	453	$[Cu(tftm)_2]^+$	23
366	$[Cd(eeac)_2]^+$	<1	396	$[Cu(tftm)(tftm\text{-}t\text{Bu})]^+$	35
308	$[Cd(eeac\text{-}Et)\text{-}(eeac\text{-}Et)]^+$	8	339	$[Cu(tftm\text{-}tBu)(tftm\text{-}t\text{Bu})]^+$	52
240	$[Cd(eeac)]^+$	2	384	$[Cu(tftm)(eeac)]^+$	5
504	$[Cd(tftm)_2]^+$	15	315	$[Cu(eeac)_2]^+$	99
447	$[Cd(tftm)(tftm\text{-}t\text{Bu})]^+$	100	286	$[Cu(eeac)(eeac\text{-}Et)]^+$	100
309	$[Cd(tftm)\ ]^+$	35	257	$[Cu(eeac\text{-}Et)(eeac\text{-}Et)]^+$	69
252	$[Cd(tftm\text{-}t\text{Bu})]^+$	18	189	$[Cu(eeac)]^+$	31
			160	$[Cu(eeac\text{-}Et)]^+$	46

Table 5.2: Relative ion abundances of the $Cd(tftm)_2$ and $Cu(eeac)_2$ species, as well as the co-sublimation of $Cd(tftm)_2$ and $Cu(eeac)_2$ as presented in Figure 5.2c.

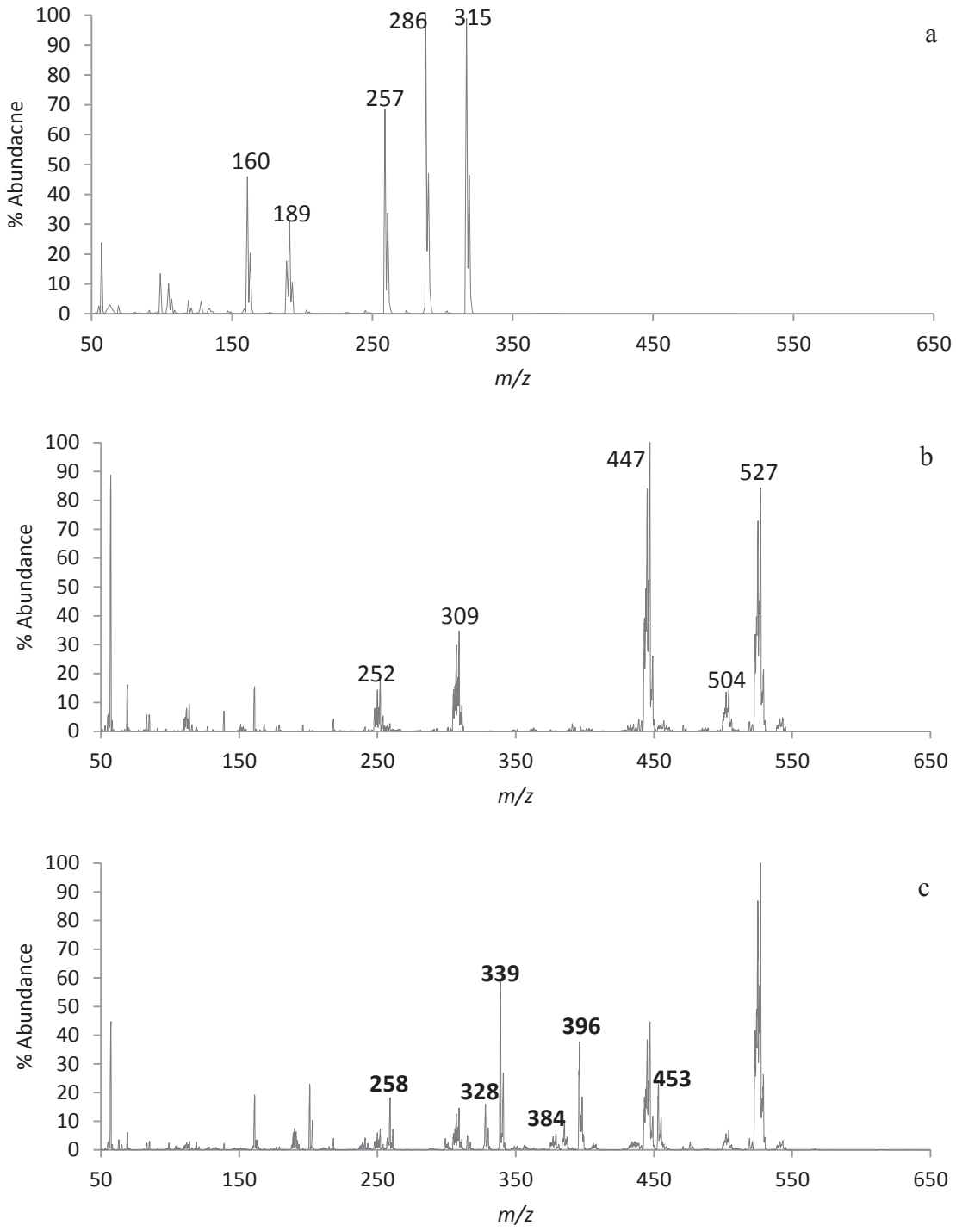

Figure 5.2: The positive EI mass spectra of (a) $Cu(eeac)_2$, (b) $Cd(tftm)_2$, and (c) the co-sublimation of $Cu(eeac)_2$ and $Cd(tftm)_2$. Masses labeled in (a) and (b) represent the molecular ion and typical fragments of their respective parent compounds. Masses labeled in (c) correspond to the intact ligand gas phase product and fragments thereof.

5.4: Co-sublimation of $Cd(tftm)_2$ and $Cu(hfac)_2$

The mass spectrometric data describing the sublimation of $Cu(hfac)_2$, $Cd(tftm)_2$, as well as the co-sublimation $Cd(tftm)_2$ and $Cu(hfac)_2$ is presented in Figure 5.3, and is vertically stacked for ease of comparison. Figure 5.3a illustrates the single $Cu(hfac)_2$ spectrum and the corresponding fragmentation pattern that is typically associated with this species. Notable peaks that can be observed in the three spectra are listed in Table 5.3, and include the parent peak $[Cu(hfac)_2]^+$ at m/z = 477 and the loss of a CF_3 group at m/z = 408. The loss of second a CF_3 group at m/z = 309, and the loss of a CF_3 group from only one intact hfac ligand at m/z = 201 are also observed.

The mass spectrum of $Cd(tftm)_2$ is reproduced in Figure 5.3b, which is the same spectrum that is represented from Figure 4.1, just over a different mass range. The co-sublimation $Cd(tftm)_2$ and $Cu(hfac)_2$ is presented in Figure 5.3c, where both species can react in the gas phase and undergo ligand exchange, whether it be a partial, mixed, or complete exchange. The ion peaks observed in Figure 5.3c are exclusive to the results following the co-sublimation ligand exchange and are not present in the individual spectrum. Table 5.4 reports the m/z ratios, the exchanged single species, mixed ligand and fragmented species, as well as the corresponding relative abundances. In assessing the ligand exchange in Figure 5.3c it would appear that the copper complex was more likely to form than the cadmium complexes, which is comparable to the data presented in Section 4.2.

Upon evaluating the spectrum of the co-sublimation of $Cd(tftm)_2$ and $Cu(hfac)_2$, it appears there are many exchanges between the gas-phase species. Although there appears to be no complete exchange of the cadmium complex, there appears to be quite a variety

of exchanges that occur within the copper species – not just partial ligand exchanges, but a complete exchange as well.

m/z	Species	Rel. Ab.	m/z	Species	Rel. Ab.
528	$[Cd(hfac)_2]^+$	<1	453	$[Cu(tftm)_2]^+$	21
516	$[Cd(hfac)(tftm)]^+$	<1	396	$[Cu(tftm)(tftm\text{-}t\text{Bu})]^+$	44
459	$[Cd(hfac)(hfac\text{-}CF_3)]^+$	5	339	$[Cu(tftm\text{-}t\text{Bu})(tftm\text{-}t\text{Bu})]^+$	100
321	$[Cd(hfac)]^+$	2	465	$[Cu(tftm)(hfac)]^+$	10
252	$[Cd(hfac\text{-}CF_3)]^+$	<1	408	$[Cu(tftm)(hfac)]^+$	31
504	$[Cd(tftm)_2]^+$	15	201	$[Cu(tftm\text{-}t\text{Bu})]^+$	93
447	$[Cd(tftm)(tftm\text{-}t\text{Bu})]^+$	100	259	$[Cu(tftm)]^+$	25
309	$[Cd(tftm)]^+$	35	477	$[Cu(hfac)_2]^+$	64
252	$[Cd(tftm\text{-}t\text{Bu})]^+$	18	408	$[Cu(hfac)(hfac\text{-}CF_3)]^+$	100
			339	$[Cu(hfac\text{-}CF_3)(hfac\text{-}CF_3)]^+$	45
			201	$[Cu(hfac\text{-}CF_3)]^+$	83

Table 5.3: Relative ion abundances of the $Cd(tftm)_2$ and $Cu(hfac)_2$ species, as well as the co-sublimation of $Cd(tftm)_2$ and $Cu(hfac)_2$ as presented in Figure 5.3c.

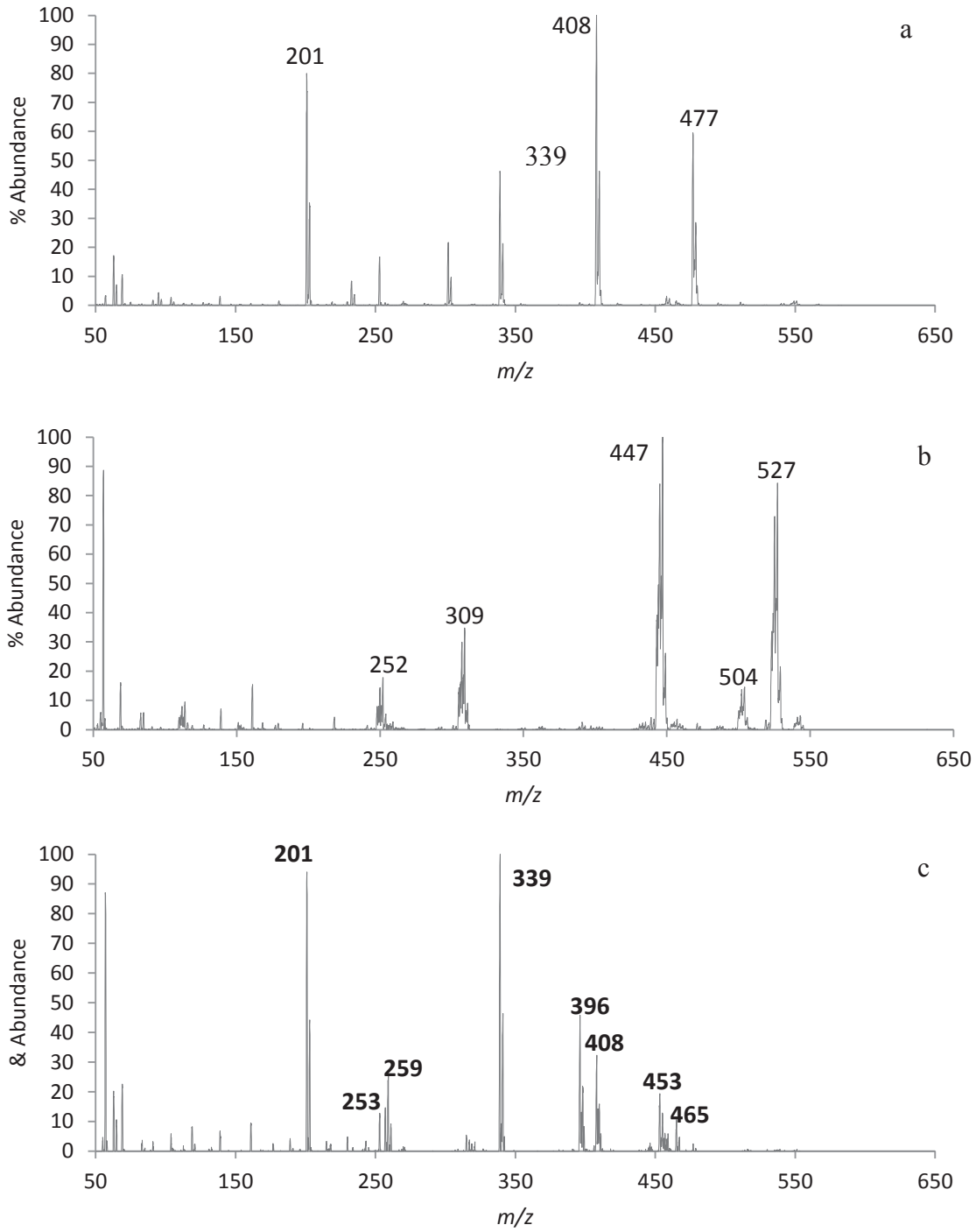

Figure 5.3: The positive EI mass spectra of (a) $Cu(hfac)_2$, (b) $Cd(tftm)_2$, and (c) the co-sublimation of $Cu(hfac)_2$ and $Cd(tftm)_2$. Masses labeled in (a) and (b) represent the molecular ion and typical fragments of their respective parent compounds. Masses labeled in (c) correspond to the intact ligand gas phase product and fragments thereof.

5.5: Co-sublimation of $Cd(tftm)_2$ and $Ni(hfac)_2$

The mass spectrometric data describing the sublimation of $Ni(hfac)_2$, $Cd(tftm)_2$, as well as the co-sublimation $Cd(tftm)_2$ and $Ni(hfac)_2$ is presented in Figure 5.4, and is vertically stacked for ease of comparison. Figure 5.4a illustrates the single $Ni(hfac)_2$ spectrum and the corresponding fragmentation pattern that is typically associated with this species. Notable peaks that can be observed in the three spectra are listed in Table 5.4, and include the parent peak $[Ni(hfac)_2]^+$ at *m/z* = 472 and the loss of a CF_3 group at *m/z* = 403. The loss of one intact ligand at *m/z* = 265, and the presence of fluorine migration, which is the loss of a CF_2 group from only one intact hfac ligand at *m/z* = 215 are also observed.

The mass spectrum of $Cd(tftm)_2$ is reproduced in Figure 5.4b, which is the same spectrum that is represented from Figure 4.1, just over a different mass range. The co-sublimation $Cd(tftm)_2$ and $Ni(hfac)_2$ is presented in Figure 5.4c, where both species can react in the gas phase and undergo ligand exchange, whether it be a partial, mixed, or complete exchange. The ion peaks observed in Figure 5.4c are exclusive to the results following the co-sublimation ligand exchange and are not present in the individual spectrum. Table 5.4 reports the m/z ratios, the exchanged single species, mixed ligand and fragmented species, as well as the corresponding relative abundances. In assessing the ligand exchange in Figure 5.3c it would appear that the copper complex was more likely to form than the cadmium complexes, which is comparable to the data presented in Section 4.2.

Again, when analyzing the peaks of the co-sublimation experiment, isobaric peaks should be taken into consideration. Here we have two similar ion masses: one at m/z =

391, which represents [Ni(tftm-tBu)(tftm)]$^+$, and a peak of *m/z* 390, indicating [Cd(hfac-CF_3)(hfac-CF_3)]$^+$. In addition to the isobaric peaks, there are several peaks present in Figure 5.4c that would yield significant data points in establishing that the reaction has successfully occurred. The complete exchange of the nickel complex appears to be present in the spectrum at *m/z* = 448 as well as the loss of *t*Bu at *m/z* = 391. Just as important as the complete exchange, the presence of mixed ligand exchanges in nickel complexes provides additional evidence that the reaction was completed successfully. Moreover, even though there does not appear to be a complete exchange of the cadmium complex, there is, however, indication of many cadmium-containing fragments. It is from these fragments and mixed ligand complexes that will help determine mechanistic pathways in future research.

m/z	Species	Rel. Ab.	m/z	Species	Rel. Ab.
528	[Cd(hfac)$_2$]$^+$	<1	448	[Ni(tftm)$_2$]$^+$	36
516	[Cd(hfac)(tftm)]$^+$	<1	391	[Ni(tftm)(tftm-*t*Bu)]$^+$	57
459	[Cd(hfac)(hfac-CF_3)]$^+$	9	334	[Ni(tftm-tBu)(tftm-*t*Bu)]$^+$	<1
390	[Cd(hfac-CF_3)(hfac-CF_3)]$^+$	3	460	[Ni(tftm)(hfac)]$^+$	4
321	[Cd(hfac)]$^+$	3	403	[Ni(tftm)(hfac)]$^+$	6
252	[Cd(hfac-CF_3)]$^+$	7	196	[Ni(hfac-CF_3)]$^+$	8
504	[Cd(tftm)$_2$]$^+$	15	472	[Ni(hfac)$_2$]$^+$	36
447	[Cd(tftm)(tftm-*t*Bu)]$^+$	100	403	[Ni(hfac)(hfac-CF_3)]$^+$	100
309	[Cd(tftm)]$^+$	35	265	[Ni(hfac)]$^+$	42
252	[Cd(tftm-*t*Bu)]$^+$	18	215	[Ni(hfac-CF_2)]$^+$	44

Table 5.4: Relative ion abundances of the Cd(tftm)$_2$ and Ni(hfac)$_2$ species, as well as the co-sublimation of Cd(tftm)$_2$ and Ni(hfac)$_2$ as presented in Figure 5.4c.

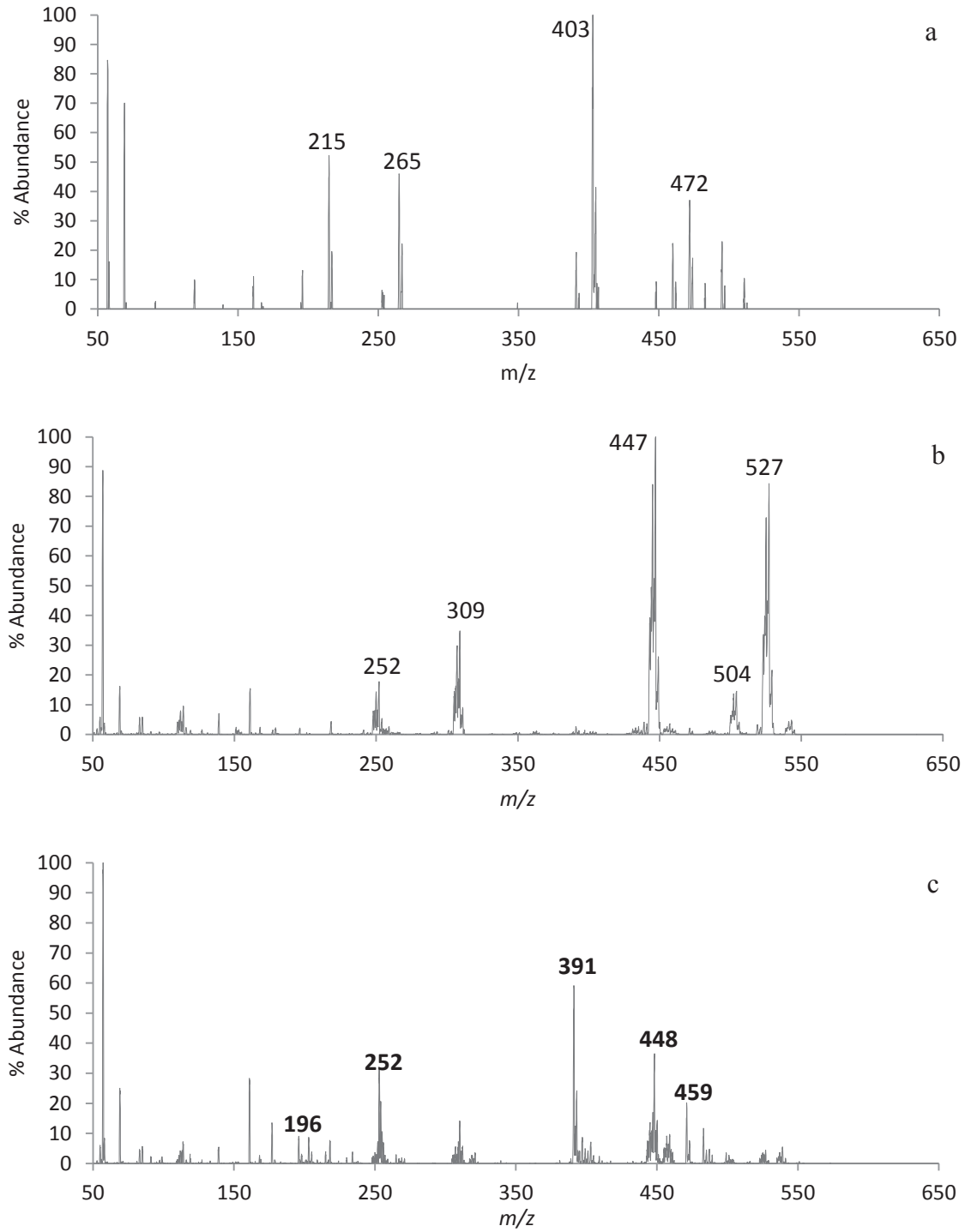

Figure 5.4: The positive EI mass spectra of (a) $Ni(hfac)_2$, (b) $Cd(tftm)_2$, and (c) the co-sublimation of $Ni(hfac)_2$ and $Cd(tftm)_2$. Masses labeled in (a) and (b) represent the molecular ion and typical fragments of their respective parent compounds. Masses labeled in (c) correspond to the intact ligand gas phase product and fragments thereof.

5.6: Co-sublimation of $Cd(tftm)_2$ and $Zn(hfac)_2$

The mass spectrometric data describing the sublimation of $Zn(hfac)_2$, $Cd(tftm)_2$, as well as the co-sublimation $Cd(tftm)_2$ and $Zn(hfac)_2$ is presented in Figure 5.5, and is vertically stacked for ease of comparison. Figure 5.5a illustrates the single $Zn(hfac)_2$ spectrum and the corresponding fragmentation pattern that is typically associated with this species. Notable peaks that can be observed in the three spectra are listed in Table 5.5, and include the parent peak $[Zn(hfac)_2]^+$ at m/z = 479 and the loss of a CF_3 group at m/z = 410. The loss of one intact ligand at m/z = 272 and the presence of fluorine migration, $-CF_2$ group, from only one intact hfac ligand at m/z = 222 are also observed.

The mass spectrum of $Cd(tftm)_2$ is reproduced in Figure 5.5b, which is the same spectrum that is represented from Figure 4.1, just over a different range. The co-sublimation $Cd(tftm)_2$ and $Zn(hfac)_2$ is presented in Figure 5.5c, where both species can react in the gas phase and undergo ligand exchange, whether it be a partial, mixed, or complete exchange. The ion peaks observed in Figure 5.5c are exclusive to the results following the co-sublimation ligand exchange and are not present in the individual spectrum. Table 5.5 reports the m/z ratios, the exchanged single species, mixed ligand and fragmented species, as well as the corresponding relative abundances. In assessing the ligand exchange in Figure 5.5c it would appear that the copper complex was more likely to form than the cadmium complexes, which is comparable to the data presented in Section 4.2.

In assessing the ligand exchange in Figure 5.5c, the trend is for the more volatile complex, which is usually the more fluorinated one, to quickly sublime and become detected first. The data presented here is quite exciting considering some of the peaks

observed in the co-sublimation spectrum, namely complete ligand exchange for both cadmium and nickel complexes at *m/z* = 528 and *m/z* = 455, respectively. In addition to the complete exchanges, there are partial ligand exchanges for both, not to mention fragmentation of the newly formed complexes. What is of particular interest in the data is the peak observed at *m/z* = 271, which is the fluorine migration that is associated with the ion signal for the hexafluoroacetylacetonate complex. Although the fluorine migration product is still present, overall ion intensity of the spectra is low.

m/z	Species	Rel. Ab.	m/z	Species	Rel. Ab.
528	$[Cd(hfac)_2]^+$	9	455	$[Zn(tftm)_2]^+$	30
516	$[Cd(hfac)(tftm)]^+$	6	398	$[Zn(tftm)(tftm\ t\text{Bu})]^+$	19
459	$[Cd(hfac)(hfac\text{-}CF_3)]^+$	54	341	$[Zn(tftm\text{-}t\text{Bu})(tftm\text{-}t\text{Bu})]^+$	1
390	$[Cd(hfac\text{-}CF_3)(hfac\text{-}CF_3)]^+$	1	467	$[Zn(tftm)(hfac)]^+$	2
321	$[Cd(hfac)]^+$	15	410	$[Zn(tftm\text{-}t\text{Bu})(hfac)]^+$	7
252	$[Cd(hfac\text{-}CF_3)]^+$	13	203	$[Zn(tftm\text{-}t\text{Bu})]^+$	2
271	$[Cd(hfac\text{-}CF_2)]^+$	8	479	$[Zn(hfac)_2]^+$	5
504	$[Cd(tftm)_2]^+$	15	410	$[Zn(hfac)(hfac\text{-}CF_3)]^+$	23
447	$[Cd(tftm)(tftm\text{-}t\text{Bu})]^+$	100	272	$[Zn(hfac)]^+$	2
309	$[Cd(tftm)]^+$	35	222	$[Zn(hfac\text{-}CF_2)]^+$	6
252	$[Cd(tftm\text{-}t\text{Bu})]^+$	18			

Table 5.5: Relative ion abundances of the $Cd(tftm)_2$ and $Zn(hfac)_2$ species, as well as the co-sublimation of $Cd(tftm)_2$ and $Zn(hfac)_2$ as presented in Figure 5.5c.

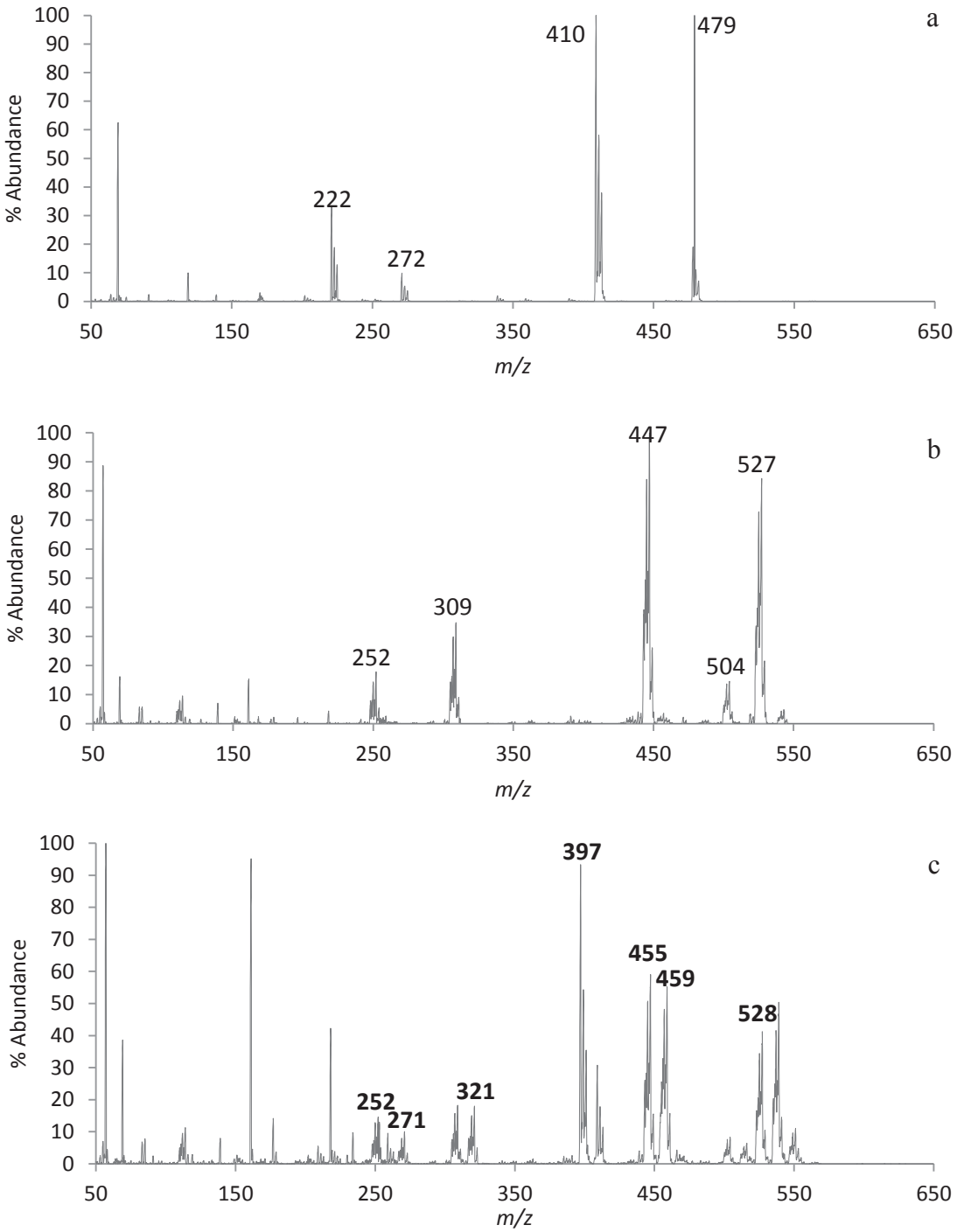

Figure 5.5: The positive EI mass spectra of (a) $Zn(hfac)_2$, (b) $Cd(tftm)_2$, and (c) the co-sublimation of $Zn(hfac)_2$ and $Cd(tftm)_2$. Masses labeled in (a) and (b) represent the molecular ion and typical fragments of their respective parent compounds. Masses labeled in (c) correspond to the intact ligand gas phase product and fragments thereof.

5.7: Co-sublimation of $Cd(tftm)_2$ and $Pd(hfac)_2$

The mass spectrometric data describing the sublimation of $Pd(hfac)_2$, $Cd(tftm)_2$, as well as the co-sublimation $Cd(tftm)_2$ and $Pd(hfac)_2$ is presented in Figure 5.6, and is vertically stacked for ease of comparison. Figure 5.6a illustrates the single $Pd(hfac)_2$ spectrum and the corresponding fragmentation pattern that is typically associated with this species. Notable peaks that can be observed in the three spectra are listed in Table 5.6, and include the parent peak $[Pd(hfac)_2]^+$ at m/z = 520, and the loss of a CF_3 group at m/z = 451. The loss of one intact ligand at m/z = 313 and the loss of a CF_3 group from only one intact *hfac* ligand at m/z = 244 are also observed.

The mass spectrum of $Cd(tftm)_2$ is reproduced in Figure 5.6b, which is the same spectrum that is represented from Figure 4.1, just over a different range. The co-sublimation $Cd(tftm)_2$ and $Pd(hfac)_2$ is presented in Figure 5.6c, where both species can react in the gas phase and undergo ligand exchange, whether it be a partial, mixed, or complete exchange. The ion peaks observed in Figure 5.6c are exclusive to the results following the co-sublimation ligand exchange and are not present in the individual spectrum. Table 5.6 reports the m/z ratios, the exchanged single species, mixed ligand and fragmented species, as well as the corresponding relative abundances. In assessing the ligand exchange in Figure 5.6c, it would appear that the copper complex was more likely to form than the cadmium complexes, which is comparable to the data presented in Section 4.2.

m/z	Species	Rel. Ab.	m/z	Species	Rel. Ab.
528	$[Cd(hfac)_2]^+$	1	496	$[Pd(tftm)_2]^+$	5
516	$[Cd(hfac)(tftm)]^+$	<1	439	$[Pd(tftm)(tftm\text{-}t\text{Bu})]^+$	2
459	$[Cd(hfac)(hfac\text{-}CF_3)]^+$	31	382	$[Pd(tftm\text{-}t\text{Bu})(tftm\text{-}t\text{Bu})]^+$	<1
390	$[Cd(hfac\text{-}CF_3)(hfac\text{-}CF_3)]^+$	<1	508	$[Pd(tftm)(hfac)]^+$	6
321	$[Cd(hfac)]^+$	22	451	$[Pd(tftm\text{-}t\text{Bu})(hfac)]^+$	3
252	$[Cd(hfac\text{-}CF_3)]^+$	3	244	$[Pd(tftm\text{-}t\text{Bu})]^+$	32
271	$[Cd(hfac\text{-}CF_2)]^+$	10	520	$[Pd(hfac)_2]^+$	21
504	$[Cd(tftm)_2]^+$	15	451	$[Pd(hfac)(hfac\text{-}CF_3)]^+$	5
447	$[Cd(tftm)(tftm\text{-}t\text{Bu})]^+$	100	313	$[Pd(hfac)]^+$	22
309	$[Cd(tftm)]^+$	35	244	$[Pd(hfac\text{-}CF_3)]^+$	25
252	$[Cd(tftm\text{-}t\text{Bu})]^+$	18			

Table 5.6: Relative ion abundances of the $Cd(tftm)_2$ and $Pd(hfac)_2$ species, as well as the co-sublimation of $Cd(tftm)_2$ and $Pd(hfac)_2$ as presented in Figure 5.6c.

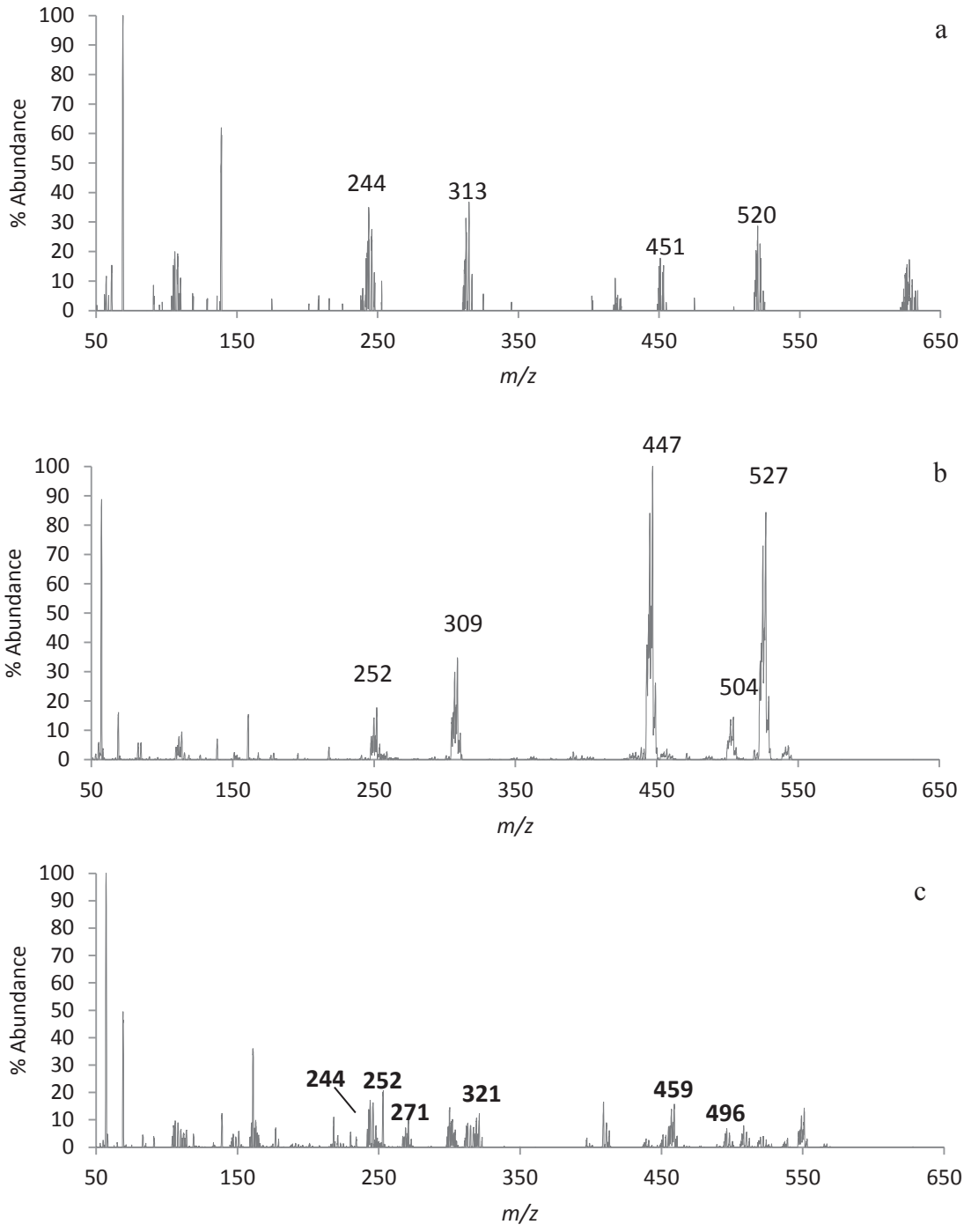

Figure 5.6: The positive EI mass spectra of (a) $Pd(hfac)_2$, (b) $Cd(tftm)_2$, and (c) the co-sublimation of $Pd(hfac)_2$ and $Cd(tftm)_2$. Masses labeled in (a) and (b) represent the molecular ion and typical fragments of their respective parent compounds. Masses labeled in (c) correspond to the intact ligand gas phase product and fragments thereof.

Chapter 6
Supplemental Homo-Metal Gas-Phase Spectra

6.1 Introduction

The remaining spectra presented in this Chapter were those that, when synthesized, appeared successful, however, when examined under co-sublimation conditions, did not yield any type of exchange – partial, mixed, or complete. Although these species were not found to be useful in co-sublimation data, four of the samples are being reported for the first time. As previously reported in Hunter's[1] thesis, $Co(tftm)_2$ is reproduced in Figure 6.1. For the first time, the 70eV positive EI mass spectra of $Co(eeac)_2$, $Mg(eeac)_2$, $Mg(tftm)_2$, and $Pd(tftm)_2$ are presented in this Chapter.

In the Sections that follow, the five synthesized complexes, two $M(eeac)_2$ and three $M(tftm)_2$ complexes, have been observed using the triple quadrupole mass spectrometer under a 70 eV ion source, while monitoring positive ions. The fragmentation patterns have been reported in previous Chapters of this research and will be described for each of the Figures presented.

6.2 $Co(eeac)_2$

The positive EI mass spectrometric distribution of $Co(eeac)_2$ is presented for the first time in Figure 6.1. The fragmentation patterns observed, for species bound to the *eeac* ligand, are consistent with what was reported for similar complexes throughout the previous Chapters. The parent peak for $[Co(eeac)_2]^+$ is observed at *m/z* = 311, with the loss of a single ethyl group at *m/z* = 282. At *m/z* = 185, the peak with one intact *eeac* ligand bound to the Co metal (i.e. $[Co(eeac)]^+$) center can be observed, and again the loss of the ethyl group is observed at *m/z* = 156.

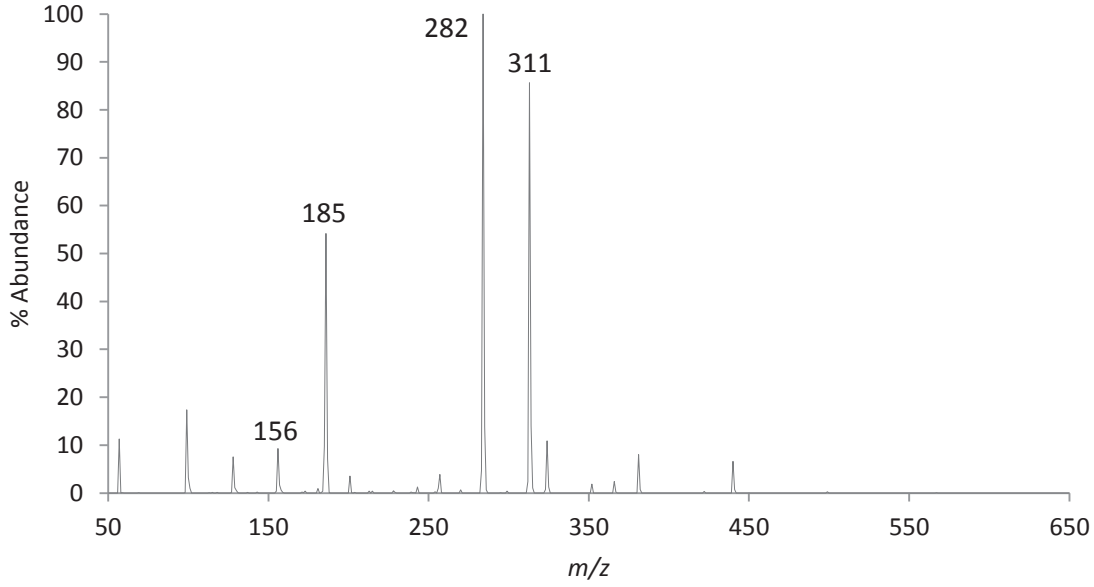

Figure 6.1: The 70 eV positive EI mass spectrum of $Co(eeac)_2$.

6.3 $Co(tftm)_2$

The positive EI mass spectrometric distribution of $Co(tftm)_2$ is presented for the first time in Figure 6.2. The fragmentation patterns observed, for species bound to the *tftm* ligand, are consistent with what was reported for similar complexes throughout the previous Chapters. The parent peak for $[Co(tftm)_2]^+$ is observed at m/z = 449, with the loss of a single *t*Bu group at m/z = 392 and the loss of a *tftm* ligand to form $[Co(tftm)]^+$ at m/z = 254.

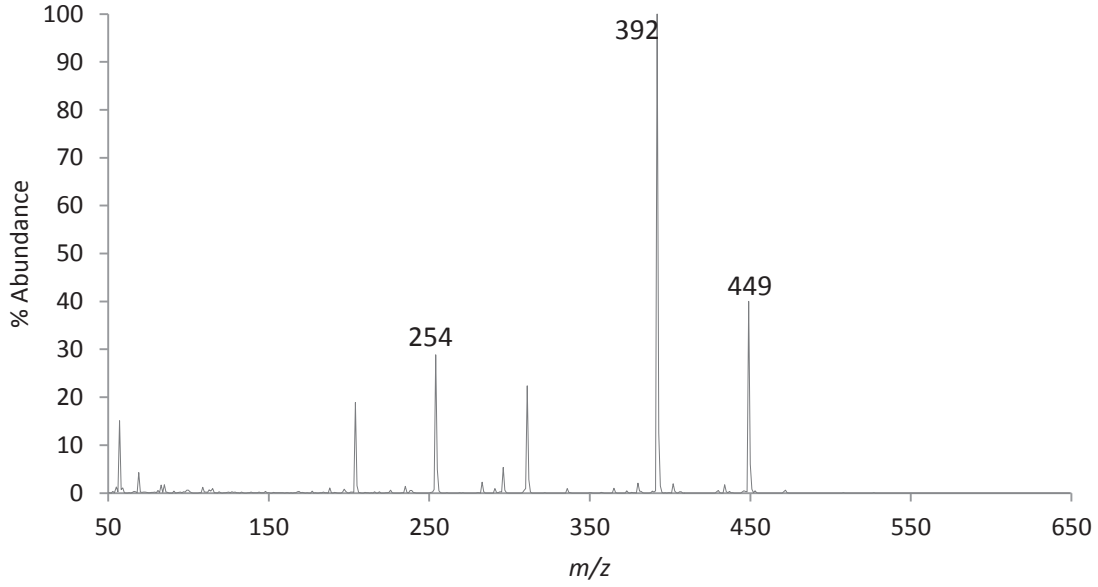

Figure 6.2: The 70 eV positive EI mass spectrum of $Co(tftm)_2$.

6.4 $Mg(eeac)_2$

The positive EI mass spectrometric distribution of $Mg(eeac)_2$ is presented for the first time in Figure 6.3. The fragmentation patterns observed, for species bound to the *eeac* ligand, are consistent with what was reported for similar complexes throughout the previous Chapters. The parent peak for $[Mg(eeac)_2]^+$ is observed at *m/z* = 276, with the loss of a single methyl group at *m/z* = 247 and the loss of an *eeac* ligand to form $[Mg(eeac)]^+$ at *m/z* = 150.

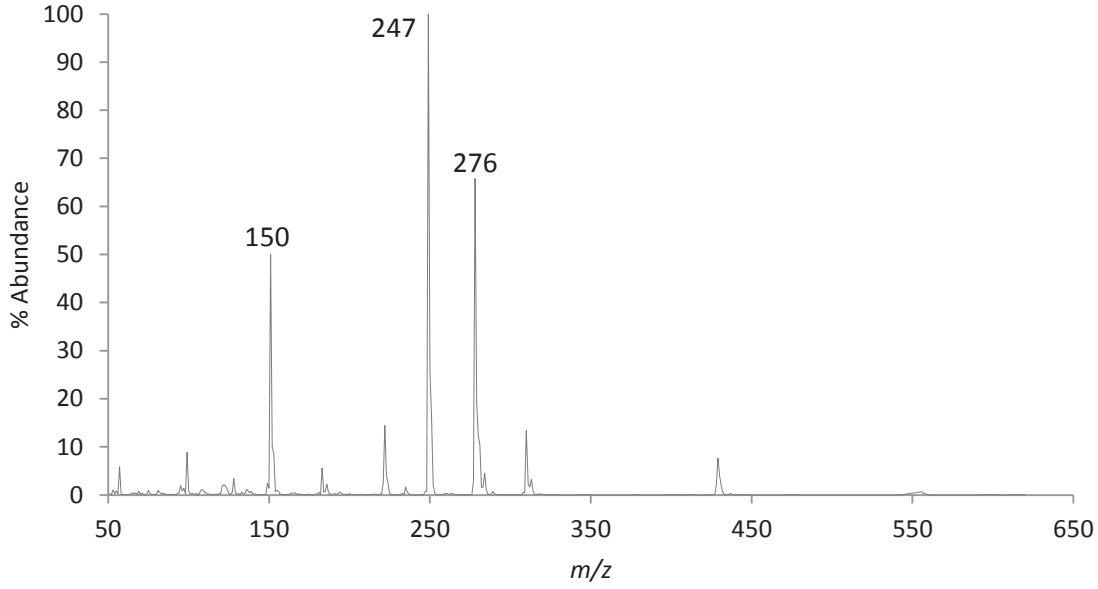

Figure 6.3: The 70 eV positive EI mass spectrum of $Mg(eeac)_2$.

6.5 $Mg(tftm)_2$

The positive EI mass spectrometric distribution of $Mg(tftm)_2$ is presented for the first time in Figure 6.4. The fragmentation patterns observed, for species bound to the *tftm* ligand, are consistent with what was reported for similar complexes throughout the previous Chapters. The parent peak for $[Mg(tftm)_2]^+$ is observed at *m/z* = 414, with the loss of a single *t*Bu group at *m/z* = 357.

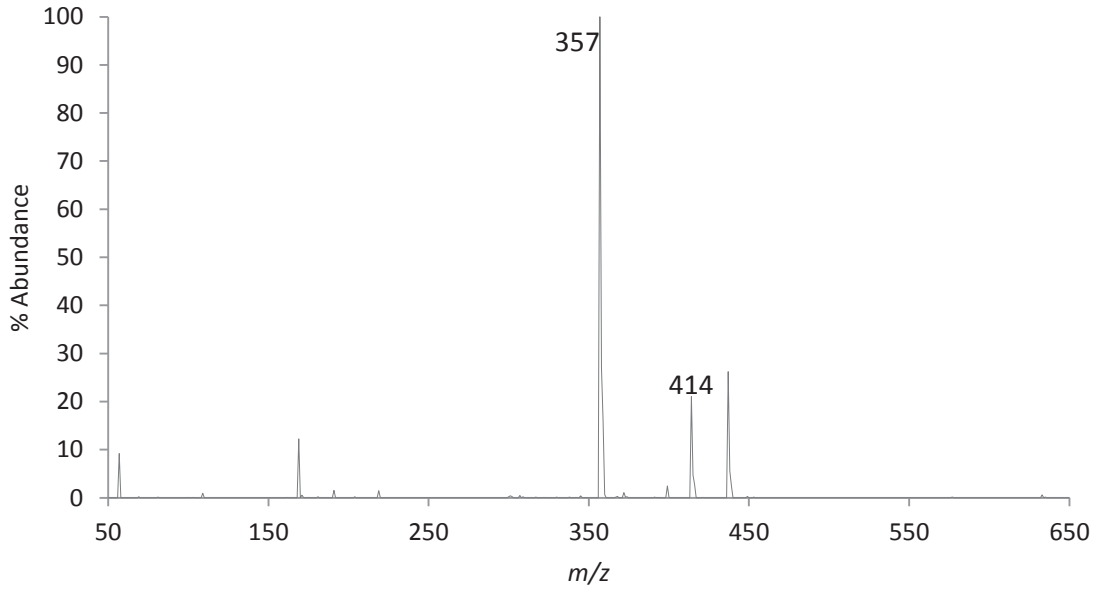

Figure 6.4: The 70 eV positive EI mass spectrum of $Mg(tftm)_2$.

6.6 $Pd(tftm)_2$

The positive EI mass spectrometric distribution of $Pd(tftm)_2$ is presented for the first time in Figure 6.5. The fragmentation patterns observed, for species bound to the *tftm* ligand, are consistent with what was reported for similar complexes throughout the previous Chapters. The parent peak $[Pd(tftm)_2]^+$ is observed at *m/z* = 496, with the loss of a single *t*Bu group at *m/z* = 439. At *m/z* = 301, the loss of a *tftm* ligand to form $[Pd(tftm)]^+$ is observed, as is the loss of a *t*Bu group at *m/z* = 244.

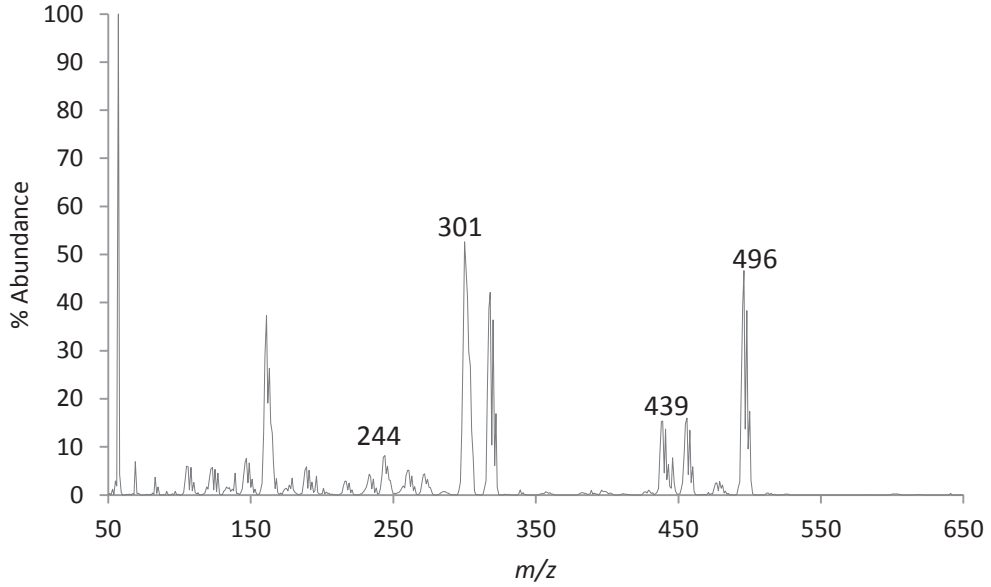

Figure 6.5: The 70 eV positive EI mass spectrum of $Pd(tftm)_2$.

Chapter 7

Conclusions and Future Work

From the research presented herein gas-phase ligand exchange is a process that is freely occuring. Regardless of the metal type of ligand present, co-sublimation of two different β-diketonates resulted in some degree of gas-phase ligand exchange, whether it was complete or a partial exchange. From the data presented, the trends of fragmentation that were reported previously are not only limited to the first row of transition metals, but are consistent with second row transition metals as well. Specific ion-neutral reactions were investigated using a collsion cell in order to gain insight into the reactions that produced the gas-phase ligand exchange products. The mass-selected experiments were implemented for the first time and were an integral part of the data collection and were instrumental in gaining a better understanding of the reactions taking place. Furthermore, the collison cell reactions enabled us to verify that an exchange was actually occuring due to the presence of the particular peaks in the spectrum.

Additional areas of future research include an expansion of the list of metal centers incorporated into the β-diketonate complex, as well as introducing new functional groups to the acetylacetonate backbone. Additional work is needed to further describe the reaction mechanisms. Morever, changing the conditions of the mass selected collision cell is also another option. When attempting to examine additional mechanisms, one can also alter the identity of both the neutral and charged species. For example, in all mass selected reactions that were presented in Chapter 4, the neutral species was each of the three different nickel complexes, while the charged species were the $Cd(tftm)_2$ cations

and fragments thereof. Not only can you change which species is held neutral and which is charged, but conducting anionic studies is another future research direction.

References

1. Hunter, G.O. The Examination of the Stability and Reactivity of Select Transition Metal β-diketonate Complexes during Gas-Phase Ligand Exchange Reactions, MS Thesis, Youngstown State University, December 2009
2. X. Yan, Q. Zhang, X. Fan. New MOCVD precursor for the iridium thin films deposition. *Mat. Lett.* **2007**, 61, 216.
3. A. C. B. Burtoloso, Copper (II) acetylacetonate: an inexpensive multifunctional catalyst. *Synlett* **2005**, 2589.
4. S. Shi, D. Ma, J. Peng. Improved electron injection in organic light-emitting devices with a lithium acetylacetonate [Li(acac)]/aluminum bilayer cathode. *Semicond. Sci. Technol.* **2007**, 22, 249.
5. Condorelli, G.G. Malandrino, G., Fragala, I.L*., Coordination Chemistry Reviews 2007 251, 1931-1950.*
6. Katok, K.V., Terttkh, V.A., Brichka, S.Y., Prikhod, G.P., *Journal of Thermal Analysis and Calorimetry* **2006** 86, 109-114
7. L. B. Belykh, T. V. Goremyka, A. V. Rokhin, Yu. Yu. Titova, V. A. Umanets, F. K. Schmidt. Reactions of Pd β-Diketonate Complexes with Triethylaluminum. *Russian Journal of Coordination Chem.***2005**, 31, 719-724.
8. Allen, G., Dwek, R.A., *Journal of the Chemical Society (B)***1966** 2, 161-163
9. Sloop, J.C., Baumgarder, C.L., Washington, G., Loehle, W.D., Sankar, S.S., Lewis, A.B., *Journal of Fluorine Chemistry* **2006** 127, 780-786
10. Schildcrout, S.M., *Journal of Physical Chemistry* **1976** 80, 2834-2838

11. Wallen, S.L., Yonker, C.R., Phelps, C.L., Wai, C.M., *Journal of the Chemical Society, Faraday Society***1997** 99, 4568-4572.

12. Wyatt, M.F., Harvard, S., Stien, B.K., Brenton, A.G., *Rapid Communications in Mass Spectrometry* **2008** 22, 11-18.

13. Dean, L.K., DiDonato, G.C., Wood, T.D., Busch, K.L., *Inorganic Chemistry* **1988** 27, 4622-4627.

14. Lerach, J.O. Investigation into the Gas-Phase Rearrangements of Some Transition Metal B-diketonate Complexes, MS Thesis, Youngstown State University, August 2008.

15. Pierce, J.L. Busch, K.L., Graham Cook, R., Walton, R.A., *Inorganic Chemistry* **1982** 27, 4622-4627.

16. MacDonald, C.G., Shannon, J.S., *Australian Journal of Chemistry* **1966** 9, 1454-1566.

17. Majer, J.R., Perry, R., *Chemical Communications* **1969** 9, 454-455.

18. Nieminen, M., Putkonen, M., Niinisto, L., *Applied Surface Science* **2001** 174, 155-165.

19. Kumar, R., Jain, S.K., Misra, R.K., Kachchwaha, M., Khatri, *International Journal of Environmental Science and Technology* **2012** 9, 79 – 84.

20. Spijksma, G.I., Seisenbaeva, G.A, Bouwmeester, H.J, Blank, D., and Kessler, V.G.. *Polyhedron* **2013** 53, 150-156.

21. Watson, W.H., Lin, C.T., *Inorganic Chemistry* **1965** 5, 1074 – 1077.

22. Lerach, J.O., Leskiw, B.D., *Rapid Communications in Mass Spectrometry* **2008** 22, 4139 – 4146.

23. Hunter, G.O., Lerach, J.O., Lockso, T.R., Leskiw, B.D., *Rapid Communications in Mass Spectrometry* **2010** 24, 129 – 137.

24. Hunter, G.O., Leskiw, B.D., *Rapid Communications in Mass Spectrometry* **2012** 26, 369 – 376.

Appendix A

Scanning Electron Microscopy (SEM) and Energy Dispersive Spectroscopy (EDS) Identification of $Cd(tftm)_2$ Formation

Secondary Electron Imaging

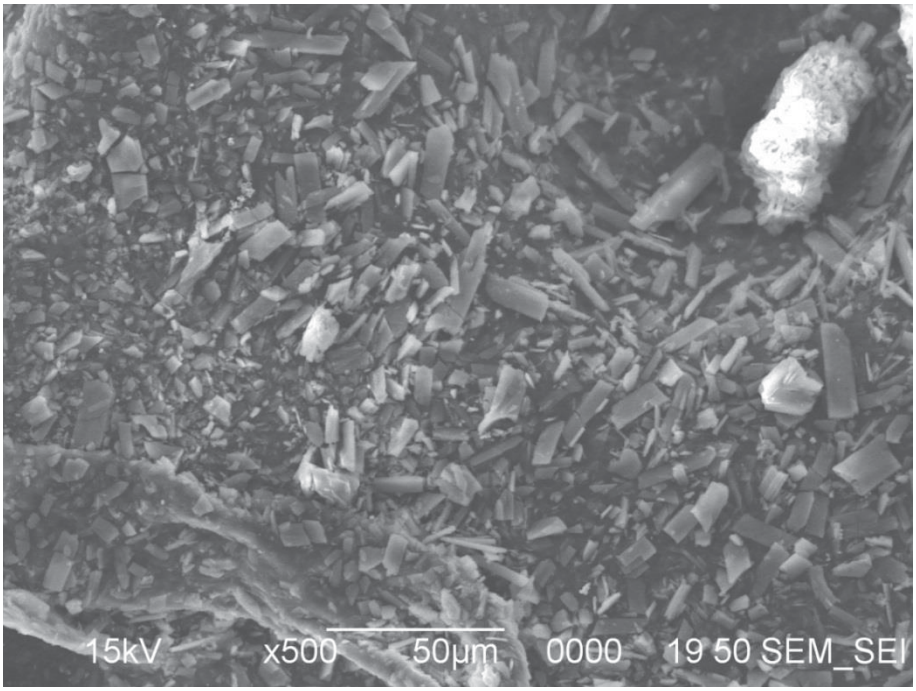

Figure A.1: $Cd(tftm)_2$ secondary electron imaging (SEI) 50µm, x500 magnification.

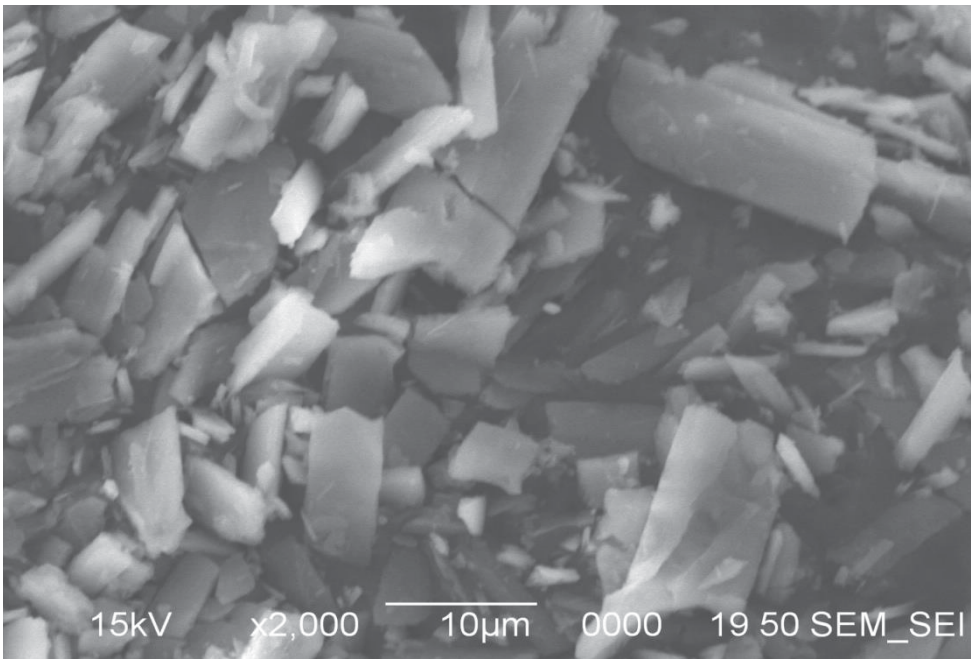

Figure A.2: $Cd(tftm)_2$ SEI, 10µm, x2000 magnification.

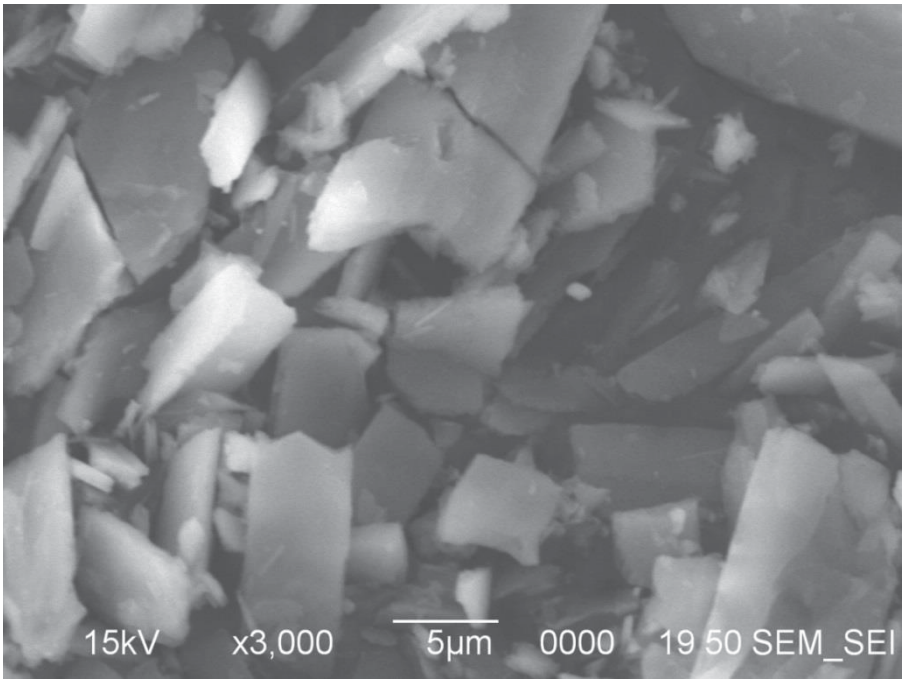

Figure A.3: $Cd(tftm)_2$ SEI 5µm, x3000 magnification.

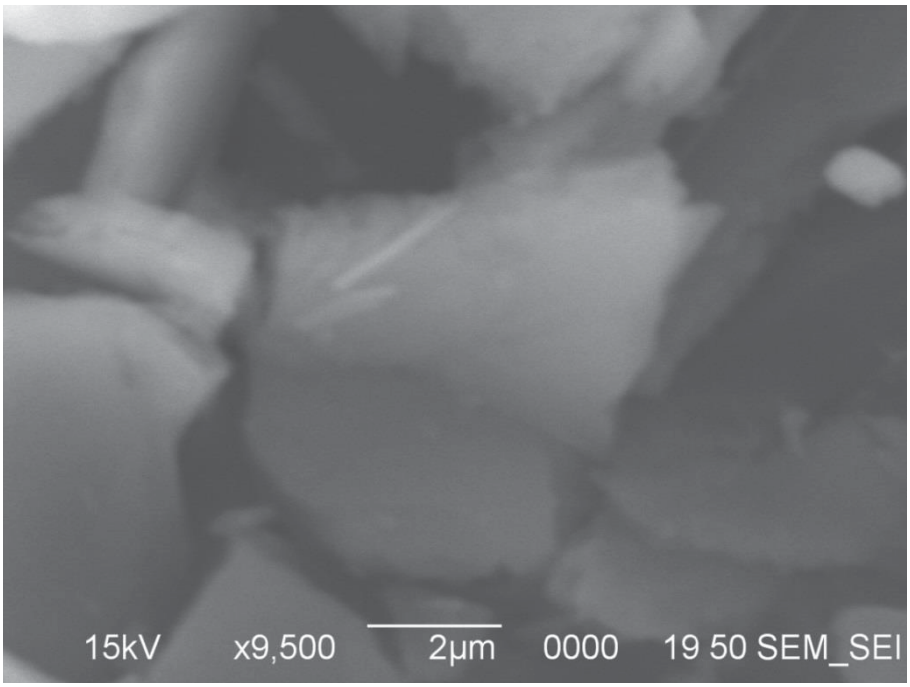

Figure A.4: $Cd(tftm)_2$ SEI 2µm, x9500 magnification**.**

Backscattered Electron Composition

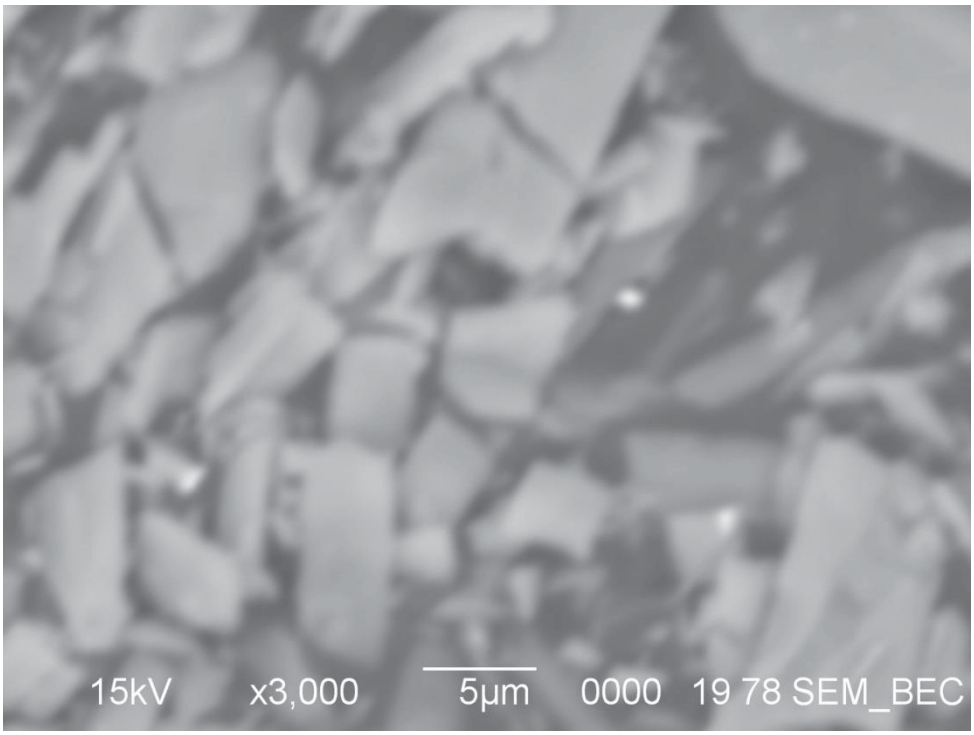

Figure A.5: $Cd(tftm)_2$ backscattered electron composition (BEC) 5µm, x3000 magnification.

Energy Dispersive X-Ray (EDX) Imaging

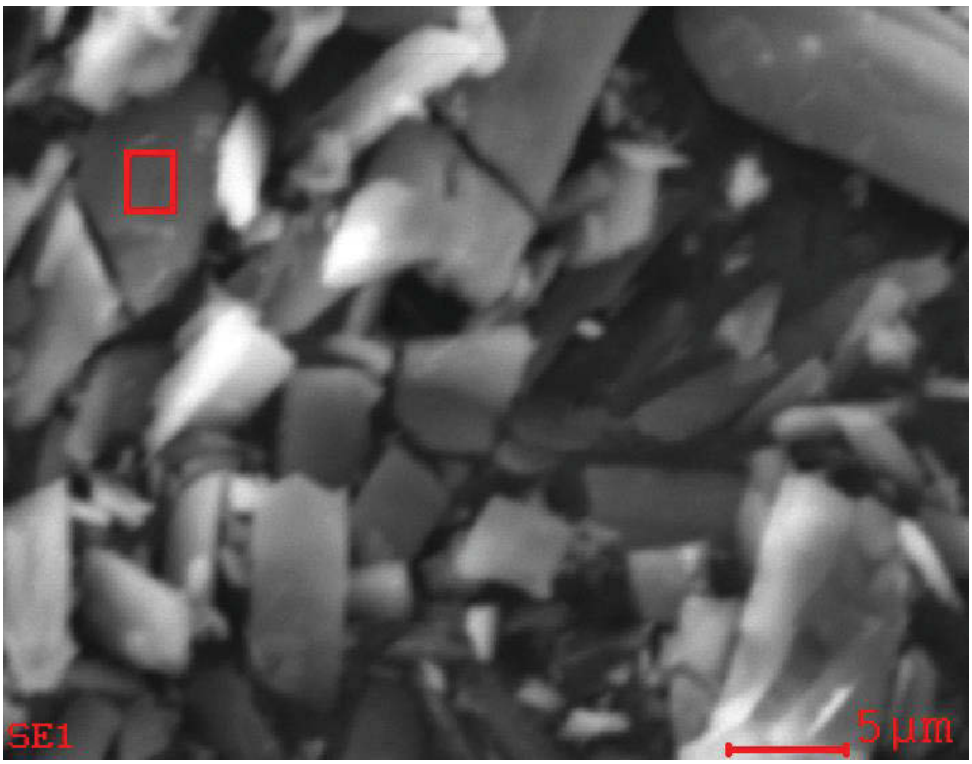

Figure A.6: $Cd(tftm)_2$ EDX 5µm.

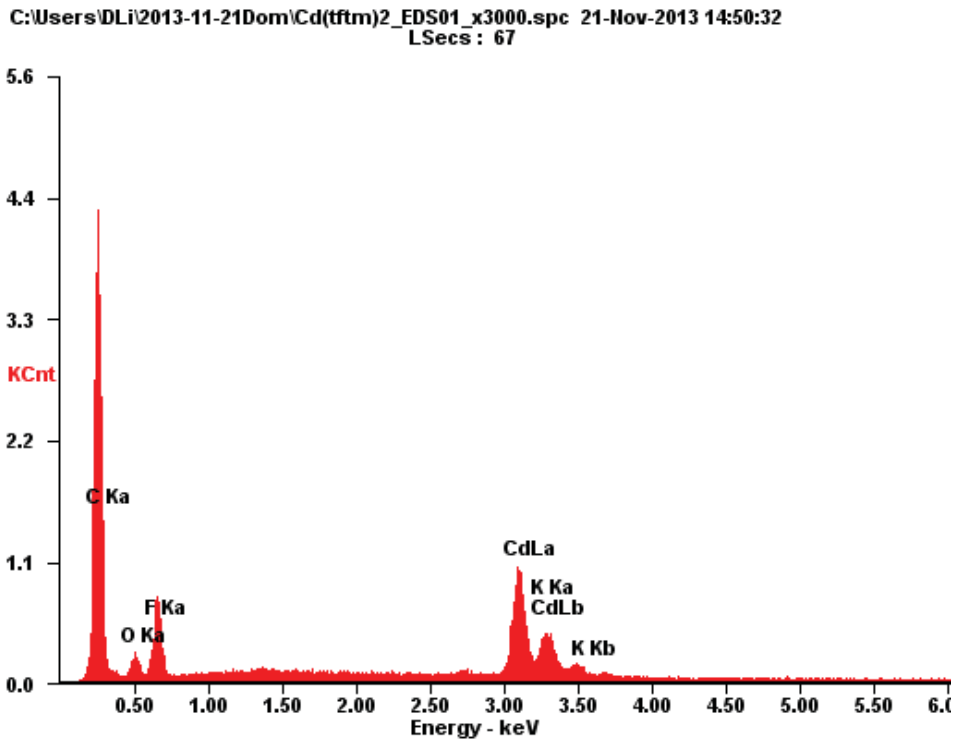

Figure A.7: EDX chemical composition spectrum of $Cd(tftm)_2$.

Element	Wt%	At%
CK	51.36	74.73
OK	6.63	7.24
FK	15.04	13.83
CdL	26.98	4.19
KK	00.00	00.00
Matrix	Correction	ZAF

Table A.1: Weight composition and atomic composition of elements present in $Cd(tftm)_2$ as presented in Figure A.7.

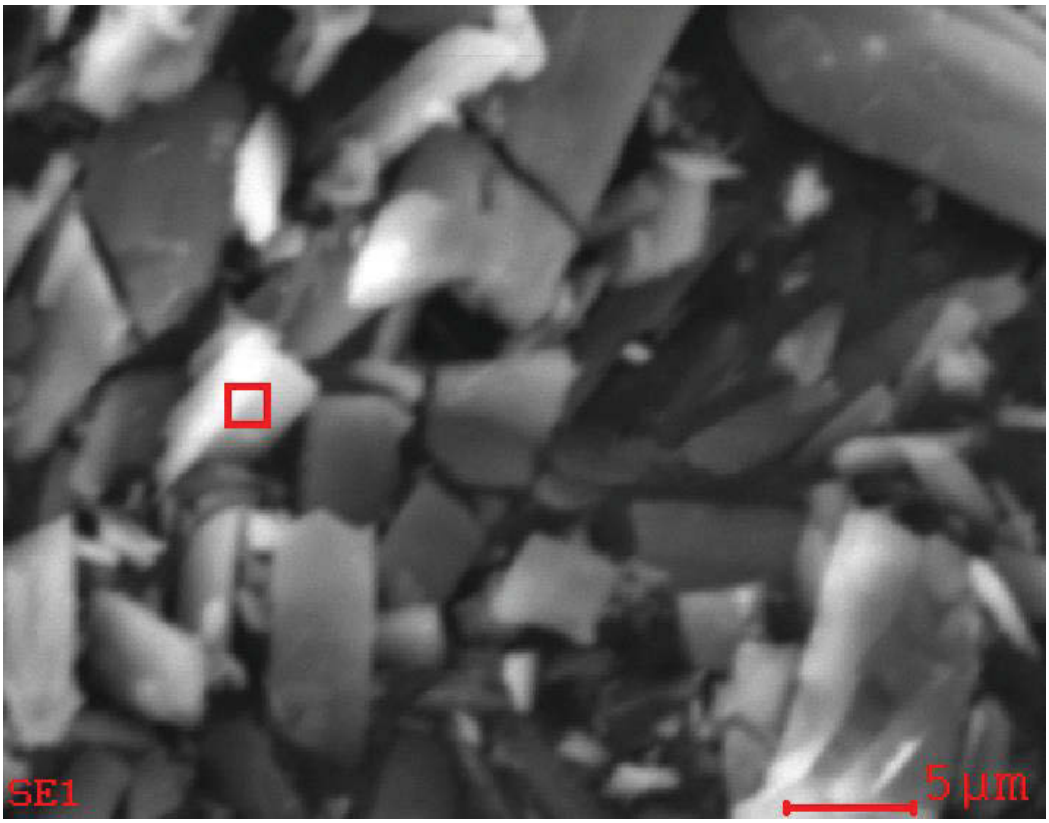

Figure A.8: $Cd(tftm)_2$ EDX 5µm.

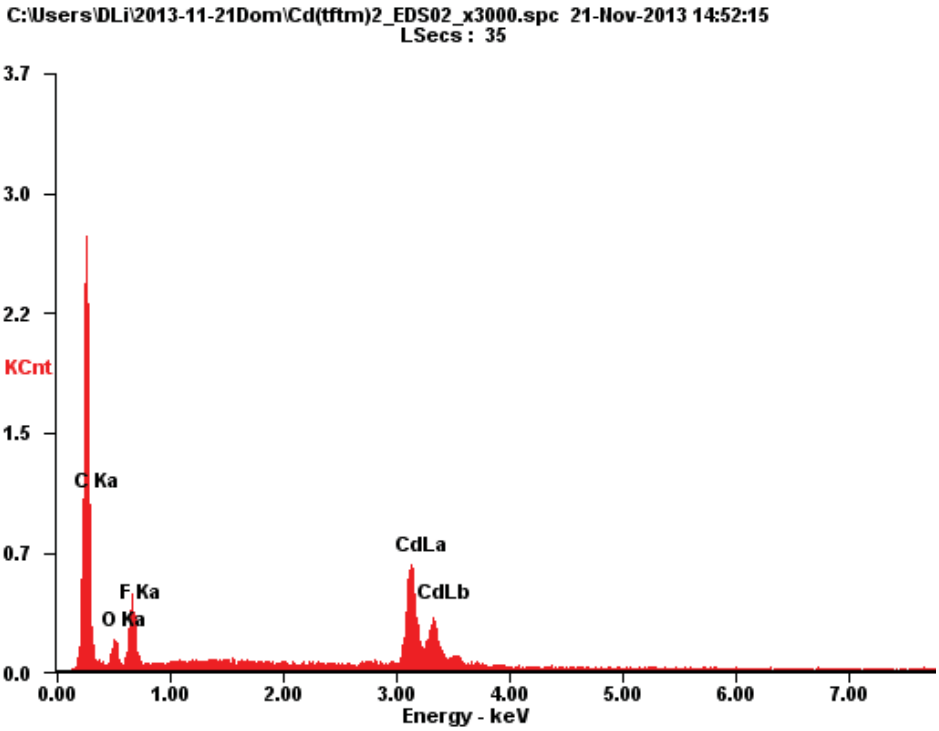

Figure A.9: EDX chemical composition spectrum of $Cd(tftm)_2$.

Element	Wt%	At%
CK	51.14	74.33
OK	7.47	8.15
FK	14.52	13.34
CdL	26.88	4.17
Matrix	Correction	ZAF

Table A.2: Weight composition and atomic composition of elements present in $Cd(tftm)_2$ as presented in Figure A.9.

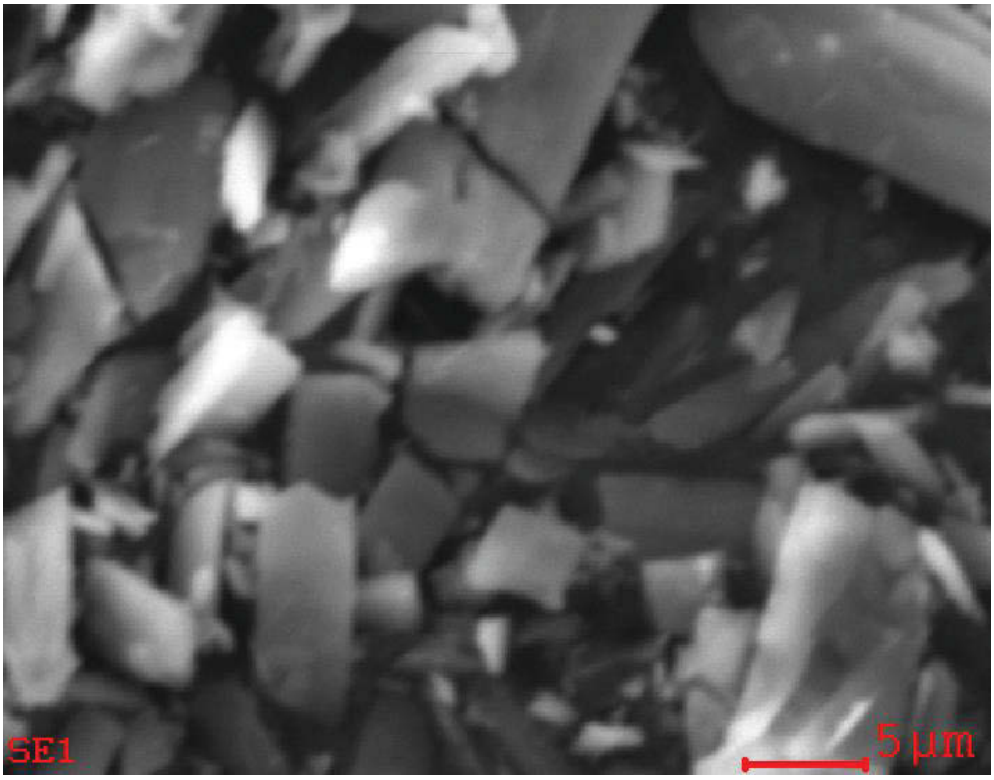

Figure A.10: $Cd(tftm)_2$ EDX 5µm.

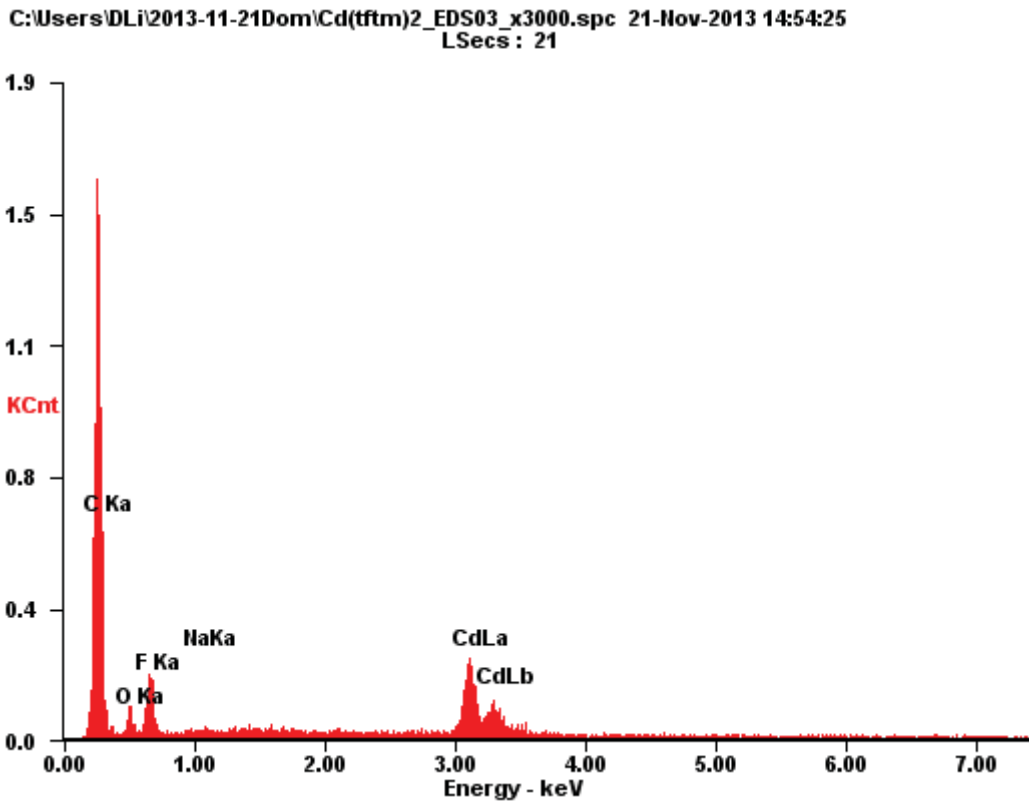

Figure A.11: EDX chemical composition spectrum of $Cd(tftm)_2$.

Element	Wt%	At%
CK	59.87	78.93
OK	7.55	7.47
FK	12.65	10.54
NaK	0.45	0.31
CdL	19.49	2.75
Matrix	Correction	ZAF

Table A.3: Weight composition and atomic composition of elements present in $Cd(tftm)_2$ as presented in Figure A.11.